

Caloric curves of self-gravitating fermions in general relativity

Giuseppe Alberti

*Laboratoire de Physique Théorique, Université Paul Sabatier,
118 route de Narbonne 31062 Toulouse, France and
Living Systems Research, Roseggerstraße 27/2, A-9020 Klagenfurt am Wörthersee, Austria*

Pierre-Henri Chavanis

Laboratoire de Physique Théorique, Université Paul Sabatier, 118 route de Narbonne 31062 Toulouse, France

We study the nature of phase transitions between gaseous and condensed states in the self-gravitating Fermi gas at nonzero temperature in general relativity. The condensed states can represent compact objects such as white dwarfs, neutron stars, or dark matter fermion balls. The caloric curves depend on two parameters: the system size R and the particle number N . When $N < N_{\text{OV}}$, where N_{OV} is the Oppenheimer-Volkoff limit, there exists an equilibrium state for any value of the temperature T and of the energy E as in the nonrelativistic case [P.H. Chavanis, *Int. J. Mod. Phys. B* **20**, 3113 (2006)]. Gravitational collapse is prevented by quantum mechanics (Pauli's exclusion principle). When $N > N_{\text{OV}}$, there is no equilibrium state below a critical energy and below a critical temperature. In that case, the system is expected to collapse towards a black hole. We plot the caloric curves of the general relativistic Fermi gas, study the different types of phase transitions that occur in the system, and determine the phase diagram in the (R, N) plane. The nonrelativistic results are recovered for $N \ll N_{\text{OV}}$ and $R \gg R_{\text{OV}}$ with NR^3 fixed. The classical results are recovered for $N \gg N_{\text{OV}}$ and $R \gg R_{\text{OV}}$ with N/R fixed. We discuss the commutation of the limits $c \rightarrow +\infty$ and $\hbar \rightarrow 0$. We study the relativistic corrections to the nonrelativistic caloric curves and the quantum corrections to the classical caloric curves. We highlight a situation of physical interest where a gaseous Fermi gas, by cooling, first undergoes a phase transition towards a compact object (white dwarf, neutron star, dark matter fermion ball), then collapses into a black hole. This situation occurs in the microcanonical ensemble when $N_{\text{OV}} < N < 3.73 N_{\text{OV}}$. We also relate the phase transitions from a gaseous state to a core-halo state in the microcanonical ensemble to the onset of red-giant structure and to the supernova phenomenon.

PACS numbers: 95.30.Sf, 95.35.+d, 04.40.Dg, 67.85.Lm, 05.70.-a, 05.70.Fh

I. INTRODUCTION

The study of phase transitions is an important problem in physics. Some examples include solid-liquid-gas phase transitions, superconducting and superfluid transitions, Bose-Einstein condensation, liquid-glass phase transition in polymers, liquid crystal phases, Kosterlitz-Thouless transition etc. Self-gravitating systems also undergo phase transitions but they are special due to the unshielded long-range attractive nature of the interaction [1]. This leads to unusual phenomena such as negative specific heats, ensembles inequivalence, long-lived metastable states, and gravitational collapse. A strict equilibrium state can exist only if the system is confined within a box, otherwise it has the tendency to evaporate (this is already the case for an ordinary gas). On the other hand, in order to define a condensed phase we need to introduce a short-range repulsion between the particles that opposes itself to the gravitational attraction.¹

In this paper, we consider the case of self-gravitating fermions where an effective short-range repulsion is due to quantum mechanics (Pauli's exclusion principle). The object of this paper is to present a complete description of phase transitions in the self-gravitating Fermi gas in general relativity. This study can have applications in relation to the formation of compact objects such as white dwarfs, neutron stars, dark matter stars, black holes etc. On the other hand, the phase transition from a gaseous state to a condensed state may be related to the onset of red-giant structure and to the supernova phenomenon. We first start by reviewing the literature on the subject. We focus our review on papers that study phase transitions in the box-confined self-gravitating Fermi gas at nonzero temperature.² We do not review the immensely vast literature related to self-gravitating fermions as models of white dwarfs, neutron stars, and dark matter halos. For a connection to this

¹ Without small-scale regularization, there is no equilibrium state (global entropy maximum) in a strict sense [2]. There can exist, however, metastable gaseous states (local entropy maxima) that are insensitive to the small-scale regularization [2, 3]. These metastable states have a very long lifetime, scaling as e^N , where

N is the number of particles in the system [4]. In practice this lifetime is much larger than the age of the Universe, making the metastable states fully relevant in astrophysics [5].

² The case of completely degenerate self-gravitating fermions at $T = 0$ and the case of classical (nondegenerate) self-gravitating systems are considered in our companion papers [6, 7] where a detailed review of the literature is made.

literature, we refer to [8–16] and references therein. For a connection to the general literature on the statistical mechanics of self-gravitating systems and systems with long-range interactions we refer to the introduction of [17] and to the reviews [1, 5, 18–21].

The statistical mechanics of nonrelativistic self-gravitating fermions at nonzero temperature enclosed within a box of radius R was first studied by Hertel & Thirring (1971) [22]. They worked in the canonical ensemble and rigorously proved that the mean field approximation (or effective field approximation) and the Thomas-Fermi (TF) approximation (which amounts to neglecting the quantum potential) become exact in a suitable thermodynamic limit $N \rightarrow +\infty$ where $R \sim N^{-1/3}$, $T \sim N^{4/3}$, $E \sim N^{7/3}$, $S \sim N$, and $F \sim N^{7/3}$ (the scaling $F \sim N^{7/3}$ was first obtained by Lévy-Leblond (1969) [23] for the ground state).³ This leads to the temperature-dependent TF equation.⁴ The existence of the TF limit for the thermodynamic functions of self-gravitating fermions was proven by Hertel *et al.* (1972) [24] for the microcanonical and canonical ensembles and by Messer (1979) [25] for the grand canonical ensemble. The convergence of the quantum-statistically defined particle density towards the TF density was proven by Baumgartner (1976) [26]. He also showed that there are no correlations in the thermodynamic limit. Narnhofer and Sewell (1980) [28] showed that when $N \rightarrow +\infty$ the equilibrium Gibbs distribution becomes a tensor product of density functions of an ideal Fermi gas which minimize the TF free energy functional. These density functions can be stable (global minima) or metastable (local minima). Finally, Narnhofer and Sewell (1982) [29] showed that when $N \rightarrow +\infty$ a quantum system of self-gravitating fermions is described by the *classical* Vlasov equation [30].

Hertel & Thirring (1971) [31] studied numerically phase transitions in the nonrelativistic self-gravitating Fermi gas in relation with the structure of neutron stars.⁵ They assumed that the gas is enclosed within a box and worked in the canonical ensemble. For a given number of particles N , they showed that a canonical first order phase transition arising from a multiplicity of solutions in the TF equation appears if the radius of the box is larger than a certain value $R_{\text{CCP}}(N) = 12.8 \hbar^2 / (N^{1/3} G m^3)$. This phase transition is characterized by a jump of en-

ergy (the energy $E = \partial(\beta F) / \partial \beta$, the first derivative of βF with respect to β , becomes discontinuous) at a transition temperature T_t determined by a Maxwell construction like in the theory of the van der Waals gas.⁶ This corresponds to a transition between a nearly homogeneous phase of medium mass density (gaseous phase) and a phase with a high density core surrounded by an atmosphere of low density (condensed phase) when the system cools down below T_t . Hertel & Thirring (1971) [31] explained that this phase transition replaces the region of negative specific heats in the microcanonical ensemble (or the piece of convex curvature in the entropy curve $S(E)$) which is associated with unstable equilibrium states in the canonical ensemble. Therefore, the microcanonical and canonical ensembles are not equivalent [24]. The region of negative specific heat in the microcanonical ensemble is bridged by a phase transition in the canonical ensemble.⁷ Hertel & Thirring (1971) [31] applied their crude model of neutron stars to a system of $N = 10^{57}$ neutrons (the corresponding mass being of the order of the solar mass) initially contained in a sphere of radius $R = 100$ km. The critical radius is $R_{\text{CCP}} = 43.1$ km. For $R = 100$ km $> R_{\text{CCP}}$, the system undergoes a first order phase transition below a critical temperature $T_t = 7.03 \times 10^{10}$ K, collapses, and forms a compact object (neutron star) containing almost all the mass. This compact object has approximately the same size, $R_C = 4.51 \hbar^2 / (N^{1/3} G m^3) = 15.1$ km, as a completely degenerate Fermi gas at $T = 0$ (equivalent, in their nonrelativistic model, to a polytrope of index $n = 3/2$) but it is surrounded by a small isothermal atmosphere. This gravitational phase transition could account for the implosion of the core in the supernova phenomenon where the energy is carried quickly by neutrinos.⁸

³ This is also equivalent to the usual thermodynamic limit $N \rightarrow +\infty$ where $R \sim N^{1/3}$, $T \sim 1$, $E \sim N$, $S \sim N$ and $F \sim N$ with $G \sim N^{-2/3}$ (see Appendix A).

⁴ It can be obtained by combining the fundamental equation of hydrostatic equilibrium with the Fermi-Dirac equation of state or, equivalently, by substituting the Fermi-Dirac density into the Poisson equation; see, e.g., Hertel (1977) [27]. For that reason, the temperature-dependent TF equation is sometimes called the Fermi-Dirac-Poisson equation.

⁵ The possibility of phase transitions in the self-gravitating Fermi gas at nonzero temperature was suggested in the Appendix IV of Lynden-Bell and Wood (1969) [3].

⁶ The phase transition arises because the TF equation has two stable solutions at the same temperature that minimize the TF free energy. A rigorous analytical proof for the existence of this phase transition was given by Messer (1981a, 1981b) [32, 33] following numerical calculations by Hertel (1977) [27]. When there are multiple solutions in the TF equation, they argue that one must choose the one with the smallest value of free energy.

⁷ Canonical phase transitions, associated with negative specific heats, have also been found by Thirring (1970) [34] in a toy model of self-gravitating systems, by Aronson and Hansen (1972) [35] for a self-gravitating hard spheres gas, by Carlitz (1972) [36] for hadronic matter, and by Hawking (1976) [37] for black holes.

⁸ Thirring (1970) [34], Hertel and Thirring (1971) [31] and Messer (1981) [33] mention the analogy between this phase transition and the formation of red giants and supernovae. However, this analogy may not be fully correct because the phase transition that they obtain just corresponds to an implosion. This is because they work in the canonical ensemble and consider relatively small systems while the phase transition leading to an implosion-explosion phenomenon, associated with a core-halo structure, occurs in the microcanonical ensemble for larger systems (see Ref. [38] and Sec. XIII). Lynden-Bell and Wood (1968) [3], considering a classical self-gravitating gas in the microcanonical ensemble, find the emergence of a core-halo structure and relate it to

Gravitational phase transitions of fermionic matter were also studied by Bilic & Viollier (1997) [39] in a cosmological setting. They considered weakly interacting massive fermions of mass $17.2 \text{ keV}/c^2$ in the presence of a large radiation-density background fixing the temperature. They studied a halo of mass $M = 10^9 M_\odot$ and radius $R = 1.68 \times 10^{-2} \text{ pc} > R_{\text{CCP}} = 6.00 \times 10^{-3} \text{ pc}$. When the system cools down below a transition temperature $T_t = 4.80 \times 10^5 \text{ K}$, a condensed phase emerges consisting of quasidegenerate supermassive fermion stars of mass $M \sim 10^9 M_\odot$ and radius $R_C = 2.10 \times 10^{-3} \text{ pc}$. They argued that these compact dark objects could play an important role in structure formation in the early Universe. In particular, these fermion stars could explain, without resorting to the black hole hypothesis, some of the features observed around supermassive compact dark objects which are reported to exist at the centers of a number of galaxies including our own and quasistellar objects (QSOs). On a technical point of view, their study is analogous to the one carried out by Hertel & Thirring (1971) [31] for neutron stars, i.e., they described the canonical first order phase transition between a “gaseous” phase and a “condensed” phase that appears below a transition temperature when the size of the object is sufficiently large.

A detailed theoretical description of phase transitions in the nonrelativistic self-gravitating Fermi gas at nonzero temperature was given by Chavanis (2002) [5] (see also Refs. [40–45]).⁹ He showed that the caloric curves $T(E)$ depend on a single control parameter $\mu = \eta_0 \sqrt{512\pi^4 G^3 M R^3}$ with $\eta_0 = gm^4/h^3$ (g is the spin multiplicity of the quantum states). For a fixed particle number N , this parameter can be seen as a measure of the size of the system since $\mu \propto R^{3/2}$. Chavanis [5] studied in detail the nature of phase transitions in the nonrelativistic self-gravitating Fermi gas in both microcanonical and canonical ensembles. He showed that there exist two critical points (one in each ensemble) at which zeroth and first order phase transitions appear. The canonical critical point $\mu_{\text{CCP}} = 83$ at which canonical phase transitions appear is equivalent to the one previously found by Hertel and Thirring (1971) [31]. The microcanonical critical point $\mu_{\text{MCP}} = 2670$ at which microcanonical phase transitions appear was not found previously. For $\mu \rightarrow +\infty$, one recovers the caloric curve of a nonrela-

tivistic self-gravitating classical gas [1]. Chavanis [4, 5] argued that first order phase transitions do not take place in practice, contrary to previous claims [31, 39], because of the very long lifetime of metastable states for systems with long-range interactions. Therefore, only zeroth order phase transitions take place at the spinodal points where the metastable branches disappear. Recently, this study of phase transitions was extended to the nonrelativistic fermionic King model [13, 14]. This model is more realistic as it avoids the need of an artificial box to confine the system.

Gravitational phase transitions of fermionic matter in general relativity were studied by Bilic and Viollier (1999) [47].¹⁰ They showed that, at some critical temperature T_t , weakly interacting massive fermionic matter with a total mass below the Oppenheimer-Volkoff (OV) limit [49] undergoes a first order gravitational phase transition from a diffuse to a clustered state, i.e., a nearly completely degenerate fermion star. This is an extension of their previous paper [47] in the Newtonian approximation. This relativistic extension allowed them to consider situations where the mass of the system is close to the OV limit so that the fermion star is strongly relativistic. For fermions masses of 10 to $25 \text{ keV}/c^2$ they argued that these fermions stars may well provide an alternative explanation for the supermassive compact dark objects that are observed at galactic centers. Indeed, a few Schwarzschild radii away from the object, there is little difference between a supermassive black hole and a fermion star of the same mass near the OV limit.¹¹ In their paper, they considered fermionic particles of mass $m = 17.2 \text{ keV}/c^2$ for which $N_{\text{OV}} = 1.4254 \times 10^{71}$, $N_{\text{OV}}m = 2.1973 \times 10^9 M_\odot$, $M_{\text{OV}} = 2.1186 \times 10^9 M_\odot$ and $R_{\text{OV}} = 8.88 \times 10^{-4} \text{ pc}$. They studied a system of $N = 0.95350 N_{\text{OV}}$ fermions, corresponding to a rest mass $Nm = 2.0951 \times 10^9 M_\odot$ which is slightly below the OV limit, in a sphere of size $R = 29.789 R_{\text{OV}} = 2.6391 \times 10^{-2} \text{ pc}$. The transition occurs at $T_t = 0.0043951 mc^2 = 8.7725 \times 10^5 \text{ K}$. This leads to a fermion star containing almost all the particles surrounded by a small atmosphere. If we approximate the fermion star by a Fermi gas at $T = 0$ containing all the rest mass $\sim 2.0951 \times 10^9 M_\odot$, we find a radius $R_C = 1.220 R_{\text{OV}} = 1.0809 \times 10^{-3} \text{ pc}$ and a mass $M_C = 0.9577 M_{\text{OV}} = 2.0290 \times 10^9 M_\odot$.

The study of Bilic and Viollier [47] is restricted to a unique value of R and N , with $N < N_{\text{OV}}$, leading to a canonical phase transition. The object of this paper is to perform a more general study of phase transitions

the onset of red giants.

⁹ In these papers, the statistical equilibrium state is obtained by maximizing the Fermi-Dirac entropy S at fixed mass M and energy E in the microcanonical ensemble and by minimizing the Fermi-Dirac free energy $F = E - TS$ at fixed mass M in the canonical ensemble, where S is obtained from a combinatorial analysis taking into account the Pauli exclusion principle. This leads to the TF (or Fermi-Dirac-Poisson) equation in a direct manner. The study of the self-gravitating Fermi gas has also applications in the statistical theory of violent relaxation developed by Lynden-Bell [46] that also leads to a Fermi-Dirac-type distribution [40].

¹⁰ In that case, the suitable thermodynamic limit corresponds to $N \rightarrow +\infty$ where $R \sim N^{2/3}$, $T \sim N^{-1/3}$, $E \sim N^{2/3}$, $S \sim N$ and $F \sim N^{2/3}$ with $m \sim N^{-1/3}$ [47]. This is also equivalent to the usual thermodynamic limit $N \rightarrow +\infty$ where $R \sim N^{1/3}$, $T \sim 1$, $E \sim N$, $S \sim N$ and $F \sim N$ with $G \sim N^{-2/3}$ (see Appendix A).

¹¹ Some difficulties with the “fermion ball” scenario to provide an alternative to supermassive black holes at the centers of the galaxies are pointed out in [50].

in the self-gravitating Fermi gas in general relativity for arbitrary values of R and N . In particular, we would like to determine what happens when $N > N_{\text{OV}}$, or what happens for larger values of R where a microcanonical phase transition is expected.

The paper is organized as follows. In Sec. II, we present the basic equations describing a general relativistic Fermi gas at statistical equilibrium in a box. In Sec. III, we expose general notions concerning the construction of the caloric curves and the description of phase transitions. In Sec. IV, we recall the results previously obtained in the nonrelativistic and classical limits. In Sec. V, we consider the case $R_{\text{CCP}} < R < R_{\text{MCP}}$ where the system undergoes a canonical phase transition from a gaseous phase to a condensed phase when $N_{\text{CCP}} < N < N_e$. In Sec. VI, we consider the case $R > R_{\text{MCP}}$ where the system undergoes a canonical phase transition when $N_{\text{CCP}} < N < N_e$ and a microcanonical phase transition when $N_{\text{MCP}} < N < N_f$ (we find that $N_e \sim N_{\text{OV}}$ and $N_f \sim 3.73 N_{\text{OV}}$). In Sec. VII, we consider the case of very large radii $R \gg R_{\text{MCP}}$ where extreme core-halo configurations with a high central density appear. They correspond to the solutions computed in [10, 12, 14] in connection to the ‘‘fermion ball’’ scenario. However, following [14], we point out that these solutions are thermodynamically unstable (hence very unlikely). In Secs. VIII and IX, we consider the cases $R_{\text{OV}} < R < R_{\text{CCP}}$ and $R < R_{\text{OV}}$ where there is no phase transition. In Sec. X, we present the complete phase diagram of the general relativistic Fermi gas in the (R, N) plane. In Sec. XI, we recover the nonrelativistic and classical results as particular limits of our general study and we discuss the commutation of the limits $\hbar \rightarrow 0$ and $c \rightarrow +\infty$. In Sec. XII, we study the relativistic corrections to the nonrelativistic caloric curves and the quantum corrections to the classical caloric curves. In Sec. XIII, we consider astrophysical applications of our results in relation to the formation of white dwarfs, neutron stars, dark matter fermion stars, and black holes. We also connect the phase transitions found in our study with the onset of the red-giant structure and with the supernova phenomenon.

II. BASIC EQUATIONS OF A GENERAL RELATIVISTIC FERMI GAS

In this section, we give the basic equations describing the structure of a general relativistic Fermi gas at nonzero temperature (see [47, 48, 51] for their derivation). Using the normalized variables introduced in Appendix B, the local number density $n(r)$, the energy density $\epsilon(r)$, the pressure $P(r)$ and the temperature $T(r)$ are related to the gravitational potential $\Phi(r)$ by

$$n(r) = \frac{1}{\pi^2} \int_0^{+\infty} \frac{y^2 dy}{1 + e^{-\alpha} e^{|\alpha| \sqrt{(y^2+1)/(\Phi(r)+1)}}}, \quad (1)$$

$$\epsilon(r) = \frac{1}{\pi^2} \int_0^{+\infty} \frac{y^2 \sqrt{1+y^2} dy}{1 + e^{-\alpha} e^{|\alpha| \sqrt{(y^2+1)/(\Phi(r)+1)}}}, \quad (2)$$

$$P(r) = \frac{1}{3\pi^2} \int_0^{+\infty} \frac{y^4 dy}{\sqrt{1+y^2} \left[1 + e^{-\alpha} e^{|\alpha| \sqrt{(y^2+1)/(\Phi(r)+1)}} \right]}, \quad (3)$$

$$T(r) = \frac{1}{|\alpha|} \sqrt{\Phi(r) + 1}, \quad (4)$$

where

$$\alpha = \frac{\mu(r)}{T(r)} = \frac{\mu_\infty}{T_\infty} \quad (5)$$

is a quantity that is uniform throughout the system. These equations define the equation of state of a relativistic Fermi gas in parametric form.

The Tolman-Oppenheimer-Volkoff (TOV) equations, which correspond to the equations of hydrostatic equilibrium in general relativity, can be written as

$$\frac{d\Phi}{dr} = -2 [\Phi(r) + 1] \frac{M(r) + 4\pi P(r)r^3}{r^2 \left[1 - \frac{2M(r)}{r} \right]}, \quad (6)$$

$$\frac{dM}{dr} = 4\pi \epsilon(r) r^2, \quad (7)$$

where $M(r)$ is the mass-energy within the sphere of radius r . They have to be solved with the boundary conditions

$$M(0) = 0, \quad \Phi(0) = \Phi_0 > -1. \quad (8)$$

We assume that the system is confined within a box of radius R . The total mass of the gas and the total particle number are given by

$$M = M(R) = \int_0^R \epsilon(r) 4\pi r^2 dr, \quad (9)$$

$$N = \int_0^R n(r) \left[1 - \frac{2M(r)}{r} \right]^{-1/2} 4\pi r^2 dr. \quad (10)$$

The temperature at infinity is given by

$$T_\infty = T(R) \left(1 - \frac{2M}{R} \right)^{1/2}, \quad (11)$$

where $T(R)$ is the temperature of the system on the edge of the box. Using Eq. (4), we obtain

$$T_\infty = \frac{1}{|\alpha|} \sqrt{\Phi(R) + 1} \left(1 - \frac{2M}{R} \right)^{1/2}. \quad (12)$$

The entropy is given by

$$S = \int_0^R \frac{P + \epsilon}{T} \left[1 - \frac{2M(r)}{r} \right]^{-1/2} 4\pi r^2 dr - \alpha N. \quad (13)$$

Finally, the free energy is given by

$$F = E - T_\infty S, \quad (14)$$

where $E = M - N$ is the binding energy.¹²

III. CALORIC CURVES AND PHASE TRANSITIONS

In order to study the phase transitions in the general relativistic Fermi gas we have to determine the caloric curves $T_\infty(E)$ relating the temperature at infinity T_∞ to the energy E . These caloric curves depend on two parameters R and N . The manner to obtain these caloric curves is detailed in Appendix C. In order to make the connection with the nonrelativistic results [5], we shall plot the caloric curves in terms of the dimensionless parameters η (inverse temperature) and Λ (minus energy) defined by

$$\eta = \frac{\beta GNm^2}{R} \quad \text{and} \quad \Lambda = \frac{-ER}{GN^2m^2}, \quad (15)$$

where $\beta = 1/(k_B T_\infty)$ and $E = Mc^2 - Nmc^2$. In terms of our normalized variables, they reduce to

$$\eta = \frac{\beta N}{R} \quad \text{and} \quad \Lambda = \frac{-ER}{N^2}, \quad (16)$$

where $\beta = 1/T_\infty$ and $E = M - N$. We shall therefore plot the caloric curves $\eta(\Lambda)$ as a function of R and N .

We recall that for systems with long-range interactions, such as self-gravitating systems, the statistical ensembles are not equivalent. In this paper, we shall consider the microcanonical and canonical ensembles separately.

In the microcanonical ensemble, the system is isolated so that its energy E is conserved. It serves as a control parameter. A stable equilibrium state is a (local) maximum of entropy S at fixed energy E and particle number N . A minimum, or a saddle point, of entropy is unstable. The global maximum of entropy corresponds to the most probable state (the one that is the most represented at the microscopic level). The microcanonical caloric curve gives the temperature at infinity $1/T_\infty = \partial S/\partial E$ as a function of the energy E .

In the canonical ensemble, the system is in contact with a heat bath so that its temperature at infinity T_∞

is fixed. It serves as a control parameter. A stable equilibrium state is a (local) minimum of free energy F at fixed temperature T_∞ and particle number N . A maximum, or a saddle point, of free energy is unstable. The global minimum of free energy corresponds to the most probable state. The caloric curve gives the average energy $E = \partial(\beta F)/\partial\beta$ as a function of the temperature at infinity T_∞ .

The equilibrium states are the same in the microcanonical and canonical ensembles. This is because an extremum (first variations) of entropy at fixed energy and particle number coincides with an extremum of free energy at fixed particle number. However, their stability (second variations) may differ in the microcanonical and canonical ensembles. A configuration that is stable in the canonical ensemble is necessarily stable in the microcanonical ensemble but the converse is wrong. As a corollary we recall that the specific heat $C = dE/dT_\infty = Nk_B\eta^2 d\Lambda/d\eta$ of stable equilibrium states is always positive in the canonical ensemble while it can be positive or negative in the microcanonical ensemble (for systems with long-range interactions).

The stability of the solutions can be determined by using the Poincaré turning point criterion [52]. We refer to the papers of Katz [53, 54] for a presentation and a generalization of this criterion, and for its application to the nonrelativistic classical self-gravitating gas. This method was applied to the nonrelativistic self-gravitating Fermi gas in [5]. We use the same method in the present paper.

In the discussion of the caloric curves, we shall only consider stable states. An equilibrium state that is a local, but not a global, extremum of the relevant thermodynamical potential (entropy in the microcanonical ensemble and free energy in the canonical ensemble) is said to be metastable. A global extremum of the thermodynamical potential is said to be fully stable. For systems with short-range interactions, metastable states have a short lifetime so that the caloric curve should contain only fully stable states. However, for systems with long-range interactions, the metastable states have a very long lifetime scaling as e^N which is usually much longer than the age of the Universe. As a result, metastable states can be as much, or even more, relevant than fully stable states [4]. The selection between a fully stable state or a metastable state depends on the initial condition and on a notion of basin of attraction. In this paper, we shall not distinguish between metastable and fully stable states. The physical caloric curve should contain all types of stable equilibrium states.¹³

For real systems, that are not in a box, the natural

¹² The binding energy is usually defined as $E_b = Nmc^2 - Mc^2$. Here, for convenience, we define it with the opposite sign, i.e., $E = Mc^2 - Nmc^2$. In the Newtonian limit, $M \simeq Nm$ and E reduces to the usual energy $E = K + W$ which is the sum of the kinetic and potential (gravitational) energies.

¹³ The existence, or nonexistence, of fully stable states for self-gravitating fermions in general relativity is an interesting problem by itself but it will not be considered in the present paper (see the Remark at the end of Sec. V C showing that this problem is not trivial).

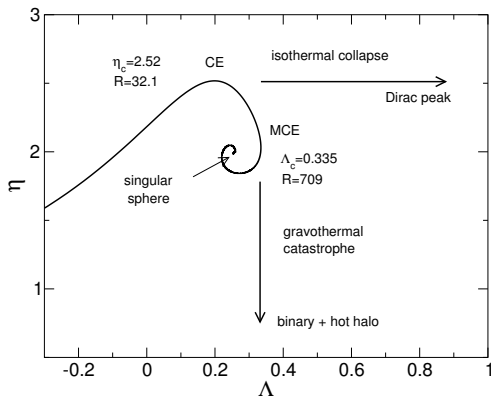


FIG. 1: Caloric curve of the nonrelativistic classical self-gravitating gas.

evolution proceeds along the series of equilibria towards larger and larger density contrasts.¹⁴ In general, this corresponds to lower and lower temperatures and energies.¹⁵ Therefore, in the discussion of the caloric curves, we shall describe the evolution of the system starting from high energies and high temperatures, and reducing the temperature and the energy until an instability takes place.

IV. PARTICULAR LIMITS

In this section, we briefly recall well-known results that correspond to particular limits of the general relativistic Fermi gas.

A. The nonrelativistic + classical limit

The thermodynamics of a nonrelativistic classical self-gravitating gas has been studied in detail in [2, 3, 53, 56, 57]. The caloric curve $\eta(\Lambda)$ forms a spiral (see Fig. 1). In the microcanonical ensemble, there is no equilibrium state below a critical energy E_c corresponding to $\Lambda_c = 0.335$. In that case, the system undergoes a

¹⁴ The reason is that, for real systems (globular clusters, dark matter halos...) such as those described by the King model, the Boltzmann or Fermi-Dirac entropy (resp. the Boltzmann or Fermi-Dirac free energy) increases (resp. decreases) with the concentration parameter; see Fig. 5 of [55] and Fig. 46 of [14]. Note that, surprisingly, for box-confined systems this is the opposite; see Fig 3 of [41].

¹⁵ This is explicitly shown in Figs. 12 and 15 below. Note that this result is valid only for mid and low energies and temperatures. At very high energies and temperatures, where the system behaves as a self-gravitating radiation, the density contrast increases with the energy and the temperature (see Figs. 2 and 3 of [7]) implying that the natural evolution of the system is towards higher and higher energies and temperatures. This situation has been discussed in [7] and will not be considered here.

gravothermal catastrophe (core collapse) leading to a binary star surrounded by a hot halo [55, 58, 59]. In the canonical ensemble, there is no equilibrium state below a critical temperature T_c , corresponding to $\eta_c = 2.52$. In that case, the system undergoes an isothermal collapse leading to a Dirac peak containing all the mass [60].

B. The nonrelativistic limit

The thermodynamics of the nonrelativistic self-gravitating Fermi gas has been studied in detail in [5]. It is shown that the caloric curves $\eta(\Lambda)$ depend on a single control parameter (it should not be confused with the chemical potential):

$$\mu = \eta_0 \sqrt{512\pi^4 G^3 N m R^3}, \quad \eta_0 = \frac{g m^4}{h^3}. \quad (17)$$

It can be written as [5]:

$$\mu = 17.3 \left(\frac{R}{R_0} \right)^{3/2}, \quad R_0 = 0.181 \frac{h^2}{G m^{8/3} g^{2/3} M^{1/3}}, \quad (18)$$

or as

$$\mu = 17.3 \left(\frac{M}{M_0} \right)^{1/2}, \quad M_0 = 5.97 \times 10^{-3} \frac{h^6}{G^3 m^8 g^2 R^3}, \quad (19)$$

where R_0 (resp. M_0) is the radius (resp. mass) of a fermion star of mass M (resp. radius R) at $T = 0$ (see Appendix F). Introducing the normalized variables of Appendix B, this parameter becomes

$$\mu = \frac{4\sqrt{2}}{\pi} (NR^3)^{1/2}. \quad (20)$$

Some caloric curves are represented in Fig. 2. They display a canonical critical point at $\mu_{CCP} = 83$ and a microcanonical critical point at $\mu_{MCP} = 2670$. When $\mu < \mu_{CCP} = 83$ there is no phase transition. When $\mu_{CCP} = 83 < \mu < \mu_{MCP} = 2670$ the system displays zeroth and first order canonical phase transitions. When $\mu > \mu_{MCP} = 2670$ the system displays zeroth and first order canonical and microcanonical phase transitions. When $\mu \rightarrow +\infty$ we recover the caloric curve of the nonrelativistic classical self-gravitating gas (spiral) represented in Fig. 1. When $\mu < +\infty$ there is a statistical equilibrium state for any accessible value of energy and temperature. The gravitational collapse of the nonrelativistic classical self-gravitating gas (gravothermal catastrophe in the microcanonical ensemble and isothermal collapse in the canonical ensemble) is prevented by quantum mechanics (Pauli's exclusion principle).

For a given box radius, the nonrelativistic canonical phase transition appears when

$$N > N_{CCP}(R) \equiv \left(\frac{\pi \mu_{CCP}}{4\sqrt{2}} \right)^2 \frac{1}{R^3} = \frac{2125}{R^3}. \quad (21)$$

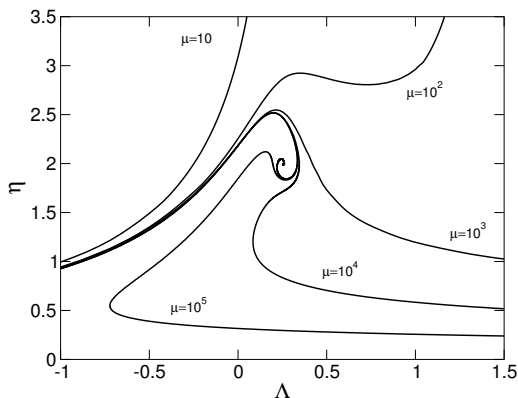


FIG. 2: Caloric curves of the nonrelativistic self-gravitating Fermi gas for different values of $\mu = (4\sqrt{2}/\pi)(NR^3)^{1/2}$.

If we consider the general relativistic problem, we must require $N \ll N_{OV}$, where $N_{OV} = 0.39853$ is the OV limit, for the validity of the nonrelativistic treatment. Therefore, we will see the nonrelativistic canonical phase transition for $N_{CCP}(R) < N \ll N_{OV}$ provided that

$$R \gg R_{CCP}^{\text{approx.}} \equiv \left(\frac{\pi \mu_{CCP}}{4\sqrt{2}} \right)^{2/3} \frac{1}{N_{OV}^{1/3}} = 17.5. \quad (22)$$

In comparison $R_{OV} = 3.3569$. This argument just provides an order of magnitude of the radius R_{CCP} above which a canonical phase transition appears for $N > N_{CCP}(R)$. By solving the general relativistic equations, we find that the exact value is $R_{CCP}^{\text{exact}} = 12.0$ (see Sec. X).

For a given box radius, the nonrelativistic microcanonical phase transition appears when

$$N > N_{MCP}(R) \equiv \left(\frac{\pi \mu_{MCP}}{4\sqrt{2}} \right)^2 \frac{1}{R^3} = \frac{2.20 \times 10^6}{R^3}. \quad (23)$$

If we consider the general relativistic problem, using the same argument as before, we will see the nonrelativistic microcanonical phase transition for $N_{MCP}(R) < N \ll N_{OV}$ provided that

$$R \gg R_{MCP}^{\text{approx.}} \equiv \left(\frac{\pi \mu_{MCP}}{4\sqrt{2}} \right)^{2/3} \frac{1}{N_{OV}^{1/3}} = 177. \quad (24)$$

This argument just provides an order of magnitude of the radius R_{MCP} above which a microcanonical phase transition appear for $N > N_{MCP}(R)$. By solving the general relativistic equations, we find that the exact value is $R_{MCP}^{\text{exact}} = 92.0$ (see Sec. X).

C. The classical limit

The thermodynamics of a classical self-gravitating gas in general relativity has been studied in detail in Refs.

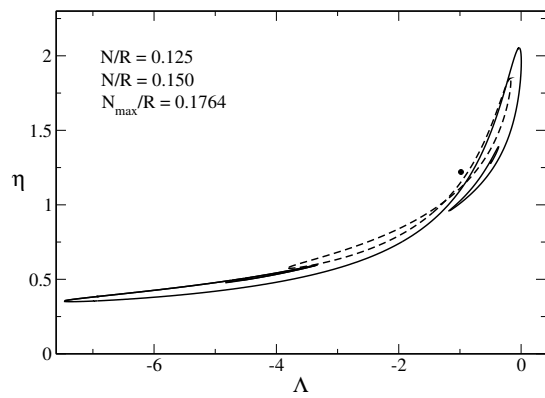


FIG. 3: Caloric curves of the classical self-gravitating gas in general relativity for different values of $\nu = N/R$.

[61] and [7]. This corresponds to the nondegenerate limit of the general relativistic Fermi gas. It is shown that the caloric curves $\eta(\Lambda)$ depend on a single control parameter

$$\nu = \frac{GNm}{Rc^2}. \quad (25)$$

It can be written as

$$\nu = \frac{R_S^*}{2R}, \quad R_S^* = \frac{2GNm}{c^2}, \quad (26)$$

or as

$$\nu = \frac{N}{2N_S^*}, \quad N_S^* = \frac{Rc^2}{2Gm}, \quad (27)$$

where R_S^* can be interpreted as a sort of Schwarzschild radius defined with the rest mass Nm instead of the mass M (reciprocally, N_S^*m is a sort of Schwarzschild rest mass of an object of radius R). Introducing the normalized variables of Appendix B this parameter becomes

$$\nu = \frac{N}{R}. \quad (28)$$

Some caloric curves are represented in Fig. 3. When $\nu \rightarrow 0$ ($N \ll N_S^*$ or $R \gg R_S^*$), we recover the caloric curve of the nonrelativistic classical self-gravitating gas (spiral) represented in Fig. 1. When $0 < \nu < \nu'_S = 0.128$ the caloric curve has the form of a double spiral exhibiting a collapse at low energies and low temperatures (cold spiral) and at high energies and high temperatures (hot spiral).¹⁶ When $\nu'_S = 0.128 < \nu < \nu_S = 0.1415$ the two spirals are amputated (truncated) and touch each other. When $\nu_S = 0.1415 < \nu < \nu_{\text{max}} = 0.1764$ the two spirals disappear and the caloric curve makes a loop resembling

¹⁶ The hot spiral corresponds to an ultrarelativistic classical gas [61] which is similar to a form of radiation described by an equation of state $P = \epsilon/3$ [62–64] (see [7] for a detailed discussion).

to the symbol “ ∞ ”. As ν increases, the loop shrinks more and more and, when $\nu = \nu_{\max} = 0.1764$, it reduces to a point located at $(\Lambda_*, \eta_*) = (-0.9829, 1.2203)$. When $\nu > \nu_{\max} = 0.1764$, no equilibrium state is possible.

For a given box radius, the spirals touch each other when

$$N > N'_S(R) = \nu'_S R = 0.128 R \quad (29)$$

and they form a loop when

$$N > N_S(R) = \nu_S R = 0.1415 R. \quad (30)$$

The caloric curve reduces to a point when

$$N = N_{\max}(R) = \nu_{\max} R = 0.1764 R. \quad (31)$$

If we consider the truly quantum problem, we must require $N \gg N_{\text{OV}} = 0.39853$ for the validity of the classical (nondegenerate) treatment. Therefore, we will see the double spiral and its evolution described previously for $N_{\text{OV}} \ll N < N_{\max}$ provided that

$$R \gg \frac{N_{\text{OV}}}{\nu_{\max}} = 2.259. \quad (32)$$

We note that $N_{\text{OV}}/\nu_{\max} = 2.259$ is of the order of $R_{\text{OV}} = 3.3569$.

Remark: For a given box radius R , coming back to dimensional variables, equilibrium states exist only when $N \leq N_{\max}(R) = 0.1764 Rc^2/Gm = 0.3528 N_S^*$. Inversely, for a given number of particles N , equilibrium states exist only when $R \geq R_{\min}(N) = 5.669 GNm/c^2 = 2.834 R_S^*$. The nonrelativistic limit corresponds to $N \ll N_{\max}(R) \sim Rc^2/2Gm \sim N_S^*$ or $R \gg R_{\min}(N) \sim 2GNm/c^2 \sim R_S^*$. These results are valid in the classical limit. For small systems, quantum effects will come into play. If we argue that $N_{\max} = \nu_{\max} Rc^2/Gm \sim N_{\text{OV}}$ when $R \sim R_{\text{OV}}$, or equivalently $R_{\min} = GNm/\nu_{\max} c^2 \sim R_{\text{OV}}$ when $N \sim N_{\text{OV}}$, we find that $\nu_{\max} \sim GN_{\text{OV}}m/R_{\text{OV}}c^2 \sim 0.1187$. This may justify the order of magnitude of this constant. Alternatively, we may just remark that $\nu_{\max} = GN_{\max}m/Rc^2 = 0.1764$ is of the same order as $GN_{\text{OV}}m/R_{\text{OV}}c^2 = 0.1187$.

D. Summary

Before treating the general case, let us summarize the previous results.

Nonrelativistic + classical limit. For a given box radius R and particle number N the system undergoes a catastrophic collapse towards a singularity at low temperatures in the canonical ensemble and at low energies in the microcanonical ensemble.

Nonrelativistic limit. For a given box radius R there is no phase transition when $N < N_{\text{CCP}}(R)$, the system can undergo a canonical phase transition when $N_{\text{CCP}}(R) < N < N_{\text{MCP}}(R)$, and the system can undergo a canonical and a microcanonical phase transition

when $N > N_{\text{MCP}}(R)$. For a given particle number N , there is no phase transition when $R < R_{\text{CCP}}(N)$, the system can undergo a canonical phase transition when $R_{\text{CCP}}(N) < R < R_{\text{MCP}}(N)$, and the system can undergo a canonical and a microcanonical phase transition when $R > R_{\text{MCP}}(N)$. Here, $R_{\text{CCP}}(N) = 12.9/N^{1/3}$ and $R_{\text{MCP}}(N) = 130/N^{1/3}$ are the reciprocal of $N_{\text{CCP}}(R) = 2125/R^3$ and $N_{\text{MCP}}(R) = 2.20 \times 10^6/R^3$. There is an equilibrium state at all temperatures $T \geq 0$ in the canonical ensemble and at all accessible energies $E \geq E_{\min}$ (where E_{\min} is the energy of the ground state) in the microcanonical ensemble.

Classical limit. For a given box radius R , the caloric curve has the form of a double spiral when $N < N'_S(R)$, the spirals touch each other when $N'_S(R) < N < N_S(R)$, the caloric curve makes a loop when $N_S(R) < N < N_{\max}(R)$, and there is no equilibrium state when $N > N_{\max}(R)$. For a given particle number N , the caloric curve has the form of a double spiral when $R > R'_S(N)$, the spirals touch each other when $R_S(N) < R < R'_S(N)$, the caloric curve makes a loop when $R_{\min}(N) < R < R_S(N)$, and there is no equilibrium state when $R < R_{\min}(N)$. Here, $R'_S(N) = 7.81 N$, $R_S(N) = 7.07 N$ and $R_{\min}(N) = 5.67 N$ are the reciprocal of $N'_S(R) = 0.128 R$, $N_S(R) = 0.1415 R$ and $N_{\max}(R) = 0.1764 R$. The system undergoes a catastrophic collapse towards a singularity at both low and high temperatures in the canonical ensemble and at both low and high energies in the microcanonical ensemble.

V. THE CASE $R_{\text{CCP}} < R < R_{\text{MCP}}$

In this section, we study the general relativistic Fermi gas in the case $R_{\text{CCP}} = 12.0 < R < R_{\text{MCP}} = 92.0$ where only a canonical phase transition may occur (see Fig. 47 below). For illustration, we select $R = 50$. For this value of R , the canonical phase transition occurs above $N_{\text{CCP}} = 0.0170$.

A. The case $N < N_{\text{CCP}}$

In Fig. 4 we have plotted the caloric curve for $N < N_{\text{CCP}} = 0.0170$. Since $N \ll N_{\text{OV}} = 0.39853$, this caloric curve coincides with the one obtained in the nonrelativistic limit [5] except at very high energies and very high temperatures (see the Remark at the end of this section).¹⁷

The series of equilibria $\eta(\Lambda)$ is monotonic. According to the Poincaré theory of linear series of equilibria, all

¹⁷ As discussed in Sec. XI the nonrelativistic limit corresponds to $N \rightarrow 0$ and $R \rightarrow +\infty$ in such a way that NR^3 is fixed (in more physical terms $N \ll N_{\text{OV}}$ and $R \gg R_{\text{OV}}$ with NR^3 fixed).

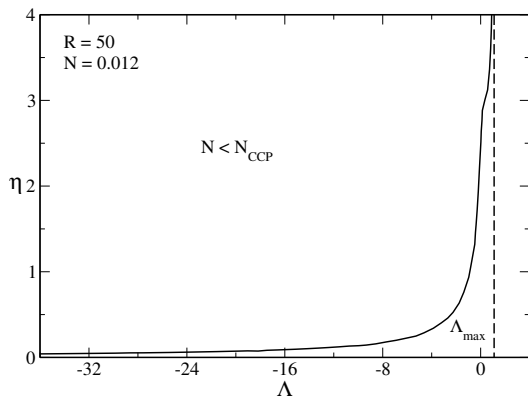


FIG. 4: Caloric curve for $N < N_{\text{CCP}} = 0.0170$ (specifically $R = 50$ and $N = 0.012$).

the equilibrium states are stable. The statistical ensembles (microcanonical and canonical) are equivalent. The caloric curve presents the following features:

- (i) There is no phase transition and no gravitational collapse.
- (ii) The specific heat is always positive. The entropy versus energy curve (not represented) is concave.

The evolution of the system is the following. At high energies and high temperatures, the system is nondegenerate (Boltzmannian). As the energy and the temperature are reduced, the system becomes more and more centrally condensed. At intermediate energies and intermediate temperatures, the Fermi gas is partially degenerate (see Appendix D). At $T = 0$, the Fermi gas is completely degenerate. This cold nonrelativistic fermion ball, equivalent to a polytrope of index $n = 3/2$, is similar to a nonrelativistic white dwarf. This is the state of minimum energy E_{min} (ground state). Since there is a stable equilibrium state at $T = 0$ (i.e. $\eta \rightarrow +\infty$) with a finite energy E_{min} , the caloric curve $\eta(\Lambda)$ presents a vertical asymptote at $\Lambda = \Lambda_{\text{max}}$.¹⁸

Remark: At very high energies and very high temperatures, the system is relativistic even though $N \ll N_{\text{OV}}$. In that case, we recover the hot spiral studied in [7, 61]. As a result, the complete caloric curve of the general relativistic Fermi gas presents a region of negative specific heat and a region of ensemble inequivalence at very high energies and very high temperatures. The system undergoes a gravitational collapse above E_{max} in the microcanonical ensemble and above T_{max} in the canonical ensemble. We note that quantum mechanics cannot prevent such a gravitational collapse since it takes place at

¹⁸ In the nonrelativistic limit $\Lambda_{\text{max}} = 0.0950N^{1/3}R$ (see Appendix F). More generally, a complete characterization of the ground state of the self-gravitating Fermi gas, in the nonrelativistic and relativistic regimes, taking into account the presence of the box is given in [6].

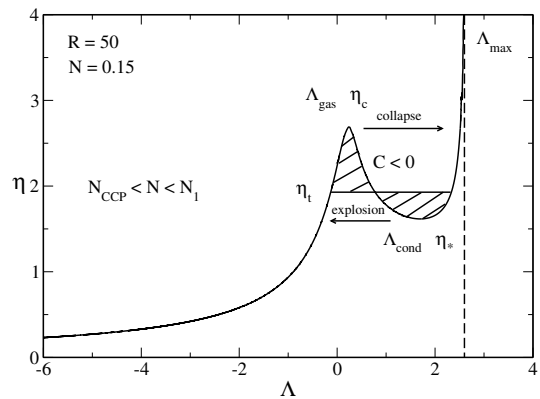


FIG. 5: Caloric curve for $N_{\text{CCP}} = 0.0170 < N < N_1 = 0.18131$ (specifically $R = 50$ and $N = 0.15$).

very high energies and very high temperatures where the system is nondegenerate. As a result, the system is expected to collapse towards a black hole. For $N \rightarrow 0$, it is shown in [7] that $\Lambda_{\text{min}} \sim -0.246/N^2 \rightarrow -\infty$ and $\eta_{\text{min}} \sim 18.3N^2 \rightarrow 0$ so that the hot spiral is rejected at infinity.¹⁹ For small values of N ($N \ll N_{\text{max}}$) the hot spiral occurs at very negative values of Λ and at very small values of η . This is why we do not see it in Fig. 4 (it is outside of the frame since $\Lambda_{\text{min}} \simeq -1708$ and $\eta_{\text{min}} \simeq 2.63 \times 10^{-3}$). The hot spiral becomes visible only for larger values of N ($N \lesssim N_{\text{max}}$) as in Fig. 22 below. In this paper, we shall not discuss the hot spiral specifically since it has been described in detail in [7, 61].

B. The case $N_{\text{CCP}} < N < N_1$

In Fig. 5 we have plotted the caloric curve for $N_{\text{CCP}} = 0.0170 < N < N_1 = 0.18131$. Since $N \ll N_{\text{OV}} = 0.39853$, the caloric curve coincides with the one obtained in the nonrelativistic limit [5]. The novelty with respect to the previous case is that the caloric curve has a N -shape structure leading to canonical phase transitions and ensembles inequivalence. This N -shape structure appears at $N = N_{\text{CCP}} = 0.0170$ where the caloric curve presents a horizontal inflexion point. Let us consider the microcanonical and canonical ensembles successively (see [5] for a more detailed discussion).

1. Microcanonical ensemble

The curve $\eta(\Lambda)$ is univalued. According to the Poincaré theory, the whole series of equilibria is stable. The caloric curve presents the following features:

¹⁹ In terms of dimensional variables this corresponds to $E_{\text{max}} \rightarrow 0.24631Rc^4/G$ and $k_B T_{\text{max}} \sim 0.0547Rc^4/NG$.

(i) There is no phase transition and no gravitational collapse.

(ii) There is a region of negative specific heats between Λ_{gas} and Λ_{cond} . In this range of intermediate energies the system is purely self-gravitating, i.e., it almost does not feel the quantum pressure (Pauli exclusion principle) nor the pressure of the box. The negative specific heat leads to a convex intruder (dip) in the entropy versus energy curve (see Fig. 25 of [5]).

The evolution of the system in the microcanonical ensemble is the following. Let us start from high energy states and decrease the energy. At high energies, the system is almost homogeneous. As energy decreases, and especially when we enter in the region of negative specific heats, the system becomes more and more concentrated and partially degenerate. At the minimum energy E_{min} (ground state) the system is completely degenerate. There is no phase transition, just a progressive clustering of the system until the ground state is reached.

2. Canonical ensemble

The curve $\Lambda(\eta)$ is multivalued leading to the possibility of phase transitions in the canonical ensemble. The left branch up to η_c corresponds to the gaseous phase and the right branch after η_* corresponds to the condensed phase. According to the Poincaré turning point criterion, these equilibrium states are stable while the equilibrium states on the intermediate branch between η_c and η_* are unstable. These equilibrium states have a core-halo structure (see below) and a negative specific heat. This is a sufficient (but not necessary) condition of instability in the canonical ensemble. The caloric curve presents the following features:

(i) When $\eta < \eta_*$ there are only gaseous states. When $\eta > \eta_c$ there are only condensed states. When $\eta_* < \eta < \eta_c$ there exist gaseous and condensed states at the same temperature. A first order phase transition is expected at a transition temperature η_t determined by the Maxwell construction (see Fig. 5) or by the equality of the free energy of the gaseous and condensed phases (see Fig. 28 of [5]). When $\eta_* < \eta < \eta_t$ the gaseous states have a lower free energy than the condensed states. When $\eta_t < \eta < \eta_c$ the condensed states have a lower free energy than the gaseous states. However, the first order phase transition does not take place in practice because of the very long lifetime of the metastable states.

(ii) There is a zeroth order phase transition at η_c from the gaseous phase to the condensed phase. It corresponds to a gravitational collapse (isothermal collapse) ultimately halted by quantum degeneracy.

(iii) There is a zeroth order phase transition at η_* from the condensed phase to the gaseous phase. It corresponds to an explosion ultimately halted by the boundary of the box.

The evolution of the system in the canonical ensemble is the following. Let us start from high temperature

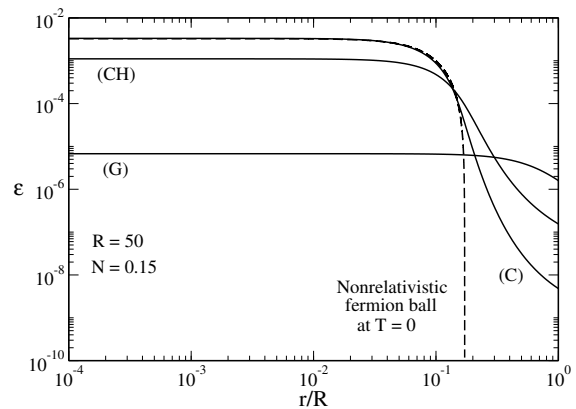


FIG. 6: Energy density profiles of gaseous, core-halo and condensed states at $\eta = \eta_t$ (specifically $\eta_t = 1.9285$). The dashed line represents the density profile of a nonrelativistic fermion ball at $T = 0$ (similar to a nonrelativistic white dwarf).

states and decrease the temperature. At high temperatures the system is in the gaseous phase. At $\eta = \eta_t$, the system is expected to undergo a first order phase transition from the gaseous phase to the condensed phase. However, in practice, this phase transition does not take place because the metastable gaseous states have a very long lifetime. At $\eta = \eta_c$ the system collapses towards the condensed phase. Complete gravitational collapse is prevented by quantum mechanics. The system reaches an equilibrium state similar to a nonrelativistic white dwarf (fermion ball). If we now increase the temperature the system remains in the condensed phase until the point η_* (again, the first order phase transition expected at η_t does not take place because the metastable condensed states have a very long lifetime) at which it explodes and returns to the gaseous phase. We have thus described an hysteretic cycle in the canonical ensemble [5].

3. Density profiles

In Fig. 6 we have plotted the density profiles of the gaseous (G), core-halo (CH) and condensed (C) states at the transition point η_t . We note that the energy density is very low confirming that we are in the nonrelativistic regime.

(i) In the gaseous phase (high energies and high temperatures), quantum mechanics is negligible and the density profile is dilute. The equilibrium state results from the competition between the gravitational attraction and the thermal pressure. The gaseous equilibrium state (G) is almost uniform because the temperature is high so that the thermal pressure overcomes the gravitational attraction. In that case, the gas is held by the walls of the box.

(ii) In the condensed phase (low energies and low temperatures), thermal effects are negligible and the density

profile is very compact. The equilibrium state results from the competition between the gravitational attraction and the quantum pressure arising from the Pauli exclusion principle. The condensed equilibrium state (C) almost coincides with a nonrelativistic fermion ball at $T = 0$ containing all the mass (see [5] and Appendix E 2 a). It is similar to a nonrelativistic white dwarf corresponding to a polytrope $n = 3/2$. In that case, gravitational collapse is prevented by quantum mechanics and the confining box is not necessary. At small but finite temperatures, we see in Fig. 6 that the dashed line corresponding to a polytrope $n = 3/2$ provides a good fit to the core of the distribution. There is a small isothermal atmosphere that becomes thinner and thinner as the temperature is reduced.

(iii) The intermediate state (CH) has a sort of core-halo structure with a degenerate core and an isothermal atmosphere. The equilibrium state results from the competition between the gravitational attraction, the thermal pressure, and the quantum pressure. The pressure of the box and the quantum pressure have a weak effect on the equilibrium of the system so it essentially behaves as a self-gravitating isothermal gas. This is why it presents a negative specific heat.

Let us recall that these three equilibrium states have the same temperature but different energies. The core-halo state (CH) is unstable in the canonical ensemble while it is stable in the microcanonical ensemble. It lies in a region of negative specific heats. The gaseous and condensed states (G) and (C) are stable in both ensembles.

C. The case $N_1 < N < N_{OV}$

In Fig. 7 we have plotted the caloric curve for $N_1 = 0.18131 < N < N_{OV} = 0.39853$. The novelty with respect to the previous case is the existence of a secondary branch presenting an asymptote at Λ'_{max} . This secondary branch appears suddenly at $N = N_1 = 0.18131$ (at that point $\Lambda'_{max} = -0.536 R$ and $\Lambda_{max} = 0.0570 R$). As detailed in [6], for $N_1 < N < N_{OV}$, there exists another equilibrium state at $T = 0$ (i.e. $\eta \rightarrow +\infty$) corresponding to a completely degenerate fermion ball distinct from the ground state. This secondary equilibrium state is unstable.²⁰ Its mass is larger than the mass of the stable ground state so that $\Lambda'_{max} \leq \Lambda_{max}$. According to the Poincaré theory, all the configurations of the secondary

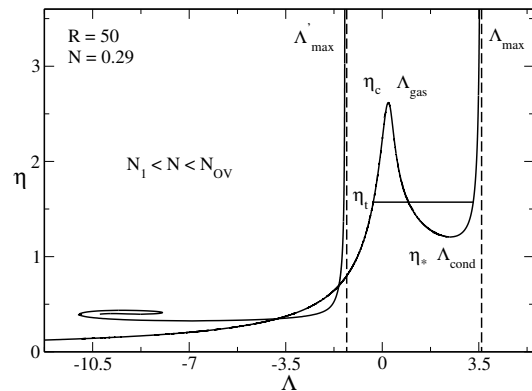


FIG. 7: Caloric curve for $N_1 = 0.18131 < N < N_{OV} = 0.39853$ (specifically $R = 50$ and $N = 0.29$).

branch are unstable.²¹ Therefore, the presence of this secondary branch does not qualitatively change the description of the caloric curve made in Sec. V B.

However, for $N > N_1$, relativistic effects start to become important. This has some consequences on the interpretation of the density profiles. In Fig. 8 we have plotted the different density profiles at η_t . We see that the energy density is low for the gaseous state (G) and for the core-halo state (CH) indicating that we are in the nonrelativistic regime. By contrast, the energy density is relatively high for the stable condensed state (C) and for the unstable condensed state (U) indicating that we are in the relativistic regime. The condensed states almost coincide with a general relativistic fermion ball at $T = 0$ containing all the mass (see Appendix E 2 a). They are similar to stable and unstable neutron stars [49]. At small but finite temperatures, we see in Fig. 8 that the dashed line obtained from the OV theory provides a good fit to the core of the distribution. There is a small atmosphere (containing a little mass) that becomes thinner and thinner as the temperature is reduced.

Remark: In Fig. 7, when the temperature is low enough, we find four solutions. The solutions (G) and (C) are stable (local minima of free energy) while the solutions (CH) and (U) are unstable (saddle points of free energy). Since we have an even number of extrema, this suggests that there is no global minimum of free energy (naively, this results from simple topological arguments if we plot a curve $f(x)$ with two minima and two maxima). The stable equilibrium state with the lowest value of free energy may be only metastable, not fully stable. This is consistent with the result of Zel'dovich [65] who showed that, at $T = 0$, the OV equilibrium states are only metastable. In Fig. 5, when $\eta_* < \eta < \eta_c$, we find

²⁰ Actually, for $N > N_1$, there can exist several unstable equilibrium states at $T = 0$ (up to an infinity) that have more and more modes of instability. They are related to the spiral structure of the mass-radius relation of the general relativistic Fermi gas at $T = 0$ [6, 9]. They give rise to additional branches (with vertical asymptotes) in the caloric curve. We shall not consider these unstable solutions here, except for the less unstable one already mentioned.

²¹ The spiral present on the left of this secondary branch will ultimately become the cold spiral of Refs. [7, 61] when N will be sufficiently large (see below).

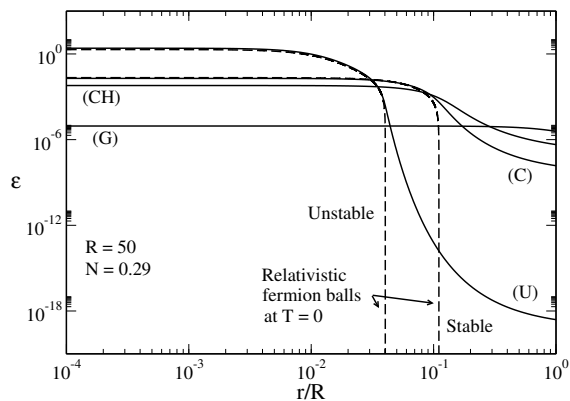


FIG. 8: Density profiles of gaseous, core-halo and (stable and unstable) condensed states at $\eta = \eta_t$ (specifically $\eta_t = 1.5722$). The dashed lines represent the density profiles of stable and unstable general relativistic fermion balls at $T = 0$ (similar to neutron stars).

three solutions. The solutions (G) and (C) are stable (local minima of free energy) while the solution (CH) is unstable (saddle point of free energy). Since we have an odd number of extrema, this suggests that the solution with the lowest value of free energy is a global minimum. This is the case in Newtonian gravity [5]. However, this is not quite clear in general relativity since the result of Zel'dovich [65] still applies for $N < N_1$. Therefore, the existence of a global minimum of free energy (fully stable state) in general relativity is not trivial and would require a more careful study. Anyway, for practical purposes, metastable states are very relevant (possibly more relevant than fully stable states) so we shall determine all types of stable equilibrium states, disregarding whether they are fully stable or just metastable.

D. The case $N_{OV} < N < N_e$

In Fig. 9 we have plotted the caloric curve for $N_{OV} = 0.39853 < N < N_e = 0.40002$. The novelty with respect to the previous case is that the two branches have merged. The merging occurs at $N = N_{OV}$ at which the two asymptotes Λ'_{max} and Λ_{max} coincide (at that point $\Lambda_{max} = \Lambda'_{max} = 0.08985R$). This is the highest value of N at which there exist an equilibrium state at $T = 0$ (ground state). When $N > N_{OV}$ there is no equilibrium state at $T = 0$ (no ground state) anymore [49]. In that case, the caloric curve presents a turning point of temperature at η'_c and a turning point of energy at Λ'_c . As a result, there is no equilibrium state at $\eta > \eta'_c$ in the canonical ensemble, i.e., below a critical temperature. Similarly, there is no equilibrium state at $\Lambda > \Lambda'_c$ in the microcanonical ensemble, i.e., below a critical energy. This means that when the system becomes strongly relativistic (i.e. when $N > N_{OV}$) quantum mechanics is not able to prevent gravitational collapse at low temperatures

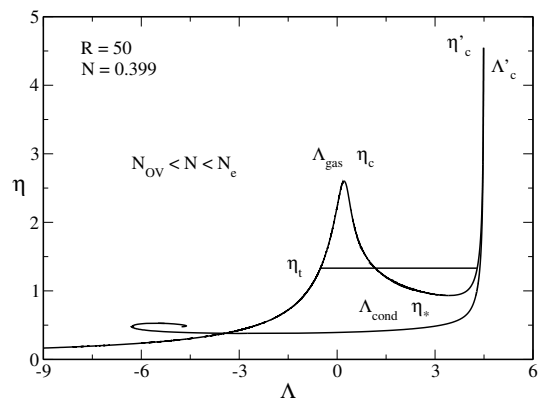


FIG. 9: Caloric curve for $N_{OV} = 0.39853 < N < N_e = 0.40002$ (specifically $R = 50$ and $N = 0.399$).

and low energies. This is a generalization of the result first obtained at $T = 0$ by Oppenheimer and Volkoff [49] in the context of neutron stars.

1. Microcanonical ensemble

Let us first consider the microcanonical ensemble. The curve $\eta(\Lambda)$ is multivalued. According to the Poincaré turning point criterion, the series of equilibria is stable up to Λ'_c and then becomes unstable. The caloric curve presents the following features:

- (i) There is no phase transition (there is only one stable equilibrium state for each $\Lambda < \Lambda'_c$).
- (ii) There are two regions of negative specific heats, one between Λ_{gas} and Λ_{cond} (as before) and another one between Λ'_{gas} (the energy corresponding to η'_c) and Λ'_c . We note that this second region of negative specific heats is extremely tiny. In Fig. 10 we clearly see the convex intruder (dip) associated with the first region of specific heat. The convex intruder associated with the second region of specific heat is imperceptible.

- (iii) There is a catastrophic collapse at Λ'_c towards a black hole.²²

In Fig. 11 we have plotted the relation $\Lambda(\Phi_0)$ between the normalized energy and the central potential. We can see that Φ_0 increases monotonically along the series of equilibria. The curve $\Lambda(\Phi_0)$ presents a peak at Λ'_c then displays damped oscillations. These oscillations correspond to the unstable equilibrium states forming the spiral of the caloric curve.

In Fig. 12 we have plotted the relation $\Lambda(\mathcal{R})$ between

²² For simplicity, when there is no equilibrium state, we shall say that the system forms a black hole. Actually, as discussed in Paper II, it is not completely clear that the system will always form a black hole in that case. We leave this interesting problem open to future works.

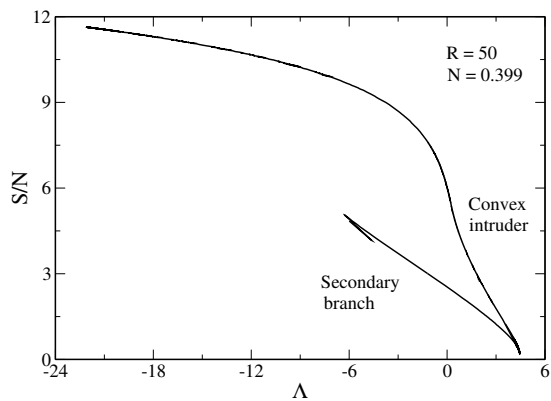


FIG. 10: Entropy per fermion as a function of the normalized energy for $N_{OV} < N < N_e$ (specifically $R = 50$ and $N = 0.399$). We can check that the unstable equilibrium states (saddle points of entropy) have an entropy lower than the stable equilibrium states (entropy maxima).

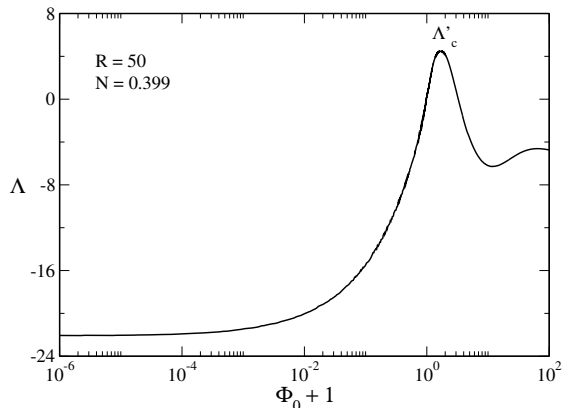


FIG. 11: Normalized energy as a function of the central potential Φ_0 for $N_{OV} < N < N_e$ (specifically $R = 50$ and $N = 0.399$).

the normalized energy and the energy density contrast $\mathcal{R} = \epsilon_0/\epsilon_R$. We can see that \mathcal{R} increases monotonically along the series of equilibria up to Λ'_c . Then, on the unstable branch, it displays a more complicated behavior.

The evolution of the system in the microcanonical ensemble is the following. Let us start from high energy states and decrease the energy. As energy decreases, the system becomes more and more concentrated. The central potential and the density contrast increase. If we keep decreasing the energy there comes a point E'_c at which the system undergoes a gravitational collapse towards a black hole. This is an instability of general relativistic origin which has no counterpart in the Newtonian theory.

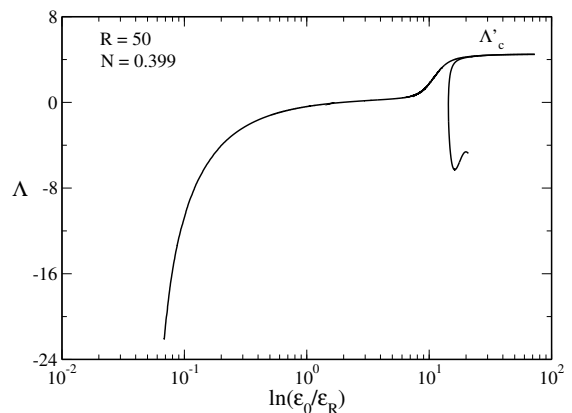


FIG. 12: Normalized energy as a function of the energy density contrast $\mathcal{R} = \epsilon_0/\epsilon_R$ for $N_{OV} < N < N_e$ (specifically $R = 50$ and $N = 0.399$).

2. Canonical ensemble

We now consider the canonical ensemble. The function $\Lambda(\eta)$ is multivalued. According to the Poincaré turning point criterion, the series of equilibria is stable up to η_c , becomes unstable between η_c and η_* , is stable again between η_* and η'_c and becomes unstable again after η'_c . The caloric curve presents the following features:

(i) When $\eta < \eta_*$ there are only gaseous states. When $\eta_c < \eta < \eta'_c$ there are only condensed states. When $\eta_* < \eta < \eta_c$ there exist gaseous and condensed states at the same temperature. A first order phase transition is expected at a transition temperature η_t determined by the Maxwell construction (see Fig. 9) or by the equality of the free energy of the gaseous and condensed phases (see Fig. 13). When $\eta_* < \eta < \eta_t$ the gaseous states have a lower free energy than the condensed states. When $\eta_t < \eta < \eta_c$ the condensed states have a lower free energy than the gaseous states. However, the first order phase transition does not take place in practice because of the very long lifetime of the metastable states.

(ii) There is a zeroth order phase transition at η_c from the gaseous phase to the condensed phase. It corresponds to a gravitational collapse (isothermal collapse) ultimately halted by quantum degeneracy.

(iii) There is a zeroth order phase transition at η_* from the condensed phase to the gaseous phase. It corresponds to an explosion ultimately halted by the boundary of the box.

(iv) There is a catastrophic collapse at η'_c from the condensed phase to a black hole.

In Fig. 14 we have plotted the relation $\eta(\Phi_0)$ between the inverse temperature and the central potential. We see that Φ_0 increases monotonically along the series of equilibria. The curve $\eta(\Phi_0)$ presents a first peak at η_c and a second peak at η'_c . Then, it displays damped oscillations. They correspond to unstable equilibrium states associated with the spiral of the caloric curve.

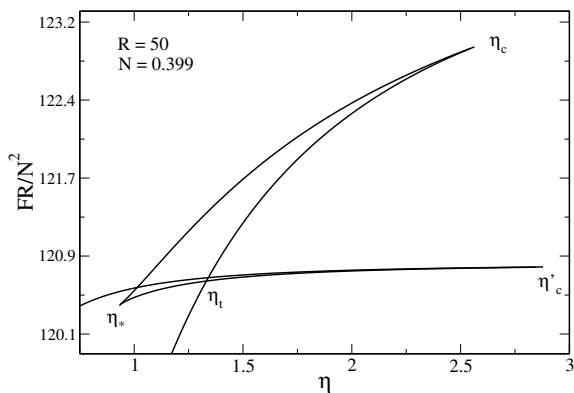


FIG. 13: Normalized free energy as a function of the normalized inverse temperature for $N_{OV} < N < N_e$ (specifically $R = 50$ and $N = 0.399$). The first derivative of βF with respect to β is discontinuous at the transition temperature β_t . This corresponds to a first order phase transition, connecting the gaseous phase to the condensed phase, which is associated with a jump of energy $E = \partial(\beta F)/\partial\beta$ in the caloric curve. On the other hand, βF is discontinuous at the spinodal points η_c and η_* . This corresponds to zeroth order phase transitions which are associated with a jump of free energy. We can check that the unstable equilibrium states (saddle points of free energy) between η_c and η_* have a free energy higher than the stable equilibrium states (minima of free energy). However, the unstable equilibrium states after η'_c can have a free energy lower than the stable equilibrium states before η_c .

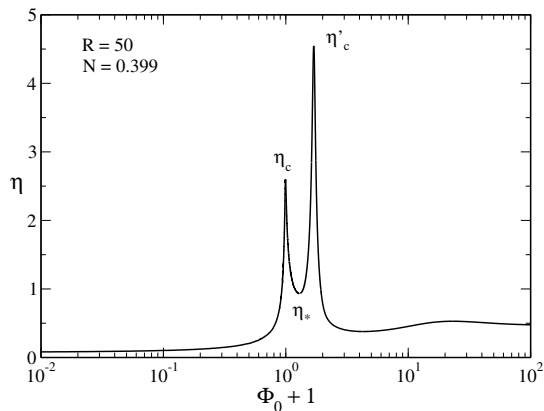


FIG. 14: Normalized inverse temperature as a function of the central potential Φ_0 for $N_{OV} < N < N_e$ (specifically $R = 50$ and $N = 0.399$).

In Fig. 15 we have plotted the relation $\eta(\mathcal{R})$ between the normalized inverse temperature and the energy density contrast $\mathcal{R} = \epsilon_0/\epsilon_R$. We can see that \mathcal{R} increases monotonically along the series of equilibria up to η'_c . Then, on the second unstable branch, it displays a more complicated behavior.

The evolution of the system in the canonical ensemble in the following. Let us start from high temperature states and decrease the temperature. At high tempera-

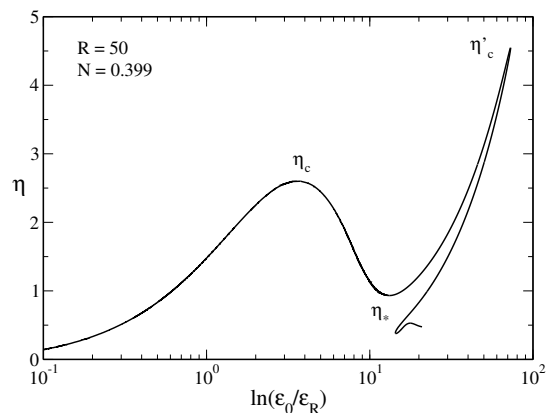


FIG. 15: Normalized inverse temperature as a function of the energy density contrast $\mathcal{R} = \epsilon_0/\epsilon_R$ for $N_{OV} < N < N_e$ (specifically $R = 50$ and $N = 0.399$).

tures, the system is in the gaseous phase. At $\eta = \eta_t$, we expect the system to undergo a first order phase transition from the gaseous phase to the condensed phase. However, in practice, this phase transition does not take place because the metastable gaseous states have a very long lifetime. The physical transition occurs at the critical temperature η_c (spinodal point) at which the gaseous phase disappears. At that point the system undergoes a zeroth order phase transition (collapse) from the gaseous phase to the condensed phase. If we keep decreasing the temperature there comes another critical point η'_c at which the system undergoes a catastrophic collapse from the condensed phase to a black hole. This is an instability of general relativistic origin which has no counterpart in the Newtonian theory. Inversely, if we increase the temperature, the system displays a zeroth order phase transition (explosion) at η_* from the condensed phase to the gaseous phase.

E. The case $N_e < N < N'_e$

In Fig. 16 we have plotted the caloric curve for $N_e = 0.40002 < N < N'_e = 0.40469$. The novelty with respect to the previous case is that now η'_c is smaller than η_c (they become equal when $N = N_e = 0.40002$).

The description in the microcanonical ensemble is the same as before.

In the canonical ensemble, the caloric curve presents the following features:

(i) When $\eta < \eta_*$ and when $\eta'_c < \eta < \eta_c$ there are only gaseous states. When $\eta_* < \eta < \eta'_c$ there exist gaseous and condensed states at the same temperature. A first order phase transition is expected at a transition temperature η_t determined by the Maxwell construction (see Fig. 16) or by the equality of the free energy of the two phases (see Fig. 17). When $\eta_* < \eta < \eta_t$ the gaseous states have a lower free energy than the condensed states.

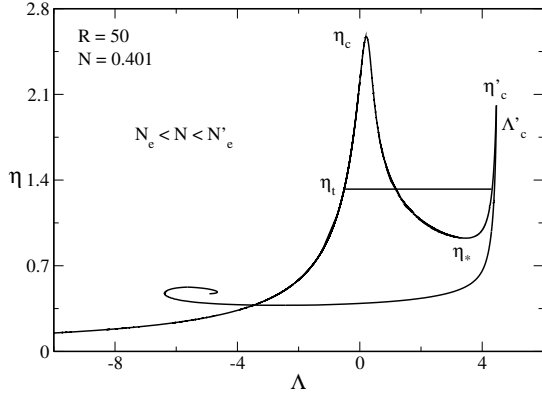


FIG. 16: Caloric curve for $N_e = 0.40002 < N < N'_e = 0.40469$ (specifically $R = 50$ and $N = 0.401$).

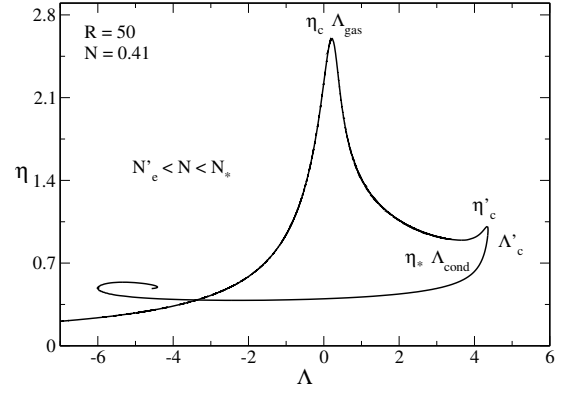


FIG. 18: Caloric curve for $N'_e = 0.40469 < N < N_* = 0.41637$ (specifically $R = 50$ and $N = 0.41$).

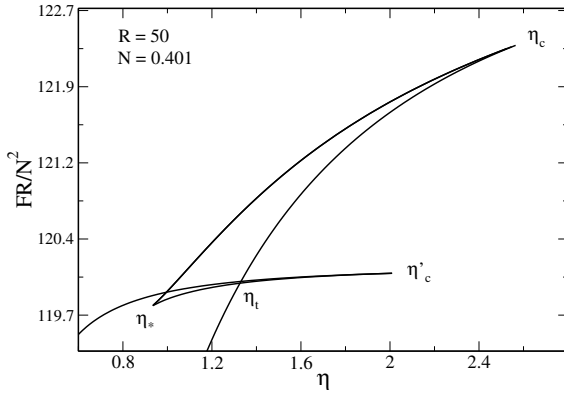


FIG. 17: Normalized free energy as a function of the inverse temperature for $N_e < N < N'_e$ (specifically $R = 50$ and $N = 0.401$).

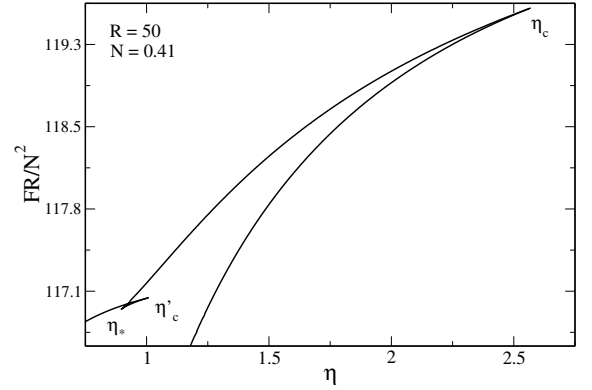


FIG. 19: Normalized free energy as a function of the inverse temperature for $N'_e < N < N_*$ (specifically $R = 50$ and $N = 0.41$).

When $\eta_t < \eta < \eta'_c$ the condensed states have a lower free energy than the gaseous states. However, the first order phase transition does not take place in practice because of the very long lifetime of the metastable states.

(ii) There is a catastrophic collapse at η_c from the gaseous phase to a black hole.

(iii) There is a catastrophic collapse at η'_c from the condensed phase to a black hole.

(iv) There is a zeroth order phase transition at η_* from the condensed phase to the gaseous phase. It correspond to an explosion ultimately halted by the boundary of the box.

The evolution of the system in the canonical ensemble is the following. Let us start from high temperature states and decrease the temperature. At high temperatures, the system is in the gaseous phase. At $\eta = \eta_t$ the system is expected to undergo a first order phase transition from the gaseous phase to the condensed phase. However, this phase transition does not take place in practice. At $\eta = \eta_c$ the system undergoes a catastrophic collapse towards a black hole. A condensed phase exists

for $\eta_* < \eta < \eta'_c$ but it is not clear how it can be reached in practice.

F. The case $N'_e < N < N_*$

In Fig. 18 we have plotted the caloric curve for $N'_e = 0.40469 < N < N_* = 0.41637$, where N'_e is defined such that $\eta'_c = \eta_t$.

The description in the microcanonical ensemble is the same as before.

In the canonical ensemble, the caloric curve presents the following features:

(i) When $\eta < \eta_*$ and when $\eta'_c < \eta < \eta_c$ there are only gaseous states. When $\eta_* < \eta < \eta'_c$ there exist gaseous and condensed states at the same temperature. However, there is no first order phase transition, even in theory, because we cannot satisfy the Maxwell construction (see Fig. 18) or the equality of the free energy of the gaseous and condensed phases (see Fig. 19). When $\eta_* < \eta < \eta'_c$ the gaseous states always have a lower free energy than

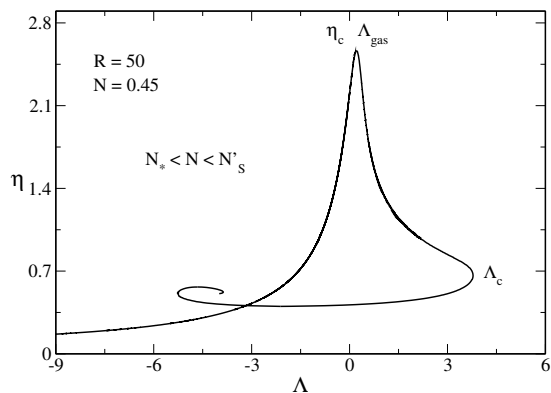


FIG. 20: Caloric curve for $N_* = 0.41637 < N < N'_S = 6.40$ (specifically $R = 50$ and $N = 0.45$).

the condensed states (see Fig. 19). Therefore, although there are several stable equilibrium states when $\eta_* < \eta < \eta'_c$ there is no phase transition from one phase to the other. This is a particularity of the relativistic situation.

(ii) There is a catastrophic collapse at η_c from the gaseous phase to a black hole.

(iii) There is a catastrophic collapse at η'_c from the condensed phase to a black hole.

(iv) There is a zeroth order phase transition at η_* from the condensed phase to the gaseous phase. It corresponds to an explosion ultimately halted by the boundary of the box.

The evolution of the system is the same as described previously.

G. The case $N > N_*$

In Fig. 20 we have plotted the caloric curve for $N > N_* = 0.41637$, where N_* is defined such that $\eta'_c = \eta_*$. From that moment, we denote the minimum energy by Λ_c instead of Λ'_c .

1. Microcanonical ensemble

Let us first consider the microcanonical ensemble. The curve $\eta(\Lambda)$ is multivalued. According to the Poincaré turning point criterion, the series of equilibria is stable up to Λ_c and then becomes unstable. The caloric curve presents the following features:

(i) There is no phase transition (there is only one stable equilibrium state for each $\Lambda < \Lambda_c$).

(ii) There is a region of negative specific heats between Λ_{gas} and Λ_c .

(iii) There is a catastrophic collapse at Λ_c towards a black hole.

The evolution of the system is the same as described previously.

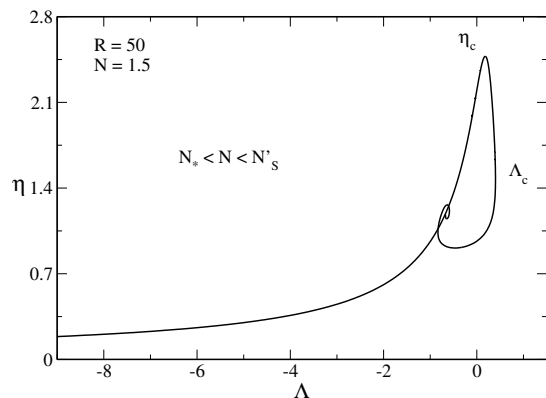


FIG. 21: Caloric curve for $N_* < N < N'_S$ (specifically $R = 50$ and $N = 1.5$).

2. Canonical ensemble

We now consider the canonical ensemble. The function $\Lambda(\eta)$ is multivalued. According to the Poincaré turning point criterion, the series of equilibria is stable up to η_c and then becomes unstable. The caloric curve presents the following features:

(i) There is no phase transition (there is only one stable equilibrium state for each $\eta < \eta_c$).

(ii) There is a catastrophic collapse at η_c towards a black hole.

The evolution of the system is the same as described previously. The only difference is that the condensed phase has disappeared.

H. Larger values of N

In Figs. 21 and 22 we have plotted the caloric curves for larger values of N . When $N \gg N_{\text{OV}} = 0.39853$, the system is nondegenerate and we recover the results of [7, 61] for a classical general relativistic gas described by the Boltzmann distribution.²³ The caloric curve exhibits a double spiral. When $N < N'_S = 6.40$ (see Fig. 7 of [7]) the two spirals are separated. When $N'_S = 6.40 < N < N_S = 7.08$ (see Fig. 8 of [7]) the two spirals are amputated (truncated) and touch each other. When $N_S = 7.08 < N < N_{\text{max}} = 8.821$ (see Fig. 9 of [7]) the spirals disappear and the caloric curve makes a “loop”. When $N \rightarrow N_{\text{max}}$, the caloric curve reduces to a “point” located at $(\Lambda_*, \eta_*) = (-0.9829, 1.2203)$.

²³ As discussed in Sec. XI the classical limit corresponds to $N \rightarrow +\infty$ and $R \rightarrow +\infty$ in such a way that N/R is fixed (in more physical terms $N \gg N_{\text{OV}}$ and $R \gg R_{\text{OV}}$ with N/R fixed).

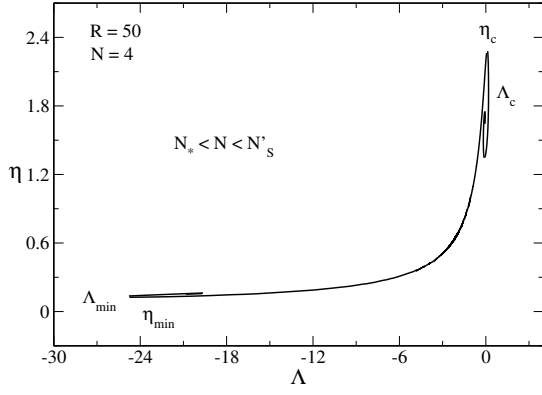


FIG. 22: Caloric curve for $N_* < N < N'_s$ (specifically $R = 50$ and $N = 4$).

I. The canonical phase diagram

In Figs. 23 and 24 we have represented the canonical phase diagram corresponding to $R_{CCP} = 12.0 < R < R_{MCP} = 92.0$ (specifically $R = 50$). It shows the evolution of the critical temperatures η_{\min} , η_c , η_* , η_t , η'_c with N . We can clearly see the canonical critical point at $N_{CCP} = 0.0170$ at which the canonical phase transition appears. We also see the point $N_{OV} = 0.39853$ above which quantum mechanics is not able to prevent gravitational collapse above $\eta'_c(N)$. Finally, we see the point $N_{\max} = 8.821$ above which there is no equilibrium state anymore.

The nonrelativistic limit [5] corresponds to the dashed lines. It provides a very good approximation of η_c , η_* and η_t for $N \ll N_{OV}$. As we approach N_{OV} general relativity must be taken into account.

The classical limit [7, 61] corresponds to the dotted lines. It provides a very good approximation of η_{\min} (hot spiral) for any N . It also provides a very good approximation of η_c (cold spiral) for $N \gg N_{OV}$. As we approach N_{OV} quantum mechanics must be taken into account.

J. The microcanonical phase diagram

In Figs. 25 and 26 we have represented the microcanonical phase diagram corresponding to $R_{CCP} = 12.0 < R < R_{MCP} = 92.0$ (specifically $R = 50$). It shows the evolution of the critical energies Λ_{\min} , Λ_{\max} , Λ'_{\max} , Λ_{gas} , Λ_{cond} , Λ'_c , Λ_c with N . We can clearly see the canonical critical point at $N_{CCP} = 0.0170$ at which the region of negative specific heat (associated with the canonical phase transition) appears. We also see the point $N_{OV} = 0.39853$ above which quantum mechanics is not able to prevent gravitational collapse above $\Lambda'_c(N)$, and the point $N_{\max} = 8.821$ above which there is no equilibrium state anymore.

The nonrelativistic limit [5] corresponds to the dashed lines. It provides a very good approximation of Λ_{\max} ,

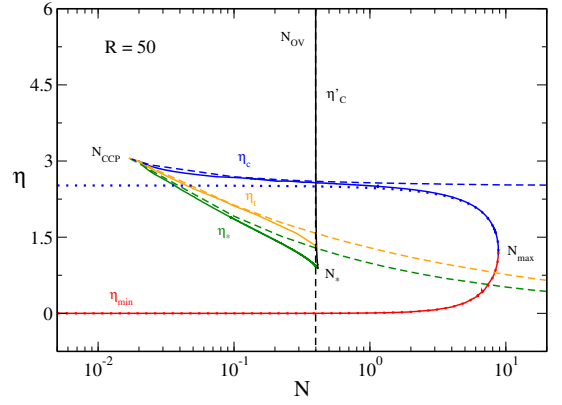


FIG. 23: Canonical phase diagram for $R_{CCP} = 12.0 < R < R_{MCP} = 92.0$ (specifically $R = 50$).

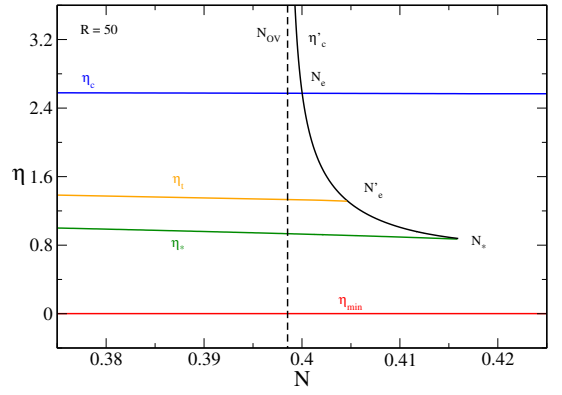


FIG. 24: Zoom of the canonical phase diagram for $R_{CCP} < R < R_{MCP}$ (specifically $R = 50$) in the region near N_{OV} . For $N \rightarrow N_{OV}^+$, we find that $\eta'_c \sim 0.104(N - N_{OV})^{-1/2}$.

Λ_{gas} and Λ_{cond} for $N \ll N_{OV}$. As we approach N_{OV} general relativity must be taken into account.

The classical limit [7, 61] corresponds to the dotted lines. It provides a very good approximation of Λ_{\min} (hot spiral) for any N . It also provides a very good approximation of Λ_c (cold spiral) for $N \gg N_{OV}$. As we approach N_{OV} quantum mechanics must be taken into account.

Remark: we recall that the minimum energy above which equilibrium states exist is Λ_{\max} (ground state) when $N < N_{OV}$ and Λ'_c or Λ_c when $N > N_{OV}$. From Fig. 25 we note that $\Lambda_{\max}(N)$ increases with N while $\Lambda'_c(N)$ and $\Lambda_c(N)$ decrease with N . We also note that the system would be a black hole if $M > Rc^2/2G$, i.e., $M > R/2$ in terms of dimensionless variables. Using Eq. (15), this leads to the condition

$$\Lambda < -\frac{\left(\frac{R}{2} - N\right) R}{N^2} \equiv \Lambda_{\text{BH}}(N, R). \quad (33)$$

One can locate the black hole energy curve $\Lambda_{\text{BH}}(N, R)$ in Fig. 25. It behaves as $\Lambda_{\text{BH}} \sim -R^2/2N^2 \rightarrow -\infty$ when

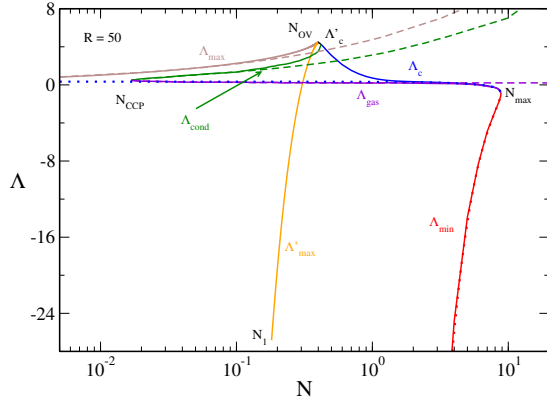


FIG. 25: Microcanonical phase diagram for $R_{\text{CCP}} = 12.0 < R < R_{\text{MCP}} = 92.0$ (specifically $R = 50$).

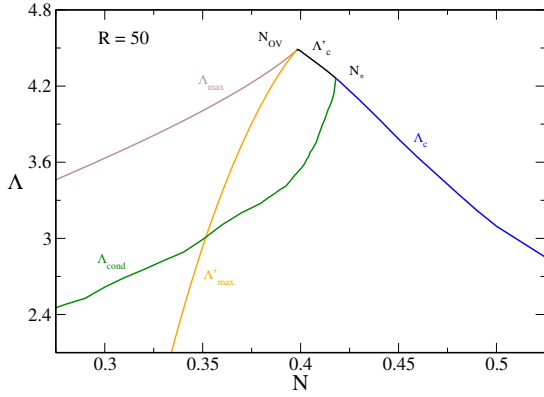


FIG. 26: Zoom of the microcanonical phase diagram for $R_{\text{CCP}} < R < R_{\text{MCP}}$ (specifically $R = 50$) in the region near N_{OV} .

$N \rightarrow 0$ and as $\Lambda_{\text{BH}} \sim R/N \rightarrow 0^+$ when $N \rightarrow +\infty$. It vanishes at $N = R/2$ and has a maximum $(\Lambda_{\text{BH}})_{\text{max}} = 1/2$ at $N = R$. One can show that the black hole energy curve never intersects the curves of Fig. 25 so that the system is never a black hole (see [7] for a detailed discussion).

VI. THE CASE $R > R_{\text{MCP}}$

We now study the case $R > R_{\text{MCP}} = 92.0$ where the system can display a canonical phase transition (as before) and a microcanonical phase transition (see Fig. 47 below). For illustration we take $R = 600$. In that case, the canonical phase transition appears above $N_{\text{CCP}} = 9.84 \times 10^{-6}$ and the microcanonical phase transition appears above $N_{\text{MCP}} = 1.02 \times 10^{-2}$.

The description of the caloric curves in the canonical ensemble is the same as before. Therefore, in the following, we only consider the microcanonical ensemble. In addition, we focus on what is new and do not treat in

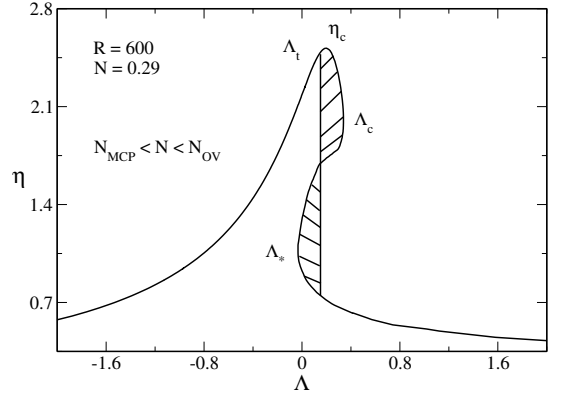


FIG. 27: Caloric curve for $N_{\text{MCP}} = 1.02 \times 10^{-2} < N < N_{\text{OV}} = 0.39853$ (specifically $R = 600$ and $N = 0.29$).

detail the situations that are similar to those described previously.

A. The case $N < N_{\text{MCP}}$

When $N < N_{\text{MCP}} = 1.02 \times 10^{-2}$, the discussion is the same as in Sec. V ($R = 50$). The canonical phase transition appears at $N_{\text{CCP}} = 9.84 \times 10^{-6}$. Since $N_{\text{MCP}} \ll N_{\text{OV}}$, we are in the nonrelativistic regime [5].

B. The case $N_{\text{MCP}} < N < N_1$

In Fig. 27 we have plotted the caloric curve for $N_{\text{MCP}} = 1.02 \times 10^{-2} < N < N_{\text{OV}} = 0.39853$. Since $N \ll N_{\text{OV}}$, the caloric curve coincides with the one obtained in the nonrelativistic limit [5]. It has a Z-shape structure leading to a microcanonical phase transition.²⁴ This Z-shape structure appears at $N = N_{\text{MCP}} = 1.02 \times 10^{-2}$ at which the caloric curve presents a vertical inflexion point. The caloric curve continues up to Λ_{max} (outside the frame of the figure) at which it presents an asymptote.

The curve $\eta(\Lambda)$ is multivalued leading to the possibility of phase transitions in the microcanonical ensemble. The upper branch up to Λ_c corresponds to the gaseous phase and the lower branch after Λ_* corresponds to the condensed phase. According to the Poincaré turning point criterion, these equilibrium states are stable while the equilibrium states on the intermediate branch between

²⁴ The caloric curve resembles a dinosaur's neck [5]. However, in Fig. 27 the dinosaur has no "chin". The "chin" appears at $N_{\text{chin}} = 0.5062$ as explained in Appendix C 2. The presence, or not, of the "chin" has no physical consequence since it concerns a region of the caloric curve where the equilibrium states are unstable.

Λ_c and Λ_* are unstable. The caloric curve presents the following features:

(i) When $\Lambda < \Lambda_*$ there are only gaseous states. When $\Lambda > \Lambda_c$ there are only condensed states. When $\Lambda_* < \Lambda < \Lambda_c$ there exist gaseous and condensed states with the same energy. A first order microcanonical phase transition is expected at a transition energy Λ_t determined by the Maxwell construction (see Fig. 27) or by the equality of the entropy of the gaseous and condensed phases (see Fig. 18 of [5]). When $\Lambda_* < \Lambda < \Lambda_t$ the gaseous states have a higher entropy than the condensed states. When $\Lambda_t < \Lambda < \Lambda_c$ the condensed states have a higher entropy than the gaseous states. However, the first order phase transition does not take place in practice because of the very long lifetime of the metastable states.

(ii) There is a zeroth order phase transition at Λ_c from the gaseous phase to the condensed phase. It corresponds to a gravitational collapse (gravothermal catastrophe) ultimately halted by quantum degeneracy.

(iii) There is a zeroth order phase transition at Λ_* from the condensed phase to the gaseous phase. It corresponds to an explosion ultimately halted by the boundary of the box.

(iv) There are two regions of negative specific heats, one between Λ_{gas} and Λ_c and another one between Λ_* and Λ_{cond} .

The evolution of the system in the microcanonical ensemble is the following. Let us start from high energies and decrease the energy. At high energies, the system is in the gaseous phase. At $\Lambda = \Lambda_t$ we expect the system to undergo a first order phase transition from the gaseous phase to the condensed phase. However, in practice, this phase transition does not take place because the metastable gaseous states have a very long lifetime. At $\Lambda = \Lambda_c$ the system collapses towards the condensed phase. Complete gravitational collapse is prevented by quantum mechanics. The system reaches an equilibrium state similar to a nonrelativistic white dwarf (fermion ball) surrounded by an isothermal atmosphere. If we now increase the energy the system remains in the condensed phase (again, the first order phase transition expected at Λ_t does not take place because the metastable condensed states have a very long lifetime) until the point Λ_* at which it explodes and returns to the gaseous phase. We have thus described an hysteretic cycle in the microcanonical ensemble [5].

In Fig. 28 we have plotted the density profiles of the gaseous (G), core-halo (CH) and condensed (C) states at the transition point Λ_t . We note that the energy density is very low confirming that we are in the nonrelativistic regime. The discussion is essentially the same as in Sec. VB3 with the difference that the fermion ball (similar to a nonrelativistic cold white dwarf) that forms in the condensed phase contains only a fraction ($\sim 1/4$) of the mass (see [5], Sec. XIII and Appendix E 2 b). The rest of the mass is diluted in a hot halo. This core-halo structure is reminiscent of a red-giant (see Sec. XIII).

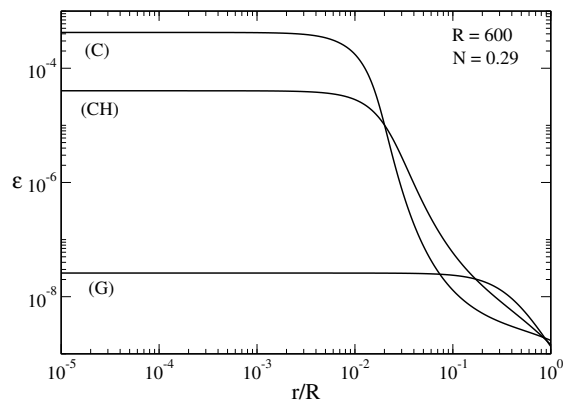


FIG. 28: Energy density profiles of gaseous, core-halo and condensed states at $\Lambda = \Lambda_t$ (specifically $\Lambda_t = 0.151$).

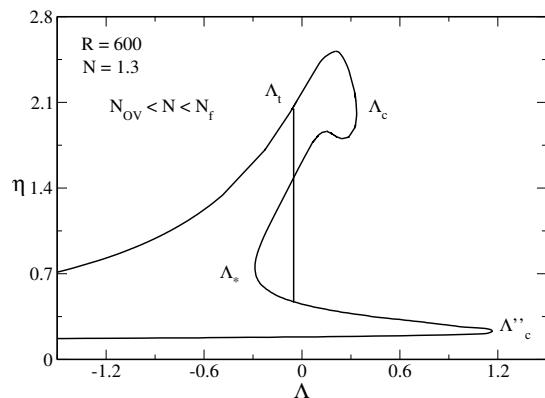


FIG. 29: Caloric curve for $N_{\text{OV}} = 0.39853 < N < N_f = 1.4854$ (specifically $R = 600$ and $N = 1.3$).

C. The case $N_1 < N < N_{\text{OV}}$

The second branch with an asymptote at Λ'_{max} appears at $N_1 = 0.18131$ but this does not change the discussion since this branch is made of unstable equilibrium states. From that moment, the system starts to be strongly relativistic.

D. The case $N_{\text{OV}} < N < N_f$

In Fig. 29 we have plotted the caloric curve for $N_{\text{OV}} = 0.39853 < N < N_f = 1.4854$.²⁵ The novelty with respect to the previous case is that the two branches have merged. As a result there is no ground state anymore (see Sec. VD). The caloric curve presents a turning point of energy which corresponds to the minimum energy. When

²⁵ We note that the “chin” of the dinosaur has appeared since $N = 1.3 > N_{\text{chin}} = 0.5062$.

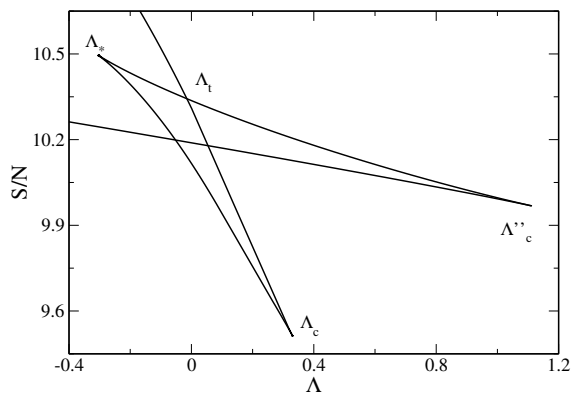


FIG. 30: Entropy per fermion as a function of the normalized energy for $N_{\text{OV}} < N < N_f$ (specifically $R = 600$ and $N = 1.3$). The first derivative of S with respect to E is discontinuous at the transition energy E_t . This corresponds to a first order phase transition, connecting the gaseous phase to the condensed phase, which is associated with a jump of temperature $\beta = \partial S / \partial E$ in the caloric curve. On the other hand, S is discontinuous at the spinodal points E_c and E_* . This corresponds to zeroth order phase transitions which are associated with a jump of entropy. We can check that the unstable equilibrium states (saddle points of entropy) between Λ_c and Λ_* have an entropy lower than the stable equilibrium states (maxima of entropy). However, the unstable equilibrium states after Λ_c'' can have an entropy higher than the stable equilibrium states before Λ_c .

$N < N_* = 0.405$ we call it Λ_c' and when $N > N_*$ we call it Λ_c'' (see Sec. V G for the definition of N_*). In the following, to be specific, we assume that $N > N_*$ but the discussion is essentially the same for $N < N_*$.

According to the Poincaré turning point criterion, the series of equilibria is stable up to Λ_c , becomes unstable between Λ_c and Λ_* , becomes stable again between Λ_* and Λ_c'' and becomes unstable again after Λ_c'' . The caloric curve presents the following features:

(i) When $\Lambda < \Lambda_*$ there are only gaseous states. When $\Lambda_c < \Lambda < \Lambda_c''$ there are only condensed states. When $\Lambda_* < \Lambda < \Lambda_c$ there exist gaseous and condensed states with the same energy. A first order phase transition is expected at a transition energy Λ_t determined by the Maxwell construction (see Fig. 29) or by the equality of the entropy of the gaseous and condensed phases (see Fig. 30). When $\Lambda_* < \Lambda < \Lambda_t$ the gaseous states have a higher entropy than the condensed states. When $\Lambda_t < \Lambda < \Lambda_c$ the condensed states have a higher entropy than the gaseous states. However, the first order phase transition does not take place in practice because of the very long lifetime of metastable states.

(ii) There is a zeroth order phase transition at Λ_c from the gaseous phase to the condensed phase. It corresponds to a gravitational collapse (gravothermal catastrophe) ultimately halted by quantum degeneracy.

(iii) There is a zeroth order phase transition at Λ_* from the condensed phase to the gaseous phase. It corresponds

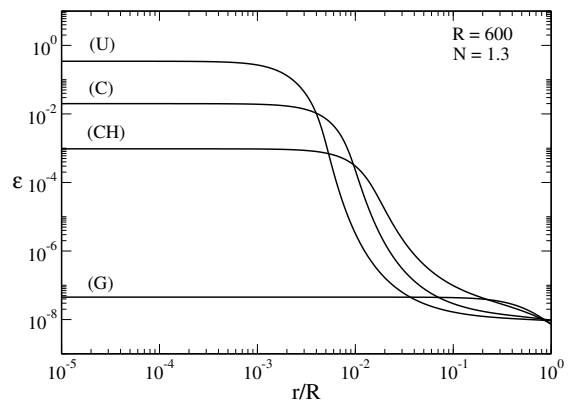


FIG. 31: Density profiles of gaseous, core-halo and (stable and unstable) condensed states at $\Lambda = \Lambda_t$ (specifically $\Lambda_t = -0.0510$).

to an explosion ultimately halted by the boundary of the box.

(iv) There is a catastrophic collapse at Λ_c'' from the condensed phase to a black hole.

(v) There are two regions of negative specific heats, one between Λ_{gas} and Λ_c and another one between Λ_* and Λ_c'' .

The evolution of the system in the microcanonical ensemble in the following. Let us start from high energies and decrease the energy. At high energies, the system is in the gaseous phase. At $\Lambda = \Lambda_t$, we expect the system to undergo a first order phase transition from the gaseous phase to the condensed phase. However, in practice, this phase transition does not take place because the metastable gaseous states have a very long lifetime. The physical transition occurs at the critical energy Λ_c (spinodal point) at which the gaseous phase disappears. At that point the system undergoes a zeroth order phase transition (collapse) from the gaseous phase to the condensed phase. If we keep decreasing the energy there comes another critical point Λ_c'' at which the system undergoes a catastrophic collapse from the condensed phase to a black hole. This is an instability of general relativistic origin which has no counterpart in the Newtonian theory. Inversely, if we increase the energy, the system displays a zeroth order phase transition (explosion) at Λ_* from the condensed phase to the gaseous phase.

In Fig. 31 we have plotted the different density profiles at Λ_t . We see that the energy density is low for the gaseous state (G) and for the core-halo state (CH) indicating that we are in the nonrelativistic regime. By contrast, the energy density is relatively high for the stable condensed state (C) and for the unstable condensed state (U) indicating that we are in the relativistic regime. The discussion is essentially the same as in Sec. V C with the difference that the fermion ball (similar to a general relativistic cold neutron star) that forms in the condensed phase contains only a fraction ($\sim 1/4$) of the mass (see Sec. XIII and Appendix E 2 b). The rest of the mass is

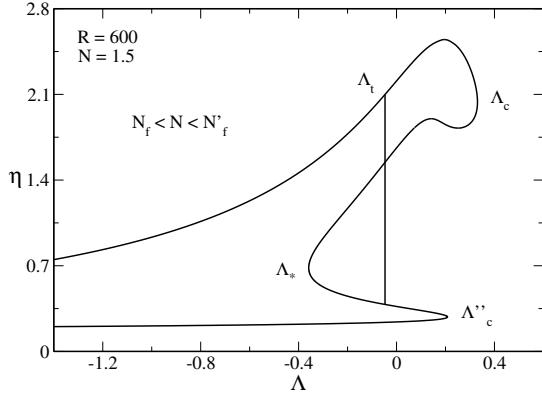


FIG. 32: Caloric curve for $N_f = 1.4854 < N < N'_f = 1.619$ (specifically $R = 600$ and $N = 1.5$).

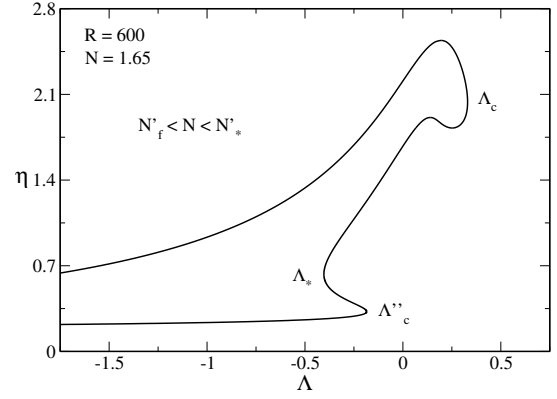


FIG. 34: Caloric curve for $N'_f = 1.619 < N < N'_* = 1.9000$ (specifically $R = 600$ and $N = 1.65$).

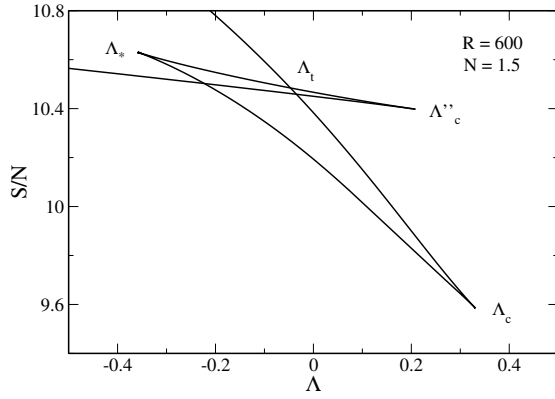


FIG. 33: Entropy per fermion as a function of the normalized energy for $N_f = 1.4854 < N < N'_f = 1.619$ (specifically $R = 600$ and $N = 1.5$).

diluted in a hot halo. This core-halo structure is reminiscent of a supernova (see Sec. XIII).

E. The case $N_f < N < N'_f$

In Fig. 32 we have plotted the caloric curve for $N_f = 1.4854 < N < N'_f = 1.619$. The novelty with respect to the previous case is that now Λ''_c is smaller than Λ_c (they become equal when $N = N_f$).

The caloric curve presents the following features:

(i) When $\Lambda < \Lambda_*$ and $\Lambda''_c < \Lambda < \Lambda_c$ there are only gaseous states. When $\Lambda_* < \Lambda < \Lambda''_c$ there exist gaseous and condensed states with the same energy. A first order phase transition is expected at a transition energy Λ_t determined by the Maxwell construction (see Fig. 32) or by the equality of the entropy of the two phases (see Fig. 33). When $\Lambda_* < \Lambda < \Lambda_t$ the gaseous states have a higher entropy than the condensed states. When $\Lambda_t < \Lambda < \Lambda''_c$ the condensed states have a higher entropy than the gaseous states. However, the first order phase transition

does not take place in practice because of the very long lifetime of the metastable states.

(ii) There is a catastrophic collapse at Λ_c from the gaseous phase to a black hole.

(iii) There is a catastrophic collapse at Λ''_c from the condensed phase to a black hole.

(iv) There is a zeroth order phase transition at Λ_* from the condensed phase to the gaseous phase. It corresponds to an explosion ultimately halted by the boundary of the box.

(v) There are two regions of negative specific heats, one between Λ_{gas} and Λ_c and another one between Λ_* and Λ''_c .

The evolution of the system in the microcanonical ensemble is the following. Let us start from high energies and decrease the energy. At high energies, the system is in the gaseous phase. At $\Lambda = \Lambda_t$ the system is expected to undergo a first order phase transition from the gaseous phase to the condensed phase. However, this phase transition does not take place in practice. At $\Lambda = \Lambda_c$ the system undergoes a catastrophic collapse towards a black hole. A condensed phase exists for $\Lambda_* < \Lambda < \Lambda''_c$ but it is not clear how it can be reached in practice.

F. The case $N'_f < N < N'_*$

In Fig. 34 we have plotted the caloric curve for $N'_f = 1.619 < N < N'_* = 1.9000$, where N'_f is defined such that $\Lambda''_c = \Lambda_t$.

The caloric curve presents the following features:

(i) When $\Lambda < \Lambda_*$ and when $\Lambda''_c < \Lambda < \Lambda_c$ there are only gaseous states. When $\Lambda_* < \Lambda < \Lambda''_c$ there exist gaseous and condensed states with the same energy. However, there is no first order phase transition, even in theory, because we cannot satisfy the Maxwell construction (see Fig. 34) or the equality of the entropy of the gaseous and condensed phases (see Fig. 35). When $\Lambda_* < \Lambda < \Lambda''_c$ the gaseous states always have an entropy higher than the

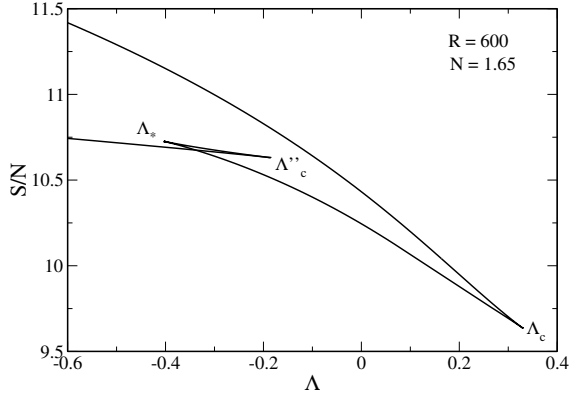


FIG. 35: Entropy per fermion as a function of the normalized energy for $N'_f = 1.619 < N < N'_* = 1.9000$ (specifically $R = 600$ and $N = 1.65$).

condensed states. Therefore, although there are several stable equilibrium states when $\Lambda_* < \Lambda < \Lambda''_c$ there is no phase transition from one phase to the other. This is a particularity of the relativistic situation.

(ii) There is a catastrophic collapse at Λ_c from the gaseous phase to a black hole.

(iii) There is a catastrophic collapse at Λ''_c from the condensed phase to a black hole.

(iv) There is a zeroth order phase transition at Λ_* from the condensed phase to the gaseous phase. It corresponds to an explosion ultimately halted by the boundary of the box.

(v) There are two regions of negative specific heats, one between Λ_{gas} and Λ_c and another one between Λ_* and Λ''_c .

The evolution of the system is the same as described previously.

G. The case $N'_* < N < N_{\text{max}}$

In Fig. 36 we have plotted the caloric curve for $N'_* = 1.9000 < N < N_{\text{max}} = 105.9$, where N'_* is defined such that $\Lambda''_c = \Lambda_*$. From that moment, we denote the minimum energy by Λ_c instead of Λ''_c . The novelty with respect to the previous case is that there is no condensed phase anymore. The discussion is the same as in Secs. V G and V H.

H. The microcanonical phase diagram

In Figs. 37 and 38 we have represented the microcanonical phase diagram corresponding to $R > R_{\text{MCP}}$. It shows the evolution of the critical energies Λ_{min} , Λ_{max} , Λ_{gas} , Λ_{cond} , Λ_c , Λ_* , Λ_t , Λ'_{max} , Λ'_c and Λ''_c with N . We can clearly see the canonical critical point at $N_{\text{CCP}} = 9.84 \times 10^{-6}$ at which the region of negative

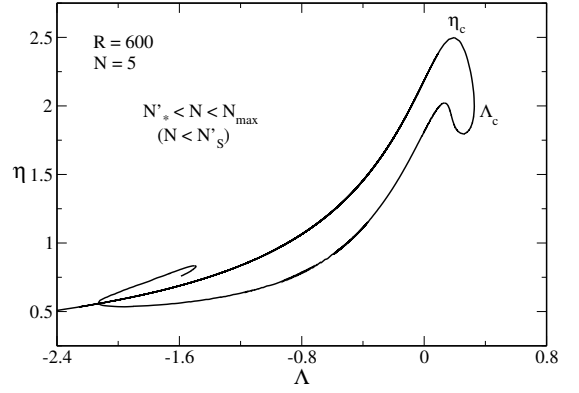


FIG. 36: Caloric curve for $N'_* = 1.9000 < N < N_{\text{max}} = 105.9$ (specifically $R = 600$ and $N = 5$).

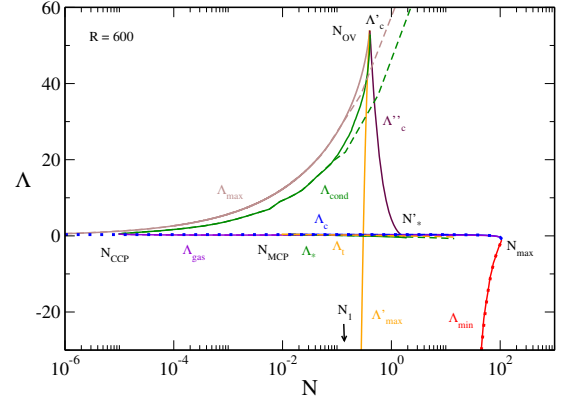


FIG. 37: Microcanonical phase diagram for $R > R_{\text{MCP}} = 92.0$ (specifically $R = 600$).

specific heat (associated with the canonical phase transition) appears and the microcanonical critical point at $N_{\text{MCP}} = 1.02 \times 10^{-2}$ at which the microcanonical phase transition appears. We also see the point $N_{\text{OV}} = 0.39853$ above which quantum mechanics is not able to prevent gravitational collapse above $\Lambda'_c(N)$ or $\Lambda''_c(N)$. Finally, we see the point $N_{\text{max}} = 105.9$ above which there is no equilibrium state anymore.

The nonrelativistic limit [5] corresponds to the dashed lines. It provides a very good approximation of Λ_{max} , Λ_{gas} , Λ_{cond} , Λ_c , Λ_* , and Λ_t for $N \ll N_{\text{OV}}$. As we approach N_{OV} general relativity must be taken into account.

The classical limit [7] corresponds to the dotted lines. It provides a very good approximation of Λ_{min} (hot spiral) for any N . It also provides a very good approximation of Λ_c (cold spiral) for $N \gg N_{\text{OV}}$. As we approach N_{OV} quantum mechanics must be taken into account.

Remark: From Fig. 37 we note that $\Lambda_{\text{max}}(N)$ increases with N while $\Lambda_c(N)$, $\Lambda'_c(N)$ and $\Lambda''_c(N)$ decrease with N .

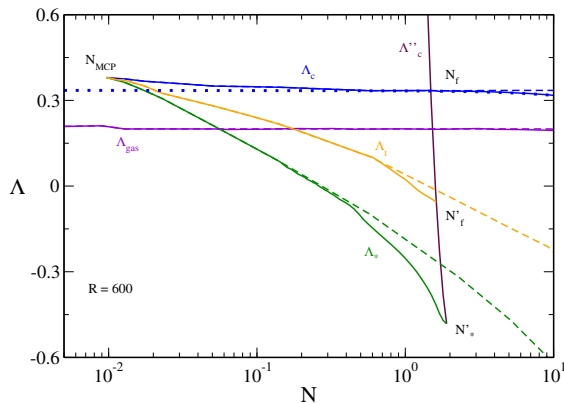


FIG. 38: Zoom of the microcanonical phase diagram for $R > R_{\text{MCP}}$ (specifically $R = 600$) in the region near N_{OV} .

VII. THE CASE $R \gg R_{\text{MCP}}$

For very large radii ($R \gg R_{\text{MCP}}$), a spiral, winding then unwinding, appears in the caloric curve at the location of the “head” of the dinosaur (this is similar to Fig. 22 of [5] and Fig. 44 of [14]). However, this spiral is made of unstable states. Therefore, if we restrict ourselves to stable equilibrium states, this mathematical complication (the proliferation of unstable states associated with the spiral) does not change the previous discussion.

Remark: The equilibrium states that are deep in the spiral have a pronounced “core-halo” structure with a large central density (see Fig. 45 of [14]). These core-halo states correspond to the configurations computed by Bilic *et al.* [10] and, more recently, by Ruffini *et al.* [12] and Chavanis *et al.* [14]. They consist in a large nondegenerate isothermal atmosphere harboring a small “fermion ball”. These solutions look very attractive at first sight because they could provide a self-consistent model of DM halos in which the fermion ball would mimic the presence of a supermassive black hole at the centers of the galaxies (an idea originally proposed in [10]). However, as argued in [14], these extreme core-halo structures are thermodynamically unstable (see Secs. VI-VIII of [14] for a detailed discussion).²⁶ These core-halo states are dynamically (Vlasov) stable meaning that if we artificially prepare the system in such a state, it will remain in this state for a long time. However, since these extreme core-halo states are thermodynamically unstable, they are very unlikely (from a thermodynamical point of view) to appear spontaneously. The fermion ball is like a “critical droplet” in nucleation processes. This may be a problem for the fermion ball scenario to mimic the effect

²⁶ By contrast, less extreme core-halo configurations, such as the solution (CH) computed in Fig. 6, can be stable in the microcanonical ensemble. They have a negative specific heat.

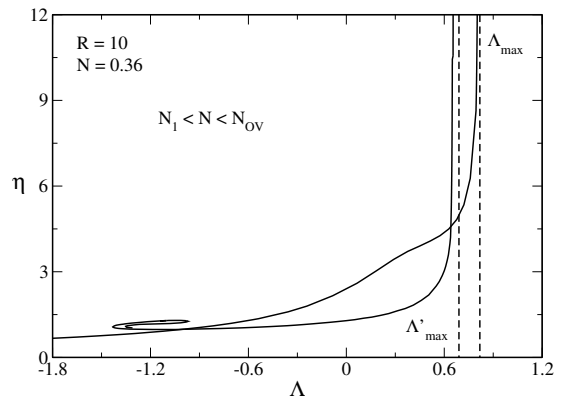


FIG. 39: Caloric curve for $N_1 = 0.18131 < N < N_{\text{OV}} = 0.39853$ (specifically $R = 10$ and $N = 0.36$).

of a black hole, as mentioned in [14]. Other problems with the fermion ball scenario are pointed out in [50].

VIII. THE CASE $R_{\text{OV}} < R < R_{\text{CCP}}$

We now study the case $R < R_{\text{CCP}} = 12.0$ where there is no phase transition (see Fig. 47 below). In this section, we assume $R > R_{\text{OV}} = 3.3569$ so that N_{OV} and N_{max} are relatively well separated. For illustration, we take $R = 10$.

A. The case $N < N_1$

When $N < N_1 = 0.18131$ the caloric curve is similar to that shown in Fig. 4. It is monotonic and presents an asymptote at Λ_{max} . The discussion is similar to that given in Sec. V A.

B. The case $N_1 < N < N_{\text{OV}}$

In Fig. 39 we have plotted the caloric curve for $N_1 = 0.18131 < N < N_{\text{OV}} = 0.39853$. The difference with the case treated in Sec. V C is that there is no canonical phase transition. The caloric curve is monotonic²⁷ and presents an asymptote at Λ_{max} . There is another branch presenting an asymptote at Λ'_{max} but it is made of unstable states. The series of equilibria of the main branch is stable in both ensembles. The specific heat is always positive. There is no phase transition and no gravitational collapse. The ensembles are equivalent.

²⁷ We see a sort of inflexion of the curve which signals the canonical first order phase transition that appears at larger radii $R > R_{\text{CCP}}$.

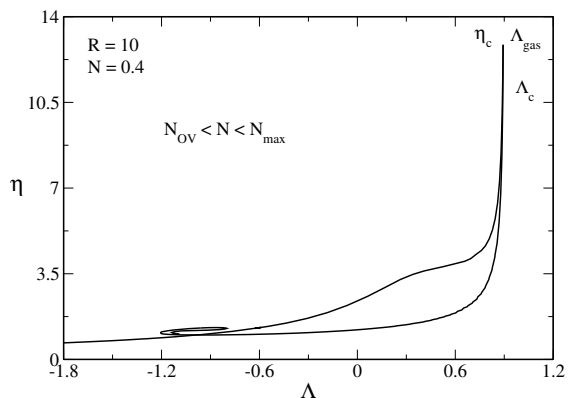


FIG. 40: Caloric curve for $N_{OV} = 0.39853 < N < N_{max} = 1.764$ (specifically $R = 10$ and $N = 0.4$).

C. The case $N_{OV} < N < N_{max}$

In Fig. 40 we have plotted the caloric curve for $N_{OV} = 0.39853 < N < N_{max} = 1.764$. The difference with the cases treated in Secs. VD-VH is that there is no phase transition. When $N > N_{OV}$ the two asymptotes have merged leading to a turning point of temperature at η_c and a turning point of energy at Λ_c . According to the Poincaré turning point criterion, the series of equilibria is stable up to η_c in the canonical ensemble and up to Λ_c in the microcanonical ensemble.

In the microcanonical ensemble, the caloric curve presents the following features:

- (i) There is no phase transition.
- (ii) There is a region of negative specific heats between Λ_{gas} and Λ_c .
- (iii) There is a catastrophic collapse at Λ_c towards a black hole.

In the canonical ensemble, the caloric curve presents the following features:

- (i) There is no phase transition.
- (ii) There is a catastrophic collapse at η_c towards a black hole.

D. The phase diagrams

In Fig. 41 we have represented the canonical phase diagram corresponding to $R < R_{CCP}$. It shows the evolution of the critical temperatures η_{max} and η_c with N . We see the point N_{OV} above which quantum mechanics is not able to prevent gravitational collapse above η_c . We also see the point N_{max} above which there is no equilibrium state anymore.

The classical limit [7] corresponds to the dotted lines. It provides a very good approximation of η_{max} (hot spiral) for any N . It also provides a very good approximation of η_c (cold spiral) for $N \gg N_{OV}$. As we approach N_{OV} quantum mechanics must be taken into account.

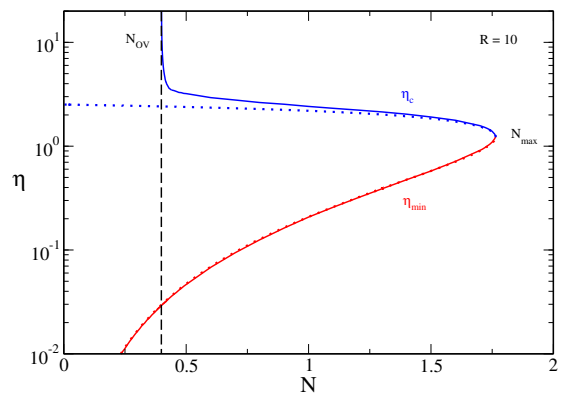


FIG. 41: Canonical phase diagram for $R_{OV} < R < R_{CCP}$ (specifically $R = 10$). For $N \rightarrow N_{OV}^+$, we find that $\eta_c \sim 0.516(N - N_{OV})^{-1/2}$.

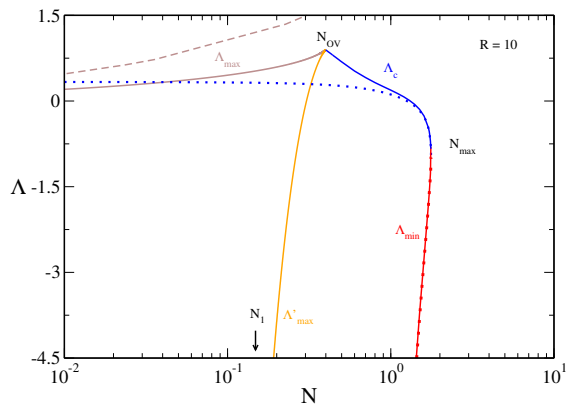


FIG. 42: Microcanonical phase diagram for $R_{OV} < R < R_{CCP}$ (specifically $R = 10$).

In Fig. 42 we have represented the microcanonical phase diagram corresponding to $R < R_{CCP}$. It shows the evolution of the critical energies Λ_{min} , Λ_{max} , Λ_c and Λ'_{max} with N . We see the point N_{OV} above which quantum mechanics is not able to prevent gravitational collapse above Λ_c . We also see the point N_{max} above which there is no equilibrium state anymore.

The nonrelativistic limit [5] corresponds to the dashed lines. It provides a very good approximation of Λ_{max} for $N \ll N_{OV}$ (this is not apparent in the figure but the curves coincide for smaller values of N). As we approach N_{OV} general relativity must be taken into account.

The classical limit [7] corresponds to the dotted lines. It provides a very good approximation of Λ_{min} (hot spiral) for any N . It also provides a very good approximation of Λ_c (cold spiral) for $N \gg N_{OV}$. As we approach N_{OV} quantum mechanics must be taken into account.

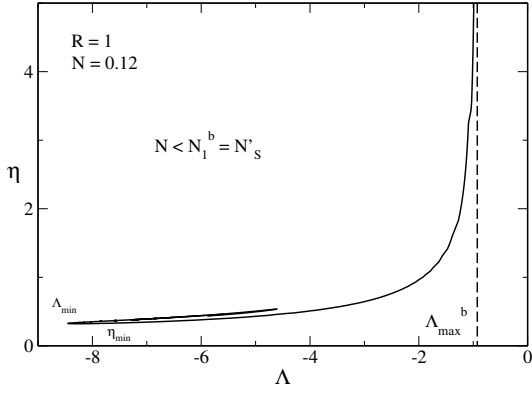


FIG. 43: Caloric curve for $N < N_1^b = 0.13627 \simeq N'_S$ (specifically $R = 1$ and $N = 0.12$).

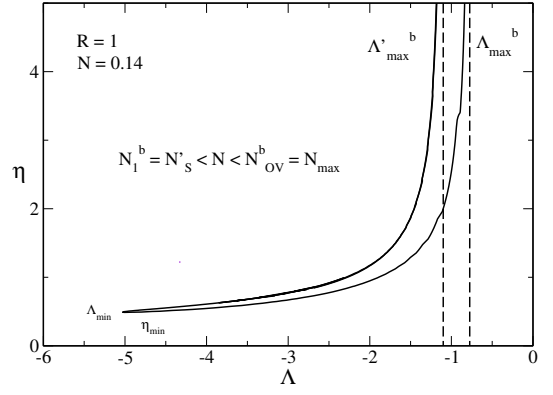


FIG. 44: Caloric curve for $N_1^b = 0.13627 \simeq N'_S < N < N_{OV}^b = 0.2015 \simeq N_{\max}$ (specifically $R = 1$ and $N = 0.14$).

IX. THE CASE $R < R_{OV}$

We now study the case $R < R_{OV} = 3.3569$. In that case, $N_{OV}^b \simeq N_{\max}$ and $N_1^b \simeq N'_S$ (see Fig. 47 below).²⁸ For illustration, we take $R = 1$.

A. The case $N < N_1^b \simeq N'_S$

In Fig. 43 we have plotted the caloric curve for $N < N_1^b = 0.13627 \simeq N'_S$. It is similar to that shown in Fig. 4. Since N is close to N_{\max} (see below), we clearly see the hot spiral that was outside the frame of Fig. 4. According to the Poincaré turning point criterion, the series of equilibria is stable up to the maximum temperature T_{\max} (corresponding to η_{\min}) in the the canonical ensemble and up to the maximum energy E_{\max} (corresponding to Λ_{\min}) in the microcanonical ensemble. Above T_{\max} and E_{\max} the system collapses into a black hole as discussed in [7, 61]. If we restrict ourselves to small and mid temperatures and energies (as in the preceding sections), there is no phase transition and no gravitational collapse. The specific heat is always positive and the ensembles are equivalent.

B. The case $N_1^b \simeq N'_S < N < N_{OV}^b \simeq N_{\max}$

In Fig. 44 we have plotted the caloric curve for $N_1^b = 0.13627 \simeq N'_S < N < N_{OV}^b = 0.2015 \simeq N_{\max}$. In that case, we have two asymptotes at Λ_{\max}^b and $(\Lambda_{\max}^b)'$

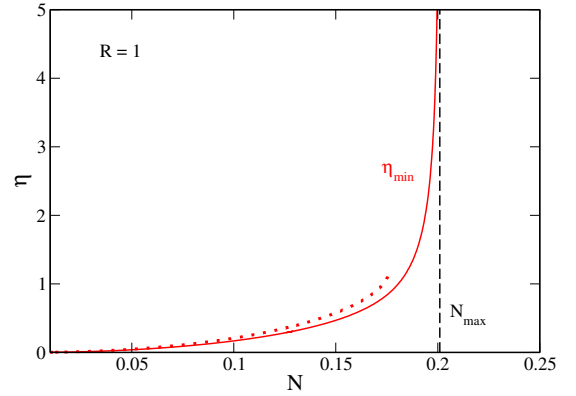


FIG. 45: Canonical phase diagram for $R < R_{OV}$ (specifically $R = 1$). For $N \rightarrow N_{\max}$, we find that $\eta_{\min} \sim 0.01 (N_{\max} - N)^{-1}$.

and a turning point of energy and temperature at Λ_{\min} and η_{\min} . According to the Poincaré turning point criterion, the series of equilibria is stable along the main branch up to the maximum temperature T_{\max} (corresponding to η_{\min}) in the the canonical ensemble and up to the maximum energy E_{\max} (corresponding to Λ_{\min}) in the microcanonical ensemble. As before, if we restrict ourselves to small and mid temperatures and energies, we conclude that there is no phase transition and no gravitational collapse. The specific heat is always positive and the ensembles are equivalent.

C. The phase diagrams

In Fig. 45 we have represented the canonical phase diagram corresponding to $R < R_{OV}$. It shows the evolution of the critical temperature η_{\min} with N . We note that η_{\min} diverges to $+\infty$ when $N \rightarrow N_{OV}^b = 0.2015 \simeq N_{\max}$ meaning that the caloric curve goes up to infinity and disappears. The classical limit [7] corresponds to the dotted

²⁸ We note that for small values of R , the values of N_1^b and N_{OV}^b (as well as $\Lambda_{\max}^b, (\Lambda_{\max}^b)'$...) are affected by the presence of the box. This is because the fermion ball at $T = 0$ and $E = E_{\min}$ (ground state) is confined by the walls of the box instead of being self-confined (see [6] for a detailed study). This is why we have added the letter b on these quantities.

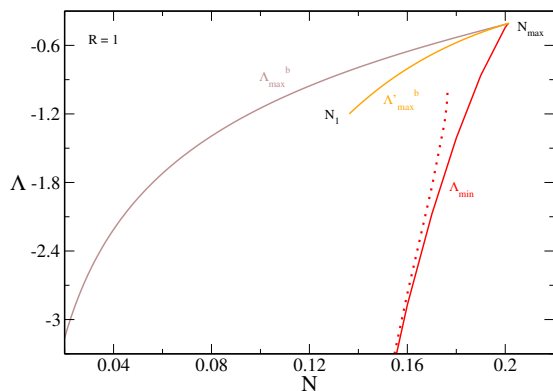


FIG. 46: Microcanonical phase diagram for $R < R_{OV}$ (specifically $R = 1$).

line. It provides a good approximation for $N \ll N_{\max}$. It is not valid for $N \sim N_{\max}$. This shows that when $R < R_{OV}$ quantum effects are still important close to N_{\max} . This is because, in the present case, $N_{\max} \simeq N_{OV}^b$ while in the previous examples $N_{\max} \gg N_{OV}$.

In Fig. 46 we have represented the microcanonical phase diagram corresponding to $R < R_{OV}$. It shows the evolution of the critical energies Λ_{\min} , Λ_{\max}^b and $(\Lambda_{\max}^b)'$ with N . The classical limit [7] corresponds to the dotted line. It provides a good approximation for $N \ll N_{\max}$. It is not valid for $N \sim N_{\max}$. When $R < R_{OV}$ quantum effects are still important close to N_{\max} .

X. THE (R, N) PHASE DIAGRAM

We can summarize our results by plotting the characteristic particle numbers $N_X(R)$ encountered in our study as a function of the box radius R . This leads to the (R, N) phase diagram represented in Fig. 47.

A. Characteristic particle numbers and characteristic radii

Let us briefly recall the meaning of the characteristic particle numbers appearing on this diagram.²⁹

(i) When $R > R_{CCP} = 12.0$, $N_{CCP}(R)$ is the particle number at which the canonical phase transition appears,

²⁹ We present the characteristic particle numbers by order of appearance in the caloric curves as we increase N for a given value of R . To fix the ideas, we take a large radius so that all kinds of phase transitions are present. We start from a small value of N . In that case, the caloric curve is monotonic with an asymptote at $\Lambda_{\max}(N, R)$ corresponding to the stable ground state of the self-gravitating Fermi gas at $T = 0$ ($\eta = \infty$). We then increase N until we meet the different characteristic particle numbers signaling a topological change of the caloric curve.

i.e., the particle number at which η_c and η_* appear in the caloric curve. When $R \gg R_{CCP}$, the function $N_{CCP}(R)$ is given by the relation $N_{CCP}(R) \sim 2.12 \times 10^3 R^{-3}$ obtained in the nonrelativistic study of [5].

(ii) When $R > R_{MCP} = 92.0$, $N_{MCP}(R)$ is the particle number at which the microcanonical phase transition appears, i.e., the particle number at which Λ_c and Λ_* appear in the caloric curve. When $R \gg R_{MCP}$, the function $N_{MCP}(R)$ is given by the relation $N_{MCP}(R) \sim 2.20 \times 10^6 R^{-3}$ obtained in the nonrelativistic study of [5].

(iii) $N_1(R)$ is the particle number at which the unstable equilibrium states at $T = 0$ appear, i.e., the particle number at which the second branch with an asymptote at $\Lambda'_{\max}(N, R)$ appears in the caloric curve. The function $N_1(R)$ is studied in [6]. When $R > R_1 = 2.0556$, the fermion star is self-confined and we have the standard value $N_1 = 0.18131$ of the OV theory. When $R < R_1$, the fermion star is box-confined and we find that $N_1^b(R)$ decreases as R decreases. When $R \rightarrow 0$, we find that $N_1^b(R) \sim 0.2492 R^{3/2}$ [6].

(iv) $N_{OV}(R)$ is the particle number above which there is no equilibrium state at $T = 0$ (no ground state) anymore. At $N = N_{OV}(R)$ the asymptotes $\Lambda_{\max}(N, R)$ and $\Lambda'_{\max}(N, R)$ merge. When $N > N_{OV}(R)$ they are replaced by a turning point η'_c in temperature and by a turning point Λ'_c in energy. The function $N_{OV}(R)$ is studied in [6]. When $R > R_{OV} = 3.3569$, the fermion star is self-confined and we have the standard value $N_{OV} = 0.39853$ of the OV theory. When $R < R_{OV}$, the fermion star is box-confined, and we find that $N_{OV}^b(R)$ decreases as R decreases. When $R \rightarrow 0$, we find that $N_{OV}^b(R) \sim 0.3104 R^{3/2}$ [6].

(v) When $R > R_{CCP} = 12.0$, $N_e(R)$ is the particle number at which the zeroth order phase transition in the canonical ensemble disappears, i.e., the particle number at which $\eta'_c = \eta_c$.

(vi) When $R > R_{CCP} = 12.0$, $N'_e(R)$ is the particle number at which the first order phase transition in the canonical ensemble disappears, i.e., the particle number at which $\eta'_c = \eta_t$.

(vii) When $R > R_{CCP} = 12.0$, $N_*(R)$ is the particle number at which the condensed phase disappears in the canonical ensemble, i.e., the particle number at which $\eta'_c = \eta_*$.

(viii) When $R > R_{MCP} = 92.0$, $N_f(R)$ is the particle number at which the zeroth order phase transition in the microcanonical ensemble disappears, i.e., the particle number at which $\Lambda''_c = \Lambda_c$.

(ix) When $R > R_{MCP} = 92.0$, $N'_f(R)$ is the particle number at which the first order microcanonical phase transition disappears, i.e., the particle number at which $\Lambda''_c = \Lambda_t$.

(x) When $R > R_{MCP} = 92.0$, $N'_*(R)$ is the particle number at which the condensed phase disappears in the microcanonical ensemble, i.e., the particle number at which $\Lambda''_c = \Lambda_*$.

(xi) When $R > R_1 = 2.0556$, $N'_S(R)$ is the value of the particle number above which the two spirals of the

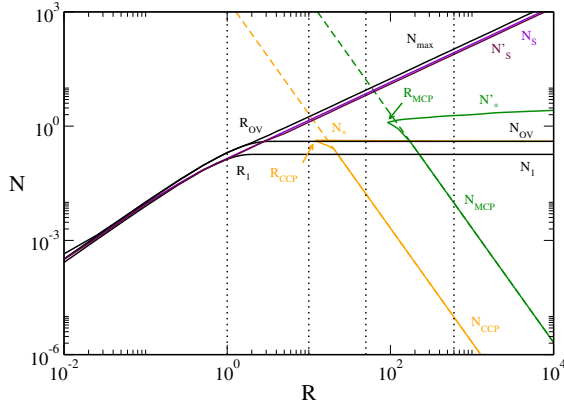


FIG. 47: The (R, N) phase diagram of the general relativistic Fermi gas. The characteristic particle numbers and radii are defined in the text. The dashed lines correspond to the nonrelativistic self-gravitating Fermi gas [5]. The dotted lines correspond to the radii $R = 1$, $R = 10$, $R = 50$ and $R = 600$ considered in the paper. Note that the quantities $N_e(R)$ and $N'_e(R)$ have not been represented because they are extremely close to $N_*(R)$. Similarly, the quantities $N_f(R)$ and $N'_f(R)$ have not been represented because they are extremely close to $N'_*(R)$.

caloric curve are amputated (truncated) and touch each other. When $R \gg R_1$, the function $N'_S(R)$ is given by the relation $N'_S(R) \sim 0.128 R$ obtained in the classical study of [7]. When $R < R_1 = 2.0556$, we find that $N'_S(R) \simeq N_1^b(R)$ [6]. Above that value, the caloric curve looks like Fig. 44 instead of looking like a double spiral.

(xii) When $R > R_1 = 2.0556$, $N_S(R)$ is the value of the particle number above which there is no spiral anymore and the caloric curve makes a “loop”. When $R \gg R_{OV}$, the function $N_S(R)$ is given by the relation $N_S(R) \sim 0.1415 R$ obtained in the classical study of [7]. When $R < R_1 = 2.0556$, we find that $N_S(R) \simeq N'_S(R) \simeq N_1^b(R)$ [6].

(xiii) $N_{\max}(R)$ is the maximum particle number below which an equilibrium state may exist for certain values of energy and temperature. For $N > N_{\max}(R)$ there is no equilibrium state, whatever the energy and the temperature. When $R \gg R_{OV}$, the function $N_{\max}(R)$ is given by the relation $N_{\max}(R) \sim 0.1764 R$ obtained in the classical study of [7, 61]. When $R < R_{OV} = 3.3569$, we find that $N_{\max}(R) \simeq N_{OV}^b(R)$ [6]. We note that $N_{\max} \gg N_{OV} = 0.39853$ when $R \gg R_{OV} = 3.3569$ while $N_{\max} \ll N_{OV}$ when $R \ll R_{OV}$. The change of regime takes place at $R \sim R_{OV}$ where $N_{\max} \sim N_{OV}$ (see the Remark at the end of Sec. IV C).

B. Summary of the main results when R is fixed and N is varied

The (R, N) phase diagram exhibits two critical points at $(R_{CCP}, N_{CCP}) = (12.0, 0.424)$ and $(R_{MCP}, N_{MCP}) =$

$(92.0, 1.25)$. $R_{CCP} = 12.0$ is the radius above which the system experiences a canonical phase transition when $N_{CCP}(R) < N < N_e(R)$. $R_{MCP} = 92.0$ is the radius above which the system experiences a microcanonical phase transition when $N_{MCP}(R) < N < N_f(R)$. Below, we summarize the essential features of the microcanonical and canonical phase transitions found for the self-gravitating Fermi gas in general relativity. In this section, we consider the situation where R is fixed and N is varied. We recall that there is a possible equilibrium state only for $N < N_{\max}(R)$. We have

$$N_{\max}(R) \sim 0.3104 R^{3/2} \quad (R \ll R_{OV}), \quad (34)$$

$$N_{\max}(R) \sim 0.1764 R \quad (R \gg R_{OV}). \quad (35)$$

As in the previous sections, we do not consider the case of very high energies and very high temperatures which has been treated in [7, 61].

1. $R < R_{CCP}$

When $N < N_{OV}(R)$, there is no phase transition and no catastrophic collapse (see Fig. 39). When $N_{OV}(R) < N < N_{\max}(R)$, there is no phase transition but there is a catastrophic collapse towards a black hole at $\eta_c(N, R)$ in the canonical ensemble and at $\Lambda_c(N, R)$ in the microcanonical ensemble (see Fig. 40).

2. $R_{CCP} < R < R'_{CCP}$

This case, in which $N_{CCP} > N_{OV}$ (see Fig. 48), was not treated explicitly in Secs. V-IX.

In the canonical ensemble when $N < N_{OV}$, there is no phase transition and no catastrophic collapse. When $N_{OV} < N < N_{CCP}(R)$, there is no phase transition but there is a catastrophic collapse toward a black hole at $\eta_c(N, R)$. When $N_{CCP}(R) < N < N_e$, there is a zeroth order phase transition from the gaseous phase to the condensed phase at $\eta_c(N, R)$ and a catastrophic collapse from the condensed phase to a black hole at $\eta'_c(N, R)$. When $N > N_e(R)$, there is no phase transition but there is a catastrophic collapse from the gaseous phase to a black hole at $\eta_c(N, R)$.

In the microcanonical ensemble, the situation is the same as before.

3. $R_{CCP} < R < R_{MCP}$

In the canonical ensemble when $N < N_{CCP}(R)$ there is no phase transition and no catastrophic collapse (see Fig. 4). When $N_{CCP}(R) < N < N_{OV}$ there is a zeroth order phase transition from the gaseous phase to the condensed phase at $\eta_c(N, R)$ and no catastrophic collapse (see Figs. 5 and 7). When $N_{OV} < N < N_e(R)$

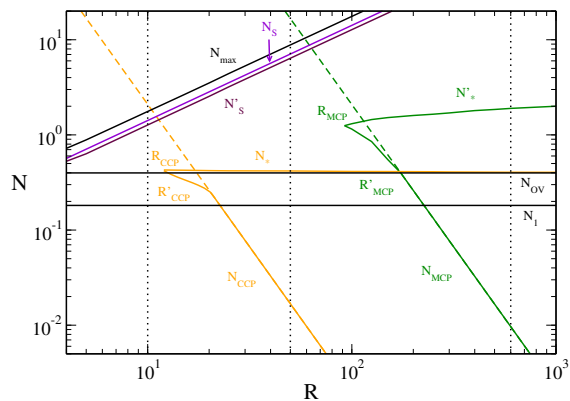


FIG. 48: Zoom of the (R, N) phase diagram of the general relativistic Fermi gas. When $R_{\text{CCP}} = 12.0 < R < R'_{\text{CCP}} = 12.6$ (resp. $R > R'_{\text{CCP}} = 12.6$) the canonical phase transition appears after (resp. before) N_{OV} . When $R_{\text{MCP}} = 92.0 < R < R'_{\text{MCP}} = 173$ (resp. $R > R'_{\text{MCP}} = 173$) the microcanonical phase transition appears after (resp. before) N_{OV} .

there is a zeroth order phase transition from the gaseous phase to the condensed phase at $\eta_c(N, R)$ and a catastrophic collapse from the condensed phase to a black hole at $\eta'_c(N, R)$ (see Fig. 9). When $N > N_e(R)$ there is no phase transition but there is a catastrophic collapse from the gaseous phase to a black hole at $\eta_c(N, R)$ (see Figs. 16, 18, 20, 21 and 22).

In the microcanonical ensemble, the situation is the same as before.

4. $R_{\text{MCP}} < R < R'_{\text{MCP}}$

This case, in which $N_{\text{MCP}} > N_{\text{OV}}$ (see Fig. 48), was not treated explicitly in Secs. V-IX.

In the canonical ensemble, the situation is the same as before so we focus on the microcanonical ensemble. When $N < N_{\text{OV}}$ there is no phase transition and no catastrophic collapse. When $N_{\text{OV}} < N < N_{\text{MCP}}(R)$ there is no phase transition but there is a catastrophic collapse towards a black hole at $\Lambda_c(N, R)$. When $N_{\text{MCP}}(R) < N < N_f(R)$ there is a zeroth order phase transition from the gaseous phase to the condensed phase at $\Lambda_c(N, R)$ and a catastrophic collapse from the condensed phase to a black hole at $\Lambda'_c(N, R)$ or $\Lambda''_c(N, R)$. When $N > N_f(R)$ there is no phase transition but there is a catastrophic collapse from the gaseous phase to a black hole at $\Lambda_c(N, R)$.

5. $R > R'_{\text{MCP}}$

In the canonical ensemble, the situation is the same as before so we focus on the microcanonical ensemble. When $N < N_{\text{MCP}}(R)$ there is no phase transition and no catastrophic collapse. When $N_{\text{MCP}}(R) < N < N_{\text{OV}}$

there is a zeroth order phase transition from the gaseous phase to the condensed phase at $\Lambda_c(N, R)$ and no catastrophic collapse (see Fig. 27). When $N_{\text{OV}} < N < N_f(R)$ there is a zeroth order phase transition from the gaseous phase to the condensed phase at $\Lambda_c(N, R)$ and a catastrophic collapse from the condensed phase to a black hole at $\Lambda''_c(N, R)$ (see Fig. 29). When $N > N_f(R)$ there is no phase transition but there is a catastrophic collapse from the gaseous phase to a black hole at $\Lambda_c(N, R)$ (see Figs. 32, 34 and 36).

C. Summary of the main results when N is fixed and R is varied

We now consider the situation where N is fixed and R is varied.³⁰ These results can be deduced from the (R, N) phase diagram of Fig. 47 by taking the inverse of the functions $N_X(R)$. This leads to the (N, R) phase diagram. We note that there is a possible equilibrium state only for $R > R_{\text{min}}(N)$ where $R_{\text{min}}(N)$ is the inverse function of $N_{\text{max}}(R)$. We have

$$R_{\text{min}}(N) \sim 2.181 N^{2/3} \quad (N \ll N_{\text{OV}}), \quad (36)$$

$$R_{\text{min}}(N) \sim 5.669 N \quad (N \gg N_{\text{OV}}). \quad (37)$$

1. $N < N_{\text{OV}}$

In the canonical ensemble when $R_{\text{min}}(N) < R < R_{\text{CCP}}(N)$ there is no phase transition and no catastrophic collapse. When $R > R_{\text{CCP}}(N)$ (with $R_{\text{CCP}}(N) \sim 12.8 N^{-1/3}$ in the nonrelativistic limit $N \ll N_{\text{OV}}$) there is a zeroth order phase transition from the gaseous phase to the condensed phase at $\eta_c(N, R)$ and no catastrophic collapse.

In the microcanonical ensemble when $R_{\text{min}}(N) < R < R_{\text{MCP}}(N)$ (with $R_{\text{MCP}}(N) \sim 130 N^{-1/3}$ in the nonrelativistic limit $N \ll N_{\text{OV}}$) there is no phase transition and no catastrophic collapse. When $R > R_{\text{MCP}}(N)$ there is a zeroth order phase transition from the gaseous phase to the condensed phase at $\Lambda_c(N, R)$ and no catastrophic collapse.

This is essentially like in the nonrelativistic limit [5]. Relativistic corrections occur only close to N_{OV} and/or close to $R_{\text{min}}(N)$.

2. $N_{\text{OV}} < N < N_{\text{CCP}} \simeq N_e$

In the canonical ensemble when $R_{\text{min}}(N) < R < R_{\text{CCP}}(N)$ there is no phase transition but there is a

³⁰ This is, for example, the viewpoint adopted by Hertel and Thirring [31] as recalled in the introduction (see also Sec. XIII).

catastrophic collapse towards a black hole at $\eta_c(N, R)$. When $R > R_{\text{CCP}}(N)$ there is a zeroth order phase transition from the gaseous phase to the condensed phase at $\eta_c(N, R)$ and a catastrophic collapse from the condensed phase to a black hole at $\eta'_c(N, R)$.

In the microcanonical ensemble when $R_{\text{min}}(N) < R < R_{\text{MCP}}(N)$ there is no phase transition but there is a catastrophic collapse towards a black hole at $\Lambda_c(N, R)$. When $R > R_{\text{MCP}}(N)$ there is a zeroth order phase transition from the gaseous phase to the condensed phase at $\Lambda_c(N, R)$ and a catastrophic collapse from the condensed phase to a black hole at $\Lambda''_c(N, R)$.

$$3. \quad N_{\text{CCP}} \simeq N_e < N < N_{\text{MCP}} \simeq N_f$$

In the canonical ensemble, when $R > R_{\text{min}}(N)$ there is no phase transition but there is a catastrophic collapse to a black hole at $\eta_c(N, R)$.

In the microcanonical ensemble, the situation is the same as before.

$$4. \quad N > N_{\text{MCP}}$$

In the canonical ensemble, the situation is the same as before. In the microcanonical ensemble when $R > R_{\text{min}}(N)$ there is no phase transition but there is a catastrophic collapse towards a black hole at $\Lambda_c(N, R)$.

This is essentially like in the classical limit [7, 61].

XI. THE NONRELATIVISTIC AND CLASSICAL LIMITS

In this section, we consider the nonrelativistic ($c \rightarrow +\infty$) and classical ($\hbar \rightarrow 0$) limits and study the commutation of these limits.

A. An apparent paradox related to the commutation of the limits $\hbar \rightarrow 0$ and $c \rightarrow +\infty$

The commutation of the limits $\hbar \rightarrow 0$ and $c \rightarrow +\infty$ leads to an apparent paradox. This can be seen from the expression of the maximum OV particle number given by

$$N_{\text{OV}} = 0.39853 \sqrt{\frac{2}{g}} \left(\frac{\hbar c}{G} \right)^{3/2} \frac{1}{m^3}. \quad (38)$$

(i) If we take the nonrelativistic limit $c \rightarrow +\infty$ first [5], we find that $N_{\text{OV}} \rightarrow +\infty$. Therefore, we always have $N < N_{\text{OV}}$. As a result, there is always an equilibrium state at low temperatures and low energies, whatever the value of \hbar , i.e., even if we consider the classical limit

$\hbar \rightarrow 0$.³¹

(ii) If we take the classical limit $\hbar \rightarrow 0$ first [7, 61], we find that $N_{\text{OV}} \rightarrow 0$. Therefore, we always have $N > N_{\text{OV}}$. As a result, the system undergoes a catastrophic collapse at low temperatures and low energies, whatever the value of c , i.e., even if we consider the nonrelativistic limit $c \rightarrow +\infty$.

Therefore, if we consider a nonrelativistic classical gas ($c \rightarrow +\infty$ and $\hbar \rightarrow 0$), the first argument tells us that there is an equilibrium state at low temperatures and low energies while the second argument tells us that there is no equilibrium state at low temperatures and low energies. How can we reconcile these two apparent contradictory situations? In the next two subsections, we re-express these results in terms of dimensionless variables, and in the third subsection we provide a solution of this apparent paradox.

B. When the nonrelativistic limit $c \rightarrow +\infty$ is taken before the classical limit $\hbar \rightarrow 0$

In this subsection, we consider the situation where the nonrelativistic limit ($c \rightarrow +\infty$) is taken before the classical limit ($\hbar \rightarrow 0$). Using the dimensionless variables of Appendix B, the nonrelativistic limit corresponds to $N \rightarrow 0$ and $R \rightarrow +\infty$ in such a way that NR^3 is fixed.³² This scaling defines an ensemble of parallel lines of constant $\mu = (4\sqrt{2}/\pi)(NR^3)^{1/2}$ in the bottom right panel of Fig. 49. In the nonrelativistic limit, the caloric curves are the same for any couple of points (R, N) belonging to a given μ -line. As μ increases, the μ -lines move to the right and the system becomes more and more classical [5].

The phase transitions occurring in a nonrelativistic self-gravitating Fermi gas have been studied in [5]. When $\mu < \mu_{\text{CCP}} = 83$ there is no phase transition (see Fig. 14 of [5]). When $\mu_{\text{CCP}} = 83 < \mu < \mu_{\text{MCP}} = 2670$ there is a

³¹ In the canonical ensemble, when $\hbar \ll 1$ and $T < T_c$, the equilibrium state corresponds to a fermion ball containing most of the mass. When $\hbar \rightarrow 0$ the fermion ball contains all the mass and its radius goes to zero. In that case, we get a Dirac peak of mass M (see Appendix E 2 a). In the microcanonical ensemble, when $\hbar \ll 1$ and $E < E_c$, the equilibrium state corresponds to a fermion ball containing a fraction of the total mass surrounded by a hot halo. When $\hbar \rightarrow 0$ the mass of the fermion ball and its radius go to zero while its potential energy goes to $-\infty$. As a result, the temperature of the halo goes to $+\infty$. In that case, we get a Dirac peak of zero mass and infinite potential energy (binary) surrounded by an infinitely hot halo (see Appendix E 2 b). Note that for $\hbar > 0$, as small as one pleases, there is always a regular equilibrium state.

³² This scaling is obtained in order to keep the parameter μ defined in [5] fixed (see also Sec. IV B). Coming back to dimensional variables, the nonrelativistic limit corresponds to $N \ll N_{\text{OV}} \sim (\hbar c/G)^{3/2}/m^3$ and $R \gg R_{\text{OV}} \sim (\hbar^3/Gc)^{1/2}/m^2$ with $\mu^2 \sim NR^3 m^9 G^3/\hbar^6$ fixed. This is consistent with the fact that $N_{\text{OV}} \rightarrow +\infty$ and $R_{\text{OV}} \rightarrow 0$ when $c \rightarrow +\infty$.

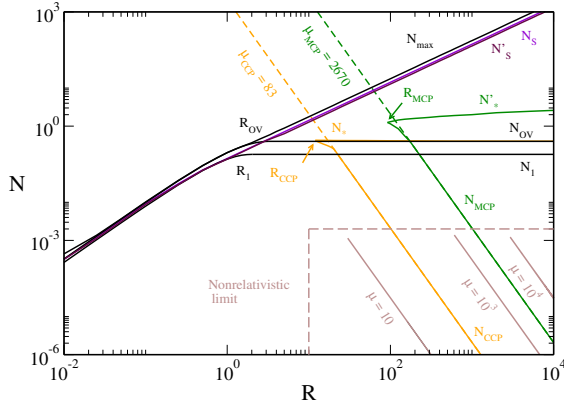


FIG. 49: Lines of constant μ in the (R, N) phase diagram of Fig. 47 characterizing the nonrelativistic limit $N \rightarrow 0$ and $R \rightarrow +\infty$ with fixed $\mu = (4\sqrt{2}/\pi)(NR^3)^{1/2}$. We have chosen $\mu = 10$, $\mu = 10^3$ and $\mu = 10^4$ (brown lines) corresponding to the values appearing in Fig. 14 of [5].

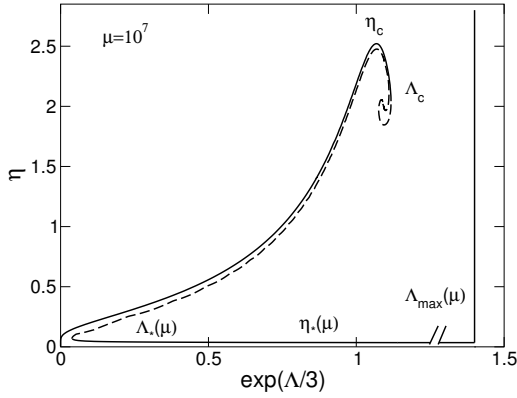


FIG. 50: Caloric curve of nonrelativistic self-gravitating fermions in the classical limit $\mu \rightarrow +\infty$ (here $\mu = 10^7$).

canonical phase transition (see Fig. 31 of [5]). When $\mu > \mu_{\text{MCP}} = 2670$ there are canonical and microcanonical phase transitions (see Fig. 21 of [5]). The classical limit corresponds to $\mu \rightarrow +\infty$ (see Fig. 22 of [5]).

For large but finite values of μ (see Fig. 50), the series of equilibria forms a spiral which finally unwinds, progresses backward along an inverse spiral until $\Lambda_*(\mu)$, turns right, forms a lower branch, and finally tends towards an asymptote at $\Lambda_{\text{max}}(\mu) = 0.0642\mu^{2/3}$ where $\eta \rightarrow +\infty$ (ground state). When $\mu \rightarrow +\infty$, the direct spiral tends to a limit curve ($\eta_c(\mu) \rightarrow 2.52$, $\Lambda_c(\mu) \rightarrow 0.335$), the inverse spiral coincides with the direct spiral, the turning point $\Lambda_*(\mu)$ is pushed towards $-\infty$, the turning point $\eta_*(\mu)$ is pushed towards 0, the lower branch coincides with the x -axis ($\eta = 0$) and the asymptote at $\Lambda_{\text{max}}(\mu)$ is pushed towards $+\infty$. In this limit, we recover the standard nonrelativistic classical caloric curve of Fig. 1 plus a singular branch at $\eta = 0$ corresponding to a Dirac peak of zero mass but infinite potential en-

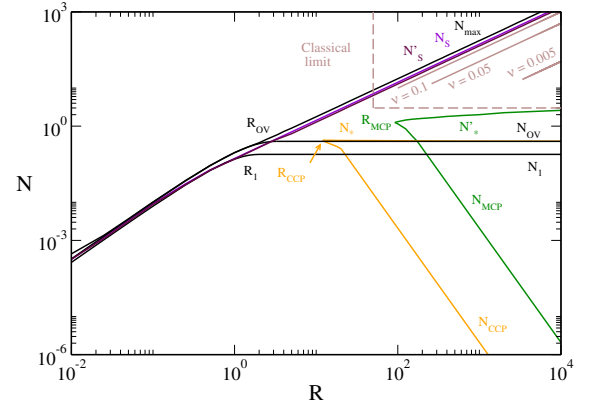


FIG. 51: Lines of constant ν in the (R, N) phase diagram of Fig. 47 characterizing the classical limit $N \rightarrow +\infty$ and $R \rightarrow +\infty$ with fixed $\nu = N/R$. We have chosen $\nu = 0.005$, $\nu = 0.05$ and $\nu = 0.1$ (brown lines) corresponding to the values appearing in Fig. 12 of [7].

ergy surrounded by a halo of infinite temperature, and a singular branch at $\Lambda = \Lambda_{\text{max}} \rightarrow +\infty$ corresponding to a Dirac peak containing all the mass (ground state).

C. When the classical limit $\hbar \rightarrow 0$ is taken before the nonrelativistic limit $c \rightarrow +\infty$

In this section, we consider the situation where the classical limit ($\hbar \rightarrow 0$) is taken before the nonrelativistic limit ($c \rightarrow +\infty$). Using the dimensionless variables of Appendix B, the classical limit corresponds to $N \rightarrow +\infty$ and $R \rightarrow +\infty$ in such a way that N/R is fixed.³³ This scaling defines an ensemble of parallel lines of constant $\nu = N/R$ in the upper right panel of Fig. 51. In the classical limit, the caloric curves are the same for any couple of points (R, N) belonging to a given ν -line. As ν decreases, the ν -lines move to the right and the system becomes less and less relativistic [7, 61].

The classical general relativistic self-gravitating gas has been studied in [7, 61]. When $\nu < \nu'_S = 0.128$ the caloric curve displays a double spiral (see Fig. 7 of [7]). When $\nu'_S = 0.128 < \nu < \nu_S = 0.1415$ the two spirals are truncated (see Fig. 8 of [7]). When $\nu_S = 0.1415 < \nu < \nu_{\text{max}} = 0.1764$ the caloric curve makes a loop (see Fig. 9 of [7]). When $\nu = \nu_{\text{max}} = 0.1764$ the caloric curve reduces to a point and disappears (see Fig. 15 of [7]). There is a gravitational collapse at low

³³ This scaling is obtained in order to keep the parameter ν defined in [7, 61] fixed (see also Sec. IV C). Coming back to dimensional variables, the classical limit corresponds to $N \gg N_{\text{OV}} \sim (\hbar c/G)^{3/2}/m^3$ and $R \gg R_{\text{OV}} \sim (\hbar^3/Gc)^{1/2}/m^2$ with $\nu \sim GNm/Rc^2$ fixed. This is consistent with the fact that $N_{\text{OV}} \rightarrow 0$ and $R_{\text{OV}} \rightarrow 0$ when $\hbar \rightarrow 0$.

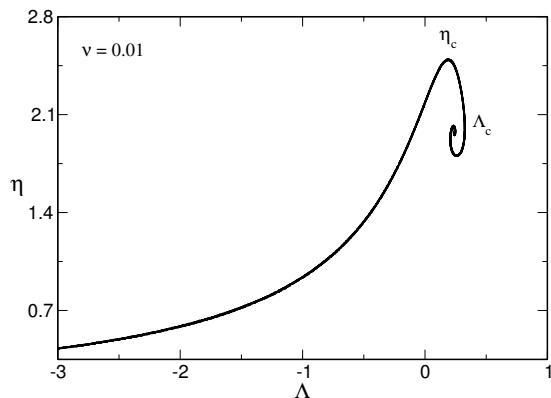


FIG. 52: Caloric curve of classical self-gravitating systems in the nonrelativistic limit $\nu \rightarrow 0$ (here $\nu = 0.01$). This figure zooms on the cold spiral.

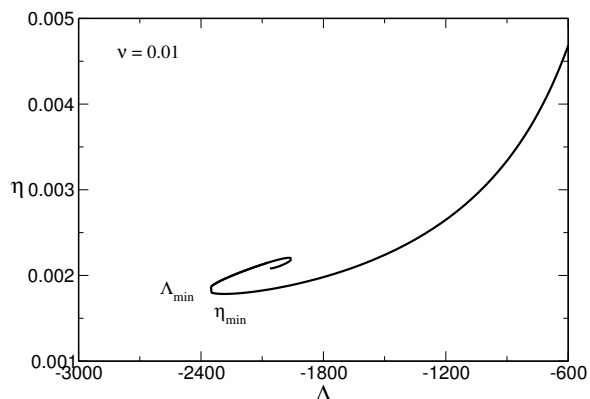


FIG. 53: Caloric curve of classical self-gravitating systems in the nonrelativistic limit $\nu \rightarrow 0$ (here $\nu = 0.01$). This figure zooms on the hot spiral.

energies and low temperatures (cold spiral) and at high energies and high temperatures (hot spiral). The nonrelativistic limit corresponds to $\nu \rightarrow 0$ (see Fig. 12 of [7]).

For small but nonzero values of ν (see Figs. 52 and 53), the series of equilibria forms two spirals very distant to each other. When $\nu \rightarrow 0$, the cold spiral tends to a limit curve ($\eta_c(\nu) \rightarrow 2.52$, $\Lambda_c(\nu) \rightarrow 0.335$) while the hot spiral is rejected to the left at infinity ($\Lambda_{\min}(\nu) \sim -0.24631/\nu^2 \rightarrow -\infty$ and $\eta_{\min}(\nu) \sim 18.27\nu^2 \rightarrow 0$) [7]. In this limit, we recover the standard nonrelativistic classical caloric curve of Fig. 1 plus a spiral at very high energies and very high temperatures ($\Lambda_{\min} \rightarrow -\infty$ and $\eta_{\min} \rightarrow 0$).

D. The solution of the apparent paradox

In the two processes described previously, in which $c \rightarrow +\infty$ and $\hbar \rightarrow 0$, we recover the standard classi-

cal nonrelativistic spiral of Fig. 1. However, the manner to obtain it is different depending on the order in which the limits are taken.

When the nonrelativistic limit $c \rightarrow +\infty$ is taken first, there is no “hot” spiral at Λ_{\min} since the hot spiral is a general relativity result associated with a form of self-gravitating radiation. By contrast, there is always an asymptote at Λ_{\max} corresponding to an equilibrium state at $T = 0$ (the ground state of the Fermi gas) because $N < N_{OV} = +\infty$. In the classical limit $\hbar \rightarrow 0$, the asymptote at Λ_{\max} is rejected at $+\infty$ (while Λ_* is pushed towards $-\infty$ and η_* towards zero) so the caloric curve has the form of a single spiral. For \hbar infinitely small but finite, we get the classical caloric curve plus singular branches $\eta \simeq 0$ (horizontal) and $\Lambda_{\max} \simeq +\infty$ (vertical) as described previously. According to the results of Appendix E, we have the scalings $E_{\min} \propto -\hbar^{-2}$, $E_* \propto \hbar^{-2}(-\ln \hbar)^{-7/3}$ and $T_* \propto \hbar^{-2}(-\ln \hbar)^{-1}$ for $\hbar \rightarrow 0$.

When the classical limit $\hbar \rightarrow 0$ is taken first, there is always a “hot” spiral at Λ_{\min} since the system is relativistic. By contrast, there is no asymptote at Λ_{\max} , i.e., there is no equilibrium state at $T = 0$ (ground state) because $N > N_{OV} = 0$. In the nonrelativistic limit $c \rightarrow +\infty$, the “hot” spiral is rejected at infinity so the caloric curve has the form of a single spiral. For c infinitely large but finite, we get the nonrelativistic caloric curve plus a spiral at very high energies Λ_{\min} and temperatures η_{\min} as described previously. According to the results of [7] (see also footnote 19), we have the scalings $E_{\max} \sim c^4$ and $T_{\max} \sim c^4$ for $c \rightarrow +\infty$.

The previous considerations lead to the following conclusion.

The nonrelativistic limit [5] corresponds to $R \gg R_{OV}$ and $N \ll N_{OV}$. This corresponds to the lower panel QNR of Fig. 54 below N_{OV} . In that case, for a fixed radius R , the caloric curve shows no phase transition below N_{CCP} , a canonical phase transition above N_{CCP} and a microcanonical phase transition (in addition to the canonical phase transition) above N_{MCP} . The classical limit corresponds to $N_{MCP} \ll N \ll N_{OV}$. This corresponds to the lower right panel CNR1 of Fig. 54 (far on the right) below N_{OV} .

The classical limit [7, 61] corresponds to $R \gg R_{OV}$ and $N \gg N_{OV}$. This corresponds to the upper panel CR of Fig. 54 above N_{OV} . In that case, for a fixed radius R , the caloric curve shows a double spiral below N'_S , a truncated double spiral above N'_S , a loop above N_S and no equilibrium states above N_{\max} . The nonrelativistic limit corresponds to $N_{OV} \ll N \ll N'_S$. This corresponds to the upper right panel CNR2 of Fig. 54 (far on the right) above N_{OV} .

Therefore, the nonrelativistic + classical limit corresponds to two distinct regions in the right panel of Fig. 54, below or above N_{OV} , depending on the order in which the limits are taken. Note also that quantum and relativistic effects are *both* important only close to R_{OV} or only close to N_{OV} . This corresponds to the region denoted QR in Fig. 54.

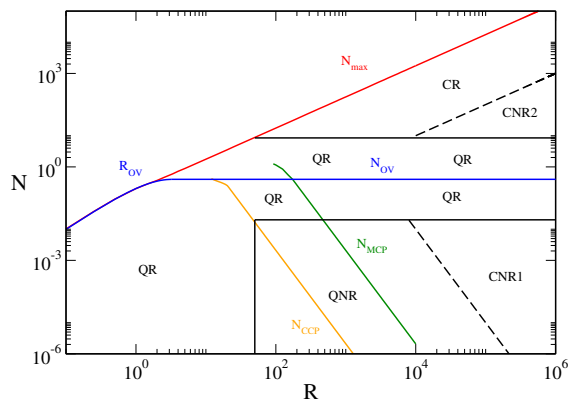


FIG. 54: Schematic representation of the different regimes of the self-gravitating Fermi gas. QR: quantum relativistic; QNR: quantum nonrelativistic; CR: classical relativistic; CNR: classical nonrelativistic (CNR1 is when the nonrelativistic limit $c \rightarrow \infty$ limit is taken before the classical limit $\hbar \rightarrow 0$; CNR2 is when the classical limit $\hbar \rightarrow 0$ is taken before the nonrelativistic limit $c \rightarrow \infty$ limit).

XII. RELATIVISTIC AND QUANTUM CORRECTIONS

A. Relativistic corrections to the nonrelativistic caloric curves

We have seen in Sec. XI B that the nonrelativistic caloric curves of the self-gravitating Fermi gas correspond to parallel lines of constant $\mu = (4\sqrt{2}/\pi)(NR^3)^{1/2}$ in the bottom right panel of Fig. 49. On a line of constant μ , the nonrelativistic limit is valid when $R \rightarrow +\infty$ and $N \rightarrow 0$ (physically $R \gg R_{OV}$ and $N \ll N_{OV}$). For small values of R and large values of N , i.e., at the top of a μ -line, relativistic corrections come into play.

1. $\mu = 10^3$

Let us first consider the case $\mu = 10^3$ corresponding to $\mu_{CCP} = 83 < \mu < \mu_{MCP} = 2670$ (see Figs. 55 and 56). When $N \rightarrow 0$, we recover the nonrelativistic caloric curve plotted in Fig. 31 of [5]. It has a N -shape structure leading to canonical phase transitions. The hot spiral is rejected at infinity. Let us increase the number of particles N at fixed μ , hence decreasing the box radius R accordingly, in order to see the relativistic corrections. The description in the change of the caloric curves as relativistic effects become more and more important is qualitatively similar to that given in Sec. V for $R = 50$ when $N > N_{CCP}$. The only difference is that we work at fixed μ (with $\mu_{CCP} < \mu < \mu_{MCP}$) instead of fixed R (with $R_{CCP} < R < R_{MCP}$). Therefore, in the (R, N) diagram, we follow the $\mu = 10^3$ oblique line (see Fig. 49) instead of the $R = 50$ vertical line (see Fig. 47). As a result, when $N \rightarrow 0$, we tend towards a limit curve (the

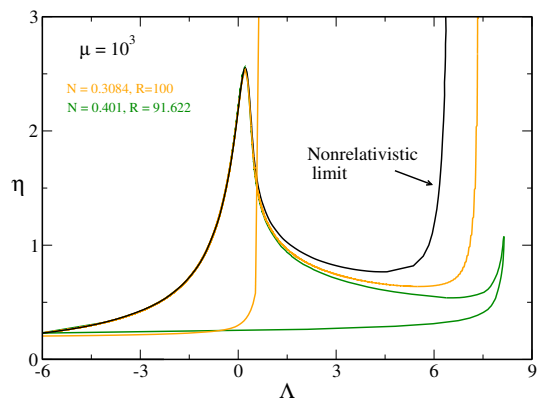


FIG. 55: Caloric curves for different values of N at fixed $\mu = (4\sqrt{2}/\pi)(NR^3)^{1/2} = 10^3$. When $N \rightarrow 0$ (black curve), we recover the nonrelativistic caloric curve with an N -shape structure obtained in Fig. 31 of [5]. The present figure illustrates the effect of general relativity on that caloric curve as N increases.

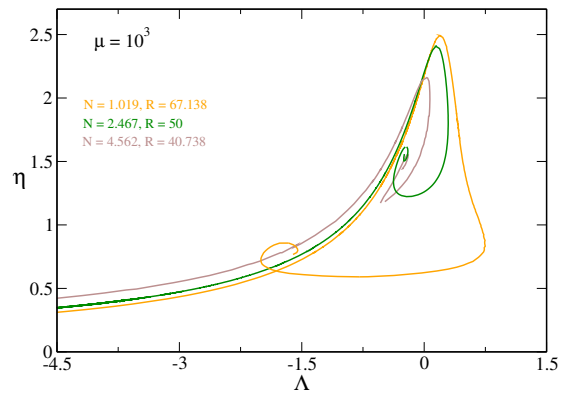


FIG. 56: Same as Fig. 55 for larger values of N .

nonrelativistic caloric curve with $\mu = 10^3$ of [5]) which presents a canonical phase transition while in the case $R = 50$ studied in Sec. V the canonical phase transition disappears when $N < N_{CCP}$.

Remark: The characteristic particle numbers N_X described in Sec. X A now depend on μ instead of R . They can be obtained by considering the intersection between the curves $N_X(R)$ and the curve $N = \pi^2 \mu^2 / (32R^3)$ with fixed μ . In this manner, we obtain $N'_S(\mu) = 0.159\sqrt{\mu}$, $N_S(\mu) = 0.172\sqrt{\mu}$, and $N_{max}(\mu) = 0.203\sqrt{\mu}$.

2. $\mu = 10^5$

Let us now consider the case $\mu = 10^5$ corresponding to $\mu > \mu_{MCP} = 2670$ (see Figs. 57-59). When $N \rightarrow 0$, we recover the nonrelativistic caloric curve plotted in Fig. 21 of [5]. It has a Z -shape structure leading to microcanon-

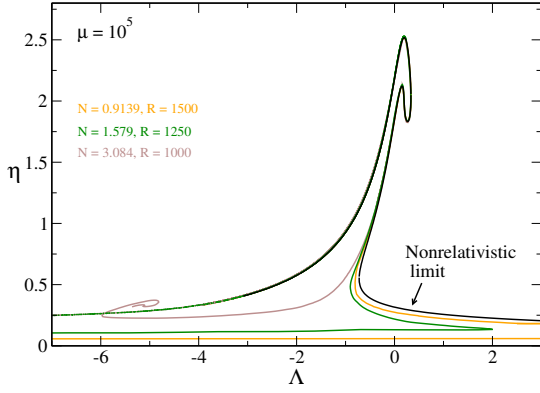


FIG. 57: Caloric curves for different values of N at fixed $\mu = (4\sqrt{2}/\pi)(NR^3)^{1/2} = 10^5$. When $N \rightarrow 0$ (black curve), we recover the nonrelativistic caloric curve with a Z-shape structure obtained in Fig. 21 of [5]. The present figure illustrates the effect of general relativity on that caloric curve as N increases.

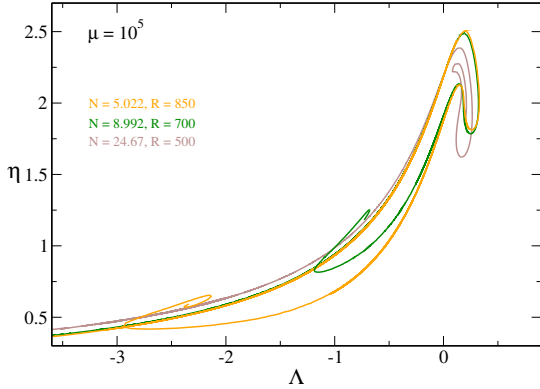


FIG. 58: Same as Fig. 57 for larger values of N .

ical phase transitions.³⁴ The vertical asymptote at Λ_{\max} is outside of the frame. The hot spiral is rejected at infinity. Let us increase the number of particles N at fixed μ , hence decreasing the box radius R accordingly, in order to see the relativistic corrections. The description in the change of the caloric curves as relativistic effects become more and more important is qualitatively similar to that given in Sec. VI for $R = 600$ when $N > N_{\text{MCP}}$. The only difference is that we work at fixed μ (with $\mu > \mu_{\text{MCP}}$) instead of fixed R (with $R > R_{\text{MCP}}$). Therefore, in the (R, N) diagram, we follow the $\mu = 10^5$ oblique line (see Fig. 49) instead of the $R = 600$ vertical line (see Fig. 47). As a result, when $N \rightarrow 0$, we tend towards a limit curve (the nonrelativistic caloric curve with $\mu = 10^5$ of [5]) which presents a microcanonical phase transition while

³⁴ The resemblance with a dinosaur's neck is clear on this figure [5].

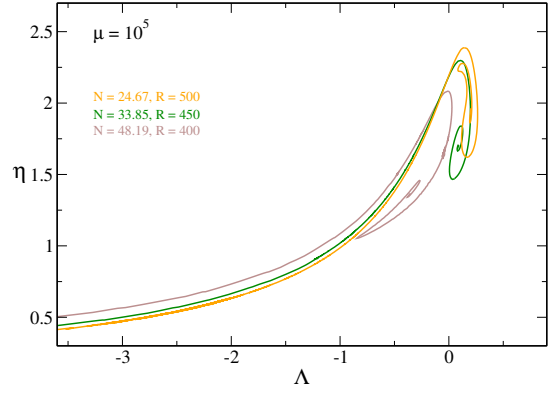


FIG. 59: Same as Figs. 57 and 58 for larger values of N .

in the case $R = 600$ studied in Sec. VI the microcanonical phase transition disappears when $N < N_{\text{MCP}}$.

B. Quantum corrections to the classical caloric curve

We have seen in Sec. XIC that the classical caloric curves of the general relativistic self-gravitating gas correspond to parallel lines of constant $\nu = N/R$ in the upper right panel of Fig. 51. On a line of constant ν , the classical limit is valid when $R \rightarrow +\infty$ and $N \rightarrow +\infty$ (physically $R \gg R_{\text{OV}}$ and $N \gg N_{\text{OV}}$). For small values of R and small values of N , i.e., on the left of a ν -line, quantum corrections come into play.

Let us consider the case $\nu = 0.1$ (see Figs. 60 and 61). When $N \rightarrow +\infty$ (black curve) we recover the classical general relativistic caloric curve plotted in Fig. 1 of [7]. It has the form of a double spiral leading to a gravitational collapse for both cold and hot systems.³⁵ Let us decrease the number of particles N at fixed ν , hence decreasing the box radius R accordingly, in order to see the quantum corrections. When $N > N_{\text{OV}} = 0.39853$ (blue and green curves), the caloric curve keeps a similar structure. When $N_1 = 0.18131 < N < N_{\text{OV}} = 0.39853$ (red curve) the caloric curve is made of two branches, each presenting an asymptote (right) and a spiral (left). When $N < N_1 = 0.18131$ (purple curve) the caloric curve has just one branch presenting an asymptote (right) and a spiral (left).

Remark: For smaller values of ν ,³⁶ we have a richer

³⁵ When $N \rightarrow +\infty$ the caloric curves of Fig. 60 and 61 tend towards a limit curve (the classical general relativistic caloric curve with $\nu = 0.1$ of [7]) which presents a double spiral while in the cases studied in Secs. V-IX the two spirals merge and disappear when $N \rightarrow N_{\text{max}}$. This is because in Secs. V-IX we work at fixed radius R while in the present case we work at fixed ν so that the radius R increases as N increases.

³⁶ This case is specifically investigated in [66].

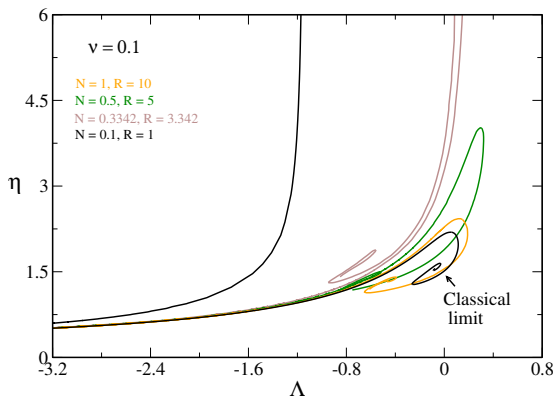


FIG. 60: Caloric curves for different values of N at fixed $\nu = N/R = 0.1$. When $N \rightarrow +\infty$ (black curve), we recover the classical caloric curve with a double spiral obtained in Fig. 1 of [7]. The present figure illustrates the effect of quantum mechanics on that caloric curve as N decreases. This figure is focused on the evolution of the cold spiral.

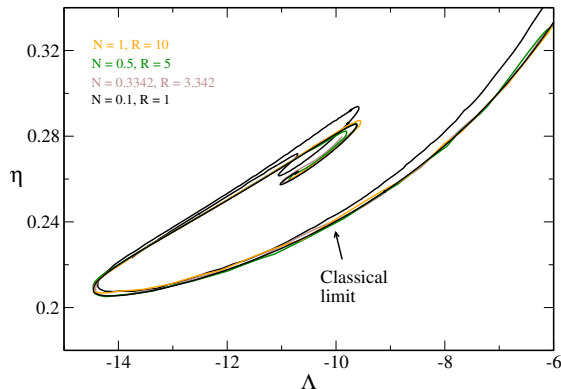


FIG. 61: Same as Fig. 60. This figure is focused on the evolution of the hot spiral.

variety of caloric curves as N decreases with the appearance of canonical and microcanonical phase transitions. This can be seen on the phase diagram of Fig. 51. The characteristic particle numbers N_X described in Sec. X A now depend on ν instead of R . They can be obtained by considering the intersection between the curves $N_X(R)$ and the line $N = \nu R$. In this manner, we obtain $N_{\text{CCP}}(\nu) = 6.79\nu^{3/4}$ and $N_{\text{MCP}}(\nu) = 38.5\nu^{3/4}$. There is no microcanonical phase transition for $\nu > \nu_{\text{MCP}} = 0.0136$ and there is no canonical phase transition for $\nu > \nu_{\text{CCP}} = 0.0353$.

XIII. ASTROPHYSICAL APPLICATIONS

A. Nonrelativistic model: collapse towards a fermion star

In this section, we discuss astrophysical applications of the nonrelativistic self-gravitating Fermi gas model [5]. This model exhibits a phase transition from a gaseous star to a compact fermion star. The fermion star can be a white dwarf, a neutron star or a DM fermion ball.³⁷ We relate this phase transition to the onset of red-giant structure and to the supernova phenomenon.

1. Canonical ensemble

Let us consider a system of nonrelativistic self-gravitating fermions in the canonical ensemble. The canonical phase transition appears for $\mu \geq \mu_{\text{CCP}} = 83$ (canonical critical point) [5] hence for

$$R \geq R_{\text{CCP}}^{\text{NR}}(N) = 0.517 \frac{h^2}{Gm^{8/3}M^{1/3}g^{2/3}}. \quad (39)$$

We assume that we are in this situation. In that case, the caloric curve has the form of Fig. 5. The natural evolution proceeds along the series of equilibria towards lower and lower temperatures (see Sec. III). We assume that the system is initially in the metastable gaseous phase. As its temperature decreases it remains in this phase up to the critical point T_c at which the metastable gaseous branch disappears.³⁸ This critical temperature is not very sensitive on quantum effects (when $\mu \gg 1$) so it can be approximated by its classical value $\eta_c = \beta_c GMm/R = 2.52$ yielding

$$k_B T_c = 0.397 \frac{GMm}{R}. \quad (40)$$

At that point, the system collapses and forms a compact fermion star. As explained in Appendix E 2 a, in the canonical ensemble, the fermion star contains almost all the mass ($M_C \simeq M$) and is surrounded by a tenuous atmosphere. If we approximate the fermion star by a Fermi gas at $T = 0$ (polytrope of index $n = 3/2$) containing all the mass, its radius is given by (see Appendix E 2 a):

$$R_C = 0.181 \frac{h^2}{Gm^{8/3}M^{1/3}g^{2/3}}. \quad (41)$$

The energy of the gaseous phase at the point of isothermal collapse is not very sensitive on quantum effects

³⁷ In this section we take $g = 2$ in the numerical applications.

³⁸ We recall that the collapse takes place at the critical (spinodal) point T_c , not at the transition point T_t , because of the tremendously long lifetime of metastable gaseous states.

(when $\mu \gg 1$) so it can be approximated by its classical value $\Lambda_{\text{gas}} = -E_{\text{gas}}R/GM^2 = 0.199$ yielding

$$E_{\text{gas}} = -0.199 \frac{GM^2}{R}. \quad (42)$$

The energy of the condensed object can be approximated by its value at $T = 0$ yielding (see Appendix E 2 a):

$$E_{\text{min}} = -2.36 \frac{G^2 m^{8/3} M^{7/3} g^{2/3}}{h^2}. \quad (43)$$

Finally, the collapse time in the canonical ensemble is of the order of the dynamical time

$$t_D \sim \frac{R^{3/2}}{(GM)^{1/2}}. \quad (44)$$

We note that the collapse in the canonical ensemble corresponds to a pure implosion since almost all the mass is in the condensate (fermion star), not in the halo. The thermodynamical reason for this implosion phenomenon is explained in Appendix E 1. It is also corroborated by the following arguments. If we calculate the density perturbation $\delta\rho$ that triggers the instability at T_c , we find that it has only one node (see Fig. 10 of [57]). Therefore, the instability develops itself in such a way that the density in the core increases while the density in the halo decreases. We also find that the velocity profile δv has no node (see Fig. 12 of [57]) so that it is purely inward. These two results confirm the implosion phenomenon.

We make below numerical applications to illustrate the preceding results. They correspond to the nonrelativistic models of neutron stars (made of neutrons of mass $m_n = 0.940 \text{ GeV}/c^2$) and dark matter halos (made of fermions of mass $m = 17.2 \text{ keV}/c^2$) respectively studied by Hertel and Thirring [31] and Bilic and Viollier [39] as recalled in the Introduction.

Neutron stars (crude model) [31]: We consider a gas of neutrons of total mass $M = 1 M_\odot$.³⁹ It contains about $N \sim 10^{57}$ neutrons. The canonical phase transition appears for $R \geq R_{\text{CCP}}^{\text{NR}}(N) = 43.1 \text{ km}$. For a gaseous star of size $R = 100 \text{ km}$, corresponding to $\mu = 294$, the collapse temperature is $T_c = 6.39 \times 10^{10} \text{ K}$ (the transition temperature is $T_t = 7.03 \times 10^{10} \text{ K}$ [31]). The radius of the neutron star of mass $M_C \simeq 1 M_\odot$ resulting from the collapse of the gaseous star is $R_C = 15.1 \text{ km}$. The energy of the gaseous star is $E_{\text{gas}} = -5.25 \times 10^{51} \text{ erg}$ and the energy of the neutron star is $E_{\text{min}} = -7.49 \times 10^{52} \text{ erg}$. The energy released during the collapse is $\Delta E = E_{\text{gas}} -$

$E_{\text{min}} = 6.96 \times 10^{52} \text{ erg}$. The collapse time is a multiple of $t_D \sim 2.74 \times 10^{-3} \text{ s}$ which is very short on an astrophysical timescale.⁴⁰

Fermion ball [39]: We consider a gas of DM fermions of total mass $M = 10 M_\odot$.⁴¹ The canonical phase transition appears for $R \geq R_{\text{CCP}}^{\text{NR}}(N) = 2.78 \text{ pc}$. For a gaseous halo of size $R = 41.3 \text{ pc}$, corresponding to $\mu = 4747$, the collapse temperature is $T_c = 9.18 \times 10^{-7} \text{ K}$ (the transition temperature is $T_t = 2.83 \times 10^{-6} \text{ K}$ [39]). The radius of the fermion ball of mass $M_C \simeq 10 M_\odot$ resulting from the collapse of the gaseous halo is $R_C = 0.974 \text{ pc}$. The energy of the gaseous halo is $E_{\text{gas}} = -4.12 \times 10^{40} \text{ erg}$ and the energy of the fermion ball is $E_{\text{min}} = -3.76 \times 10^{42} \text{ erg}$. The energy released during the collapse is $\Delta E = E_{\text{gas}} - E_{\text{min}} = 3.72 \times 10^{42} \text{ erg}$. The collapse time is a multiple of $t_D \sim 1.25 \text{ Gyrs}$ which is quite long (possibly irrelevant).

Supermassive fermion ball (crude model) [39]: We consider a gas of DM fermions of total mass $M = 10^9 M_\odot$.⁴² The canonical phase transition appears for $R \geq R_{\text{CCP}}^{\text{NR}}(N) = 6.00 \times 10^{-3} \text{ pc}$. For a gaseous halo of size $R = 1.68 \times 10^{-2} \text{ pc}$, corresponding to $\mu = 389$, the collapse temperature is $T_c = 2.26 \times 10^5 \text{ K}$ (the transition temperature is $T_t = 3.02 \times 10^5 \text{ K}$ [39]). The radius of the fermion ball of mass $M_C \simeq 10^9 M_\odot$ resulting from the collapse of the gaseous halo is $R_C = 2.10 \times 10^{-3} \text{ pc}$. The energy of the gaseous halo is $E_{\text{gas}} = -1.01 \times 10^{60} \text{ erg}$ and the energy of the fermion ball is $E_{\text{min}} = -1.74 \times 10^{61} \text{ erg}$. The energy released during the collapse is $\Delta E = E_{\text{gas}} - E_{\text{min}} = 1.64 \times 10^{61} \text{ erg}$. The collapse time is a multiple of $t_D \sim 1.03 \text{ yrs}$, which is very short on a cosmological timescale.

2. Microcanonical ensemble

We now consider a system of nonrelativistic self-gravitating fermions in the microcanonical ensemble.

³⁹ The maximum mass and minimum radius of an ideal neutron star set by general relativity are $M_{\text{OV}} = 0.710 M_\odot$ and $R_{\text{OV}} = 9.16 \text{ km}$. Therefore, the value of the mass chosen by [31] is larger than the maximum mass. If general relativity were taken into account (see below) the system would not form a neutron star but would collapse towards a black hole (assuming that all the initial mass goes in the compact object).

⁴⁰ Note that the prefactor of the collapse time is uncertain and could be of order 10^3 or larger. As a result, our estimate of the collapse time is not inconsistent with the duration of the supernova phenomenon which can be as short as a few seconds. For supernovae, the energy ΔE may be carried quickly by neutrinos. The release of gravitational energy in a supernova ($W \sim GM^2/R \sim Nmc^2$) is comparable with the energy of fusion processes which kept the star shining during the first 10^{10} years of its life. However, this takes place in a few seconds (or days) instead of 10^{10} years leading to a huge luminosity. This explains why a star can become as bright as the whole galaxy.

⁴¹ This is the typical mass of a DM halo surrounding a baryonic star of mass $\sim 1 M_\odot$ since the present fraction of baryons and dark matter are $\Omega_{\text{b},0} = 0.0487273$ and $\Omega_{\text{dm},0} = 0.2645$ respectively. Here and in the following we consider DM fermions of mass $m = 17.2 \text{ keV}/c^2$. The maximum mass and minimum radius set by general relativity are $M_{\text{OV}} = 2.12 \times 10^9 M_\odot$ and $R_{\text{OV}} = 8.86 \times 10^{-4} \text{ pc}$. Since $M \ll M_{\text{OV}}$, the nonrelativistic model is justified in that case.

⁴² In that case, general relativity should be taken into account (see below) since $M \sim M_{\text{max}}$.

The microcanonical phase transition appears for $\mu \geq \mu_{\text{MCP}} = 2670$ (microcanonical critical point) [5] hence for

$$R \geq R_{\text{MCP}}^{\text{NR}}(N) = 5.22 \frac{h^2}{Gm^{8/3}M^{1/3}g^{2/3}}. \quad (45)$$

We assume that we are in this situation.⁴³ In that case, the caloric curve has the form of Fig. 27. The natural evolution proceeds along the series of equilibria towards lower and lower energies (see Sec. III). We assume that the system is initially in the metastable gaseous phase. As its energy decreases it remains in this phase up to the critical point E_c at which the metastable gaseous branch disappears.⁴⁴ This critical energy is not very sensitive on quantum effects (when $\mu \gg 1$) so it can be approximated by its classical value $\Lambda_c = -E_c R/GM^2 = 0.335$ yielding

$$E_c = -0.335 \frac{GM^2}{R}. \quad (46)$$

At that point, the system collapses and forms a compact fermion star. As explained in Appendix E 2 b, in the microcanonical ensemble, the fermion star contains only a fraction of the total mass ($M_C < M$) and is surrounded by a massive and very hot atmosphere. If we approximate the fermion star by a Fermi gas at $T = 0$ containing a mass $M_C = \alpha_C M$, its radius is given by (see Appendix E 2 b):

$$R_C = 0.181 \frac{h^2}{Gm^{8/3}\alpha_C^{1/3}M^{1/3}g^{2/3}}. \quad (47)$$

On the other hand, the temperature of the halo in the condensed phase is given by (see Appendix E 2 b):

$$k_B T_{\text{cond}} = 1.57 \frac{\alpha_C^{7/3}}{1 - \alpha_C} \frac{G^2 M^{4/3} m^{11/3} g^{2/3}}{h^2}. \quad (48)$$

From the analytical model developed in [41] one finds that the fraction of mass in the core is approximately given by (see Appendix E 2 b):

$$\alpha_C \simeq \frac{7}{4 \ln \mu}. \quad (49)$$

In many applications, it is sufficient to consider that $\alpha_C \simeq 1/4$ (see footnote 45). The temperature of the gaseous phase at the point of gravothermal catastrophe is not very sensitive on quantum effects (when $\mu \gg 1$)

so it can be approximated by its classical value $\eta_{\text{gas}} = \beta_{\text{gas}} GMm/R = 2.03$ yielding

$$k_B T_{\text{gas}} = 0.493 \frac{GMm}{R}. \quad (50)$$

The relaxation time depends on the physical process governing the dynamical evolution of the system so it will not be discussed here.

We note that the collapse in the microcanonical ensemble corresponds to an implosion of the core and a heating of the halo. In the box model, the atmosphere is held by the walls of the box. Without the box, it would be expelled at large distances (see Figs. 38 and 41 of [14] for an illustration in the context of the fermionic King model). Therefore, in the microcanonical ensemble, the collapse leads to the formation of a fermion star and to the expulsion of a hot atmosphere. This core-halo structure is reminiscent of the onset of a red-giant before the white dwarf stage. The implosion of the core and the explosion of the halo is also similar to the supernova phenomenon leading to the formation of a neutron star. These ideas are further developed and illustrated in [38]. The thermodynamical reason for this implosion-explosion phenomenon is explained in Appendix E 1 b. It is also corroborated by the following arguments. If we calculate the density perturbation $\delta\rho$ that triggers the instability at E_c , we find that it has two nodes, corresponding to a core-halo structure (see Fig. 6b of [56]). Therefore, the instability develops itself in such a way that the density increases in the core and in the halo while it decreases between them (the intermediate shell is depopulated). We also find that the velocity profile δv has one node (see Fig. 4.b of [38]) so the velocity is directed inward in the core and outward in the halo. These two results confirm the implosion-explosion phenomenon similar to the red-giant structure and to the supernova phenomenon previously described.

We make below numerical applications to illustrate the preceding results.⁴⁵

Neutron stars (crude model) [31]: We consider a gas of neutrons of total mass $M = 1 M_\odot$. The microcanonical phase transition appears for $R \geq R_{\text{MCP}}^{\text{NR}}(N) = 435 \text{ km}$. For a gaseous star of size $R = 4875 \text{ km}$ the collapse energy is $E_c = -1.81 \times 10^{50} \text{ erg}$ (the transition energy is $E_t = 1.51 \times 10^{50} \text{ erg}$). The mass of the neutron star resulting from the collapse of the gaseous star is $M_C = 0.220 M_\odot$ and its radius is $R_C = 25.0 \text{ km}$. The temperature of the gaseous star is $T_{\text{gas}} = 1.63 \times 10^9 \text{ K}$ and the temperature

⁴³ When $R \leq R_{\text{MCP}}^{\text{NR}}(N)$ the whole series of equilibria is stable. When $R_{\text{CCP}}^{\text{NR}}(N) \leq R \leq R_{\text{MCP}}^{\text{NR}}(N)$ the system evolves, as energy decreases, from the gaseous states to the core-halo states (with a negative specific heat) without instability or phase transition.

⁴⁴ We recall that the collapse takes place at the critical (spinodal) point E_c , not at the transition point E_t , because of the tremendously long lifetime of metastable gaseous states.

⁴⁵ In the numerical applications, we have chosen the values of M and R in order to have $\mu = 10^5$. From Fig. 21 of [5] we find that $\eta_{\text{cond}} = 0.290$. From the relation $\eta_{\text{cond}} \sim 7(1 - \alpha_C)/(2\lambda\mu^{2/3}\alpha_C^{7/3})$ with $\lambda = 0.149736\dots$, equivalent to Eq. (48), we find that $\alpha_C = 0.220$. This can be compared to the approximate value $\alpha_C \simeq 0.125$ obtained from Eq. (49). The agreement is reasonable in view of the numerous approximations and the logarithmic corrections.

of the halo surrounding the neutron star is $T_{\text{cond}} = 1.14 \times 10^{10}$ K.

Fermion ball [39]: We consider a gas of DM fermions of total mass $M = 10 M_{\odot}$. The microcanonical phase transition appears for $R \geq R_{\text{MCP}}^{\text{NR}}(N) = 28.1$ pc. For a gaseous halo of size $R = 315$ pc the collapse energy is $E_c = -9.10 \times 10^{39}$ erg (the transition energy is $E_t = 7.61 \times 10^{39}$ erg). The mass of the fermion ball resulting from the collapse of the gaseous halo is $M_C = 2.20 M_{\odot}$ and its radius is $R_C = 1.61$ pc. The temperature of the gaseous halo is $T_{\text{gas}} = 1.50 \times 10^{-7}$ K and the temperature of the halo surrounding the fermion ball is $T_{\text{cond}} = 1.05 \times 10^{-6}$ K.

Supermassive fermion ball (crude model) [39]: We consider a gas of DM fermions of total mass $M = 10^9 M_{\odot}$. The microcanonical phase transition appears for $R \geq R_{\text{MCP}}^{\text{NR}}(N) = 6.06 \times 10^{-2}$ pc. For a gaseous halo of size $R = 0.679$ pc the collapse energy is $E_c = -4.22 \times 10^{58}$ erg (the transition energy is $E_t = 3.53 \times 10^{58}$ erg). The mass of the fermion ball resulting from the collapse of the gaseous halo is $M_C = 2.20 \times 10^8 M_{\odot}$ and its radius is $R_C = 3.48 \times 10^{-3}$ pc. The temperature of the gaseous halo is $T_{\text{gas}} = 6.94 \times 10^3$ K and the temperature of the halo surrounding the fermion ball is $T_{\text{cond}} = 4.86 \times 10^4$ K.

B. Relativistic model with $N < N_{\text{OV}}$: Collapse towards a fermion star

We now consider the truly general relativistic Fermi gas model. We first assume that $N < N_{\text{OV}}$ so that the collapse always leads to a fermion star (not a black hole). The discussion is essentially the same as before. However, we make below new numerical applications to see the effect of relativistic corrections when $N \lesssim N_{\text{OV}}$. These numerical applications are based on the general relativistic models of dark matter halos studied by Bilic and Viollier [47] as recalled in the Introduction.⁴⁶ We consider their adaptation to the case of neutron stars. We restrict ourselves to the canonical ensemble.

Supermassive fermion ball [47]: For a fermionic particle of mass $m = 17.2$ keV/c² the OV limits are $N_{\text{OV}} = 1.4254 \times 10^{71}$, $N_{\text{OV}}m = 2.1973 \times 10^9 M_{\odot}$, $M_{\text{OV}} = 2.1186 \times 10^9 M_{\odot}$ and $R_{\text{OV}} = 8.8859 \times 10^{-4}$ pc. We consider a gas of $N = 0.95350 N_{\text{OV}}$ fermions, corresponding to a rest mass $Nm = 2.0951 \times 10^9 M_{\odot}$. According to Fig. 47, the canonical phase transition appears for $R \geq R_{\text{CCP}}(N) = 3.93 R_{\text{OV}} = 3.4818 \times 10^{-3}$ pc (the nonrelativistic value is $R_{\text{CCP}}^{\text{NR}}(N) = 4.6894 \times 10^{-3}$ pc). For a system of initial size $R = 29.789 R_{\text{OV}} = 2.6391 \times 10^{-2}$ pc,

the collapse temperature is $T_c = 3.0112 \times 10^5$ K (the transition temperature is $T_t = 0.0043951 mc^2 = 8.7725 \times 10^5$ K [47]). The collapse of the gaseous halo leads to a supermassive fermion ball containing almost all the particles surrounded by a tenuous atmosphere. Since the particle number is slightly below the OV limit, the fermion ball is strongly relativistic. If we approximate the fermion ball by a Fermi gas at $T = 0$ containing all the rest mass $Nm \sim 2.0951 \times 10^9 M_{\odot}$, we find a radius $R_C = 1.220 R_{\text{OV}} = 1.0809 \times 10^{-3}$ pc and a mass $M_C = 0.9577 M_{\text{OV}} = 2.0290 \times 10^9 M_{\odot}$ [6] (the nonrelativistic values are $R_C^{\text{NR}} = 1.6399 \times 10^{-3}$ pc and $M_C^{\text{NR}} = 2.0951 \times 10^9 M_{\odot}$). The energy of the gaseous halo is $E_{\text{gas}} = -2.8324 \times 10^{60}$ erg and the energy of the fermion ball is $E_{\text{min}} = (M_C - Nm)c^2 = -1.1822 \times 10^{62}$ erg (the nonrelativistic value is $E_{\text{min}}^{\text{NR}} = -9.7925 \times 10^{61}$ erg). The energy released during the collapse is $\Delta E = E_{\text{gas}} - E_{\text{min}} = 1.1539 \times 10^{62}$ erg (the nonrelativistic value is $\Delta E^{\text{NR}} = 9.5092 \times 10^{61}$ erg). The collapse time is a multiple of $t_D \sim 1.3973$ yrs.

Neutron stars: For the neutrons of mass $m_n = 0.940$ GeV/c², the OV limits are $N_{\text{OV}} = 8.7448 \times 10^{56}$, $N_{\text{OV}}m = 0.73636 M_{\odot}$, $M_{\text{OV}} = 0.71000 M_{\odot}$ and $R_{\text{OV}} = 9.1614$ km. We consider a gas of $N = 0.95350 N_{\text{OV}}$ neutrons, corresponding to a rest mass $Nm = 0.70212 M_{\odot}$. The canonical phase transition appears for $R \geq R_{\text{CCP}}(N) = 3.93 R_{\text{OV}} = 36.0$ km (the nonrelativistic value is $R_{\text{CCP}}^{\text{NR}}(N) = 48.5$ km). For a system of initial size $R = 29.789 R_{\text{OV}} = 272.91$ km, the collapse temperature is $T_c = 1.6449 \times 10^{10}$ K (the transition temperature is $T_t = 0.0043951 mc^2 = 4.7921 \times 10^{10}$ K). The collapse of the gaseous star leads to a neutron star containing almost all the particles surrounded by a tenuous atmosphere. Since the particle number is slightly below the OV limit, the system is strongly relativistic. If we approximate the neutron star by a Fermi gas at $T = 0$ containing all the rest mass $Nm \sim 0.70212 M_{\odot}$, we find a radius $R_C = 1.220 R_{\text{OV}} = 11.177$ km and a mass $M_C = 0.9577 M_{\text{OV}} = 0.67996 M_{\odot}$ (the nonrelativistic values are $R_C^{\text{NR}} = 16.957$ km and $M_C^{\text{NR}} = 0.70212 M_{\odot}$). The energy of the gaseous star is $E_{\text{gas}} = -9.4919 \times 10^{50}$ erg and the energy of the neutron star is $E_{\text{min}} = (M_C - Nm)c^2 = -3.9618 \times 10^{52}$ erg (the nonrelativistic value is $E_{\text{min}}^{\text{NR}} = -3.28167 \times 10^{52}$ erg). The energy released during the collapse is $\Delta E = E_{\text{gas}} - E_{\text{min}} = 3.8669 \times 10^{52}$ erg (the nonrelativistic value is $\Delta E^{\text{NR}} = 3.1867 \times 10^{52}$ erg). The collapse time is a multiple of $t_D \sim 1.4767 \times 10^{-2}$ s.

Remark: For the value of N considered in the previous examples, we find from Fig. 47 that the microcanonical phase transition appears for $R \geq R_{\text{MCP}}(N) = 52.4 R_{\text{OV}}$ (the nonrelativistic value is $R_{\text{MCP}}^{\text{NR}}(N) = 53.4 R_{\text{OV}}$). Since R is below this critical value, the system does not display any phase transition in the microcanonical ensemble.

⁴⁶ In terms of the dimensionless variables defined in Appendix B they take $N = 0.38$, which is slightly below the OV limit $N_{\text{OV}} = 0.39853$, and $R = 100$. The radius of the completely degenerate fermion ball corresponding to $N = 0.38$ is $R_C = 4.095 = 1.22 R_{\text{OV}}$ [6].

C. Relativistic model with $N_{OV} < N < N_c$: Collapse towards a fermion star followed by a collapse towards a black hole

We now assume that $N_{OV} < N < N_c$ (where $N_c^{CE} = N_e$ and $N_c^{MCE} = N_f$) so that, by cooling, the system undergoes two successive collapses: a collapse towards a fermion star followed by a collapse towards a black hole.

We consider a system of relativistic self-gravitating fermions in the canonical ensemble. We assume that $N_{OV} < N < N_e(R)$. The caloric curve has the form of Fig. 9. We assume that the system is initially in the gaseous phase. At its temperature decreases, the system collapses from the gaseous phase to the condensed phase at T_c then undergoes a catastrophic collapse from the condensed phase to a black hole at T'_c . We note that the interval $(\Delta N)_{CE} = N_e(R) - N_{OV}$ is extremely narrow since $N_{OV} = 0.39853$ and $N_e = 0.40002$ for $R = 50$ (we see in Fig. 47 that $N_e(R)$ does not change much with R). We have $(\Delta N)_{CE}/N_{OV} = 3.81 \times 10^{-3} \ll 1$ so that

$$N_c^{CE} \simeq N_{OV}. \quad (51)$$

The reason why $(\Delta N)_{CE}/N_{OV} \ll 1$ is easy to understand. We have previously explained that the fermion star contains almost all the particles ($N_C \sim N$). Therefore, as soon as N is larger than N_{OV} the fermion star becomes unstable ($N_C > N_{OV}$) and collapses towards a black hole (see Appendix G).

We consider a system of relativistic self-gravitating fermions in the microcanonical ensemble. We assume that $N_{OV} < N < N_f(R)$. The caloric curve has the form of Fig. 29. We assume that the system is initially in the gaseous phase. At its energy decreases, the system collapses from the gaseous phase to the condensed phase at E_c then undergoes a catastrophic collapse from the condensed phase to a black hole at E'_c . The interval $(\Delta N)_{MCE} = N_f(R) - N_{OV}$ is much larger than in the canonical ensemble since $N_{OV} = 0.39853$ and $N_f \simeq 1.4854$ for $R = 600$ (we see in Fig. 47 that $N_f(R)$ remains in the range 1 – 2). We have $(\Delta N)_{MCE}/N_{OV} = 2.73$ so that

$$N_c^{MCE} \simeq 3.73 N_{OV}. \quad (52)$$

Again, the reason why $(\Delta N)_{MCE}/N_{OV} \sim 1$ is easy to understand. We have previously explained that the fermion star contains only a fraction of the particles ($N_C \sim N/4$). Therefore, if N is only slightly larger than N_{OV} , the fermion ball is stable ($N_C < N_{OV}$). It is only when N is substantially larger than N_{OV} (by a factor of ~ 4) that the fermion ball becomes unstable ($N_C > N_{OV}$) and collapses towards a black hole.

D. Relativistic model with $N > N_c$: Direct collapse towards a black hole

We finally assume that $N > N_c$ so that, by cooling, the system directly collapses towards a black hole, without

forming a fermion star.

We consider a system of relativistic self-gravitating fermions in the canonical ensemble. We assume that $N > N_e(R)$. The caloric curve has the form of Figs. 16, 18, 20, 21, and 22. We assume that the system is initially in the gaseous phase. As its temperature decreases, the system undergoes a catastrophic collapse from the gaseous phase to a black hole at T_c . This situation corresponds to $N > N_c^{CE}$, where $N_c^{CE} \simeq N_{OV}$ [see Eq. (51)]. This result shows that, in the canonical ensemble, there is no condensed configurations in the general relativistic Fermi gas at nonzero temperature as soon as N is slightly larger than N_{OV} . The reason is that almost of all the particles are in the degenerate core, the rest forming a tenuous isothermal atmosphere.

We consider a system of relativistic self-gravitating fermions in the microcanonical ensemble. We assume that $N > N_f(R)$. The caloric curve has the form of Figs. 32, 34 and 36. We assume that the system is initially in the gaseous phase. At its energy decreases, the system undergoes a catastrophic collapse from the gaseous phase to a black hole at E_c . This situation corresponds to $N > N_c^{MCE}$, where $N_c^{MCE} \simeq 3.73 N_{OV}$ [see Eq. (52)]. This result shows that, in the microcanonical ensemble, there exist condensed configurations in the general relativistic Fermi gas at nonzero temperature with $N_{OV} < N < 3.73 N_{OV}$. The reason is that only about 1/4 of the particles are in the degenerate core (so that $N_C < N_{OV}$), the rest forming an isothermal atmosphere.

E. Summary

In this section, we summarize the possible evolution of a gaseous star when its temperature (canonical ensemble) or its energy (microcanonical ensemble) is reduced below a critical value.

1. Canonical ensemble

When $N < N_{OV}$ and $R_{\min}(N) < R < R_{CCP}(N)$, there is no collapse.

When $N < N_{OV}$ and $R > R_{CCP}(N)$, the gaseous star collapses below T_c towards a fermion star (white dwarf, neutron star, DM fermion ball). The fermion star contains almost all the mass and is surrounded by a very tenuous atmosphere. Therefore, the collapse corresponds just to an implosion.

When $N_{OV} < N < N_c^{CE} \simeq N_{OV}$ and $R > R_{CCP}(N)$ the gaseous star first collapses below T_c toward a fermion star, then the fermion star collapses below T'_c towards a black hole.

When $N_{OV} < N < N_c^{CE} \simeq N_{OV}$ and $R_{\min}(N) < R < R_{CCP}(N)$ or when $N > N_c^{CE} \simeq N_{OV}$ the gaseous star directly collapses towards a black hole.

2. Microcanonical ensemble

When $N < N_{\text{OV}}$ and $R_{\text{min}}(N) < R < R_{\text{MCP}}(N)$, there is no collapse.

When $N < N_{\text{OV}}$ and $R > R_{\text{MCP}}(N)$, the gaseous star collapses below E_c towards a fermion star (white dwarf, neutron star, DM fermion ball). The fermion star contains only a fraction of the total mass and is surrounded by a very hot atmosphere. Therefore, the system has a core-halo structure which is similar to the onset of red-giants or to the supernova phenomenon. This core-halo structure results from an implosion of the core and an explosion of the halo.

When $N_{\text{OV}} < N < N_c^{\text{MCE}} \simeq 3.73 N_{\text{OV}}$ and $R > R_{\text{MCP}}(N)$ the gaseous star first collapses below E_c toward a fermion star + halo, then the fermion star collapses below E'_c towards a black hole.

When $N_{\text{OV}} < N < N_c^{\text{MCE}} \simeq 3.73 N_{\text{OV}}$ and $R_{\text{min}}(N) < R < R_{\text{MCP}}(N)$ or when $N > N_c^{\text{MCE}} \simeq 3.73 N_{\text{OV}}$ the gaseous star directly collapses towards a black hole.

XIV. CONCLUSION

In this paper we have studied the nature of phase transitions in the general relativistic Fermi gas. This is the most general situation that we can imagine since both quantum and relativistic effects are taken into account in a rigorous manner. We have obtained the complete phase diagram of the system in the (R, N) plane (see Fig. 47).

When $N < N_{\text{OV}}$, the results are similar to those obtained in the nonrelativistic limit (recovered for $N \ll N_{\text{OV}}$ and $R \gg R_{\text{OV}}$ with NR^3 fixed) [5]. In that case, there exists an equilibrium state for any value of the temperature $T \geq 0$ and any value of the energy $E \geq E_{\text{min}}$. Catastrophic collapse towards a black hole is prevented by quantum mechanics (Pauli's exclusion principle). Small systems ($R_{\text{min}} < R < R_{\text{CCP}}$) do not experience phase transition. Intermediate size systems ($R_{\text{CCP}} < R < R_{\text{MCP}}$) experience a canonical phase transition. Large systems ($R > R_{\text{MCP}}$) experience canonical and microcanonical phase transitions. A zeroth order phase transition takes place, below a critical temperature T_c or below a critical energy E_c , from a gaseous phase to a condensed phase. The gaseous phase corresponds to a radiative star, a molecular cloud or a primordial DM nebula. The condensed phase corresponds to a compact object (fermion star) such as a white dwarf, a neutron star or a DM fermion ball. In the canonical ensemble the fermion star contains almost all the mass (or is surrounded by a tenuous isothermal atmosphere). The phase transition corresponds to an implosion. In the microcanonical ensemble the compact object contains only a fraction of the total mass ($\sim 1/4$ to fix the ideas) and is surrounded by a hot isothermal atmosphere that contains the remaining mass. Therefore, the condensed phase has a core-halo structure. In the box model the

atmosphere is held by the walls of the box. Without the box it would be expelled at large distances. The phase transition corresponds to an implosion of the core and an explosion of the halo.

When $N_c < N < N_{\text{max}}$ (where $N_c \simeq N_{\text{OV}}$ in the canonical ensemble and $N_c \simeq 3.73 N_{\text{OV}}$ in the microcanonical ensemble), the results are similar to those obtained in the classical limit (recovered for $N \gg N_{\text{OV}}$ and $R \gg R_{\text{OV}}$ with N/R fixed) [7, 61]. In that case, there is no condensed phase. Below a critical temperature T_c or below a critical energy E_c , the system undergoes a catastrophic collapse from the gaseous phase to a black hole (presumably). Indeed, quantum mechanics cannot prevent this singularity.

When $N_{\text{OV}} < N < N_c$, the results are new and more complex because the system is both relativistic and quantum. In that case, the system can experience two successive collapses: a zeroth order phase transition at T_c (when $R > R_{\text{CCP}}$) or E_c (when $R > R_{\text{MCP}}$) from the gaseous phase to the condensed phase (representing a white dwarf, a neutron star, or a DM fermion ball) followed by a catastrophic collapse at T'_c or E'_c from the condensed phase to a black hole (presumably). This behavior occurs in a very narrow range of parameters in the canonical ensemble ($N_c \simeq N_{\text{OV}}$) and in a wider range of parameters ($N_c \simeq 3.73 N_{\text{OV}}$) in the microcanonical ensemble.

The previous results apply to mid and low values of energy and temperature. At very high energies and very high temperatures, the system is ultrarelativistic and behaves like a form of self-gravitating radiation. Above a maximum energy E_{max} or above a maximum temperature T_{max} , there is no equilibrium state and the system is expected to collapse towards a black hole (presumably) [7, 61].

The astrophysical applications of our results remain limited by the introduction of an artificial confining box. This is necessary in order to have isothermal equilibrium states with a finite mass and thus investigate phase transitions rigorously. A more astrophysically relevant model with a finite mass is provided by the general relativistic fermionic King model. Phase transitions in the nonrelativistic fermionic King model have been studied in detail in [13, 14] and give results that are qualitatively similar to those obtained with the box model [5]. We believe that similar results would be obtained with the general relativistic fermionic King model.

We have suggested that the microcanonical phase transitions occurring in the self-gravitating Fermi gas may be related to the onset of red-giant structure or to the supernova phenomenon. In these spectacular events, the collapse of the core of the system (resulting ultimately in the formation of a white dwarf or a neutron star) is accompanied by the explosion and the expulsion of a hot

envelope.⁴⁷ Similarly, in the self-gravitating Fermi gas, the microcanonical phase transition from a gaseous state to a condensed state corresponds to the implosion of the core (leading to a fermion star) and the explosion of the halo. These analogies are further developed in [38]. We may wonder if similar phenomena can occur in the context of DM as suggested in [14]. It would also be interesting to develop dynamical models of gravitational collapse towards a black hole when no equilibrium state is possible to ensure that the system really forms a black hole. These topics will be considered in future works.

Acknowledgement: One of us (PHC) would like to dedicate this paper to the memory of Donald Lynden-Bell (1935-2018) who was a pioneer in the statistical mechanics of self-gravitating systems.

Appendix A: Thermodynamic limit

The thermodynamic limit of nonrelativistic self-gravitating fermions corresponds to $N \rightarrow +\infty$ in such a way that $\eta = \beta GMm/R$, $\Lambda = -ER/GM^2$ and $\mu = (gm^4/h^3)\sqrt{512\pi^4 G^3 NmR^3}$ are $O(1)$. Taking $m \sim h \sim G \sim 1$, this corresponds to $N \rightarrow +\infty$ with $R \sim N^{-1/3}$, $T \sim N^{4/3}$, $E \sim N^{7/3}$, $S \sim N$, and $F \sim N^{7/3}$. These scalings are given in [5, 22]. Taking $m \sim h \sim N/V \sim 1$ (with $V \sim R^3$), this corresponds to $N \rightarrow +\infty$ with $R \sim N^{1/3}$, $G \sim N^{-2/3}$, $T \sim 1$, $E \sim N$, $S \sim N$, and $F \sim N$.

The thermodynamic limit of relativistic classical self-gravitating systems corresponds to $N \rightarrow +\infty$ in such a way that $\eta = \beta GNm^2/R$, $\Lambda = -ER/GN^2m^2$ (with $E = (M - Nm)c^2$) and $\nu = GNm/Rc^2$ are $O(1)$. Taking $m \sim c \sim G \sim 1$ this corresponds to $N \rightarrow +\infty$ with $R \sim N$, $T \sim 1$, $E \sim N$, $S \sim N$, and $F \sim N$. To the best of our knowledge, these scalings have not been given previously. Taking $m \sim c \sim N/V \sim 1$ (with $V \sim R^3$) this corresponds to $N \rightarrow +\infty$ with $R \sim N^{1/3}$, $G \sim N^{-2/3}$, $T \sim 1$, $E \sim N$, $S \sim N$, and $F \sim N$.

The thermodynamic limit of relativistic self-gravitating fermions corresponds to $N \rightarrow +\infty$ in such a way that $\eta = \beta GNm^2/R$, $\Lambda = -ER/GN^2m^2$ (with $E = (M - Nm)c^2$), $\mu = (gm^4/h^3)\sqrt{512\pi^4 G^3 NmR^3}$ and $\nu = GNm/Rc^2$ are $O(1)$. Taking $h \sim c \sim G \sim 1$ this corresponds to $N \rightarrow +\infty$ with $R \sim N^{2/3}$, $m \sim N^{-1/3}$, $T \sim N^{-1/3}$, $E \sim N^{2/3}$, $S \sim N$, and $F \sim N^{2/3}$. These scalings were given in [47]. Taking $m \sim c \sim h \sim N/V \sim 1$ (with $V \sim R^3$) this corresponds to $N \rightarrow +\infty$ with $R \sim N^{1/3}$, $G \sim N^{-2/3}$, $T \sim 1$, $E \sim N$, $S \sim N$, and $F \sim N$.

The thermodynamic limit of nonrelativistic classical self-gravitating systems is discussed in Appendix A of

[67] where several possible scalings are given.

We note that the different situations considered above can be unified by considering a thermodynamic limit of the form $N \rightarrow +\infty$ with $R \sim N^{1/3}$, $G \sim N^{-2/3}$, $T \sim 1$, $E \sim N$, $S \sim N$, and $F \sim N$, corresponding to $m \sim c \sim h \sim N/V \sim 1$ (with $V \sim R^3$). This is the standard thermodynamic limit with a renormalized gravitational constant. To the best of our knowledge this result has not been highlighted previously.

Appendix B: Dimensionless quantities

According to the OV theory [49], the maximum mass, the maximum particle number and the minimum radius of a general relativistic fermion star at $T = 0$ are⁴⁸

$$M_{\text{OV}} = 0.38426 \sqrt{\frac{2}{g}} \left(\frac{\hbar c}{G}\right)^{3/2} \frac{1}{m^2}, \quad (\text{B1})$$

$$N_{\text{OV}} = 0.39853 \sqrt{\frac{2}{g}} \left(\frac{\hbar c}{G}\right)^{3/2} \frac{1}{m^3}, \quad (\text{B2})$$

$$R_{\text{OV}} = 8.7360 \frac{GM_{\text{OV}}}{c^2} = 3.3569 \sqrt{\frac{2}{g}} \left(\frac{\hbar^3}{Gc}\right)^{1/2} \frac{1}{m^2}. \quad (\text{B3})$$

We note that $W_{\text{OV}} \sim GM_{\text{OV}}^2/R_{\text{OV}} \sim M_{\text{OV}}c^2$. We introduce the mass, particle number and length scales

$$M_* = \sqrt{\frac{2}{g}} \frac{M_P^3}{m^2} = \left(\frac{2\hbar^3 c^3}{gm^4 G^3}\right)^{1/2}, \quad (\text{B4})$$

$$N_* = \frac{M_*}{m} = \sqrt{\frac{2}{g}} \frac{M_P^3}{m^3} = \left(\frac{2\hbar^3 c^3}{gm^6 G^3}\right)^{1/2}, \quad (\text{B5})$$

$$R_* = \sqrt{\frac{2}{g}} \frac{\hbar M_P}{m^2 c} = \sqrt{\frac{2}{g}} \frac{M_P^2}{m^2} l_P = \left(\frac{2\hbar^3}{gm^4 c G}\right)^{1/2}, \quad (\text{B6})$$

where $M_P = (\hbar c/G)^{1/2}$ is the Planck mass and $l_P = (\hbar G/c^3)^{1/2}$ is the Planck length. We then define

$$r = R_* \tilde{r}, \quad M = M_* \tilde{M}, \quad \epsilon = \frac{M_* c^2}{R_*^3} \tilde{\epsilon}, \quad (\text{B7})$$

$$N = N_* \tilde{N}, \quad n = \frac{N_*}{R_*^3} \tilde{n}, \quad \Phi = c^2 \tilde{\Phi}, \quad (\text{B8})$$

⁴⁷ Newtonian gravity is sufficient to describe white dwarfs (and the planetary nebula) that follow the red-giant stage while general relativity is necessary to describe neutron stars or black holes formed from supernova explosion.

⁴⁸ Qualitatively, the scaling of the maximum mass $M_{\text{OV}} \sim (\hbar c/G)^{3/2}/m^2$ can be obtained from the mass-radius relation $MR^3 \sim \hbar^6/(m^8 G^3)$ of nonrelativistic fermion stars (see Appendix F) by determining when the radius R of the configuration becomes comparable to the Schwarzschild radius $R_S = 2GM/c^2$.

$$P = \frac{M_* c^2}{R_*^3} \tilde{P}, \quad T = \frac{m c^2}{k_B} \tilde{T}, \quad \mu = m c^2 \tilde{\mu}, \quad (\text{B9})$$

$$S = N_* k_B \tilde{S}, \quad F = M_* c^2 \tilde{F}, \quad (\text{B10})$$

where the tilde variables are dimensionless. We note that

$$\frac{M_* c^2}{R_*^3} = \frac{g m^4 c^5}{2 \hbar^3}, \quad \frac{N_*}{R_*^3} = \frac{g m^3 c^3}{2 \hbar^3}, \quad (\text{B11})$$

$$N_* R_*^3 = \frac{4 \hbar^6}{g^2 m^9 G^3}, \quad \frac{G M_*}{R_* c^2} = 1. \quad (\text{B12})$$

In the main text, in order to simplify the notations, we do not write the tildes anymore. This amounts to taking $\hbar = c = G = m = g/2 = 1$ in the dimensional expressions. In particular, we have

$$M_{\text{OV}} = 0.38426, \quad (\text{B13})$$

$$N_{\text{OV}} = 0.39853, \quad (\text{B14})$$

$$R_{\text{OV}} = 3.3569. \quad (\text{B15})$$

Appendix C: Connexion between the $N_\alpha(\Phi_0)$ curves and the caloric curves $\eta(\Lambda)$

In this Appendix, we explain how we obtained the caloric curves of self-gravitating fermions in general relativity following the method given by Bilic and Viollier [47].⁴⁹

Let us illustrate this procedure with a simple example. In order to construct the caloric curve $\eta(\Lambda)$ corresponding to $R = 50$ and $N = 0.15$ (see Fig. 5), we proceed as follows. For a given value of α and Φ_0 , we can solve the differential equations (6) and (7) up to $r = R$ and determine N from Eq. (10) [we can also determine η and Λ with the aid of Eqs. (9), (10), (12) and (16)]. By varying the central potential Φ_0 from -1 to $+\infty$, we can obtain the curve $N_\alpha(\Phi_0)$. It is usually nonmonotonic and displays damped oscillations for large values of Φ_0 . As example is represented in Fig. 62 for $R = 50$ and $\alpha = 750.24$ (see also Figs. 65 and 66 below).

Let us introduce some notations that will be useful in the following. We call $\mathcal{N}(\alpha)$ the maximum value of the curve $N_\alpha(\Phi_0)$ and we denote by $\Psi(\alpha)$ the value of the central potential Φ_0 corresponding to this maximum. By varying α from $-\infty$ to $+\infty$, we find that the peaks $\mathcal{N}(\alpha)$ of the curves $\{N_\alpha(\Phi_0)\}$ reach a maximum $N_{\text{max}}(R) =$

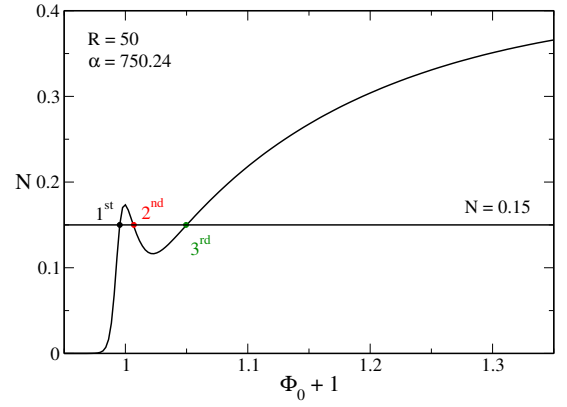


FIG. 62: Particle number N as a function of the central potential Φ_0 for $R = 50$ and $\alpha = 750.24$. The intersections between the curve $N_\alpha(\Phi_0)$ and the line level $N = 0.15$ determine three equilibrium states with central potentials $(\Phi_0)_1 = 0.9954$, $(\Phi_0)_2 = 1.0069$ and $(\Phi_0)_3 = 1.0495$. Their corresponding energy and temperature are $(\Lambda_1, \eta_1) = (-0.0242, 2.2725)$, $(\Lambda_2, \eta_2) = (0.5067, 2.2447)$ and $(\Lambda_3, \eta_3) = (2.4468, 2.2794)$. Each solution is represented by a bullet in the caloric curve of Fig. 64. The first solution (black) belongs to the gaseous phase, the second solution (red) belongs to the core-halo phase and the third solution (green) belongs to the condensed phase.

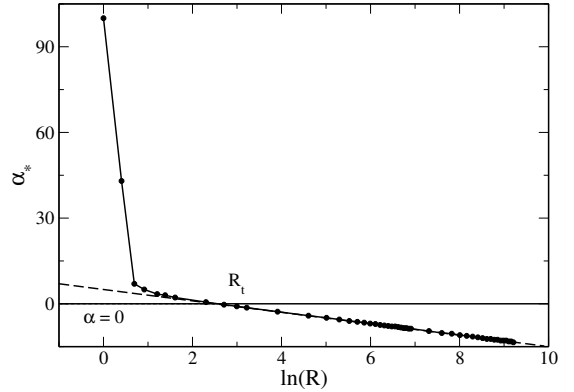


FIG. 63: Evolution of $\alpha_*(R)$ as a function of R . The dashed line represents the scaling law $\alpha_*(R) = 5.0119 - 2 \ln R$ obtained in [7] for classical systems. In the case of fermions, this law is asymptotically valid for $R \gg 1$. We have also indicated the radius $R_t = 12.255$ at which $\alpha_*(R)$ passes from negative values to positive values as the box radius decreases.

$\mathcal{N}(\alpha_*(R))$ at $\alpha = \alpha_*(R)$ (see Figs. 65 and 66 below). The evolution of α_* as a function of R is plotted in Fig. 63.

Let us come back to the curve of Fig. 62. The intersections $(\Phi_0)_{i \in \{1, \dots, n\}}$ between the curve $N_\alpha(\Phi_0)$ and the line level $N = 0.15$, and the corresponding values of Λ and η at these intersections, determine n points in the caloric curve $\eta(\Lambda)$ of Fig. 64. In the present example, $n = 3$. By varying α these points form n branches in the caloric curve $\eta(\Lambda)$. These branches have been rep-

⁴⁹ This Appendix is technical and can be skipped for a first reading. It is nevertheless important to understand where the critical values of N (such as N_1 , N_{OV} , N_{CCP} , N_* etc) obtained in the main text come from.

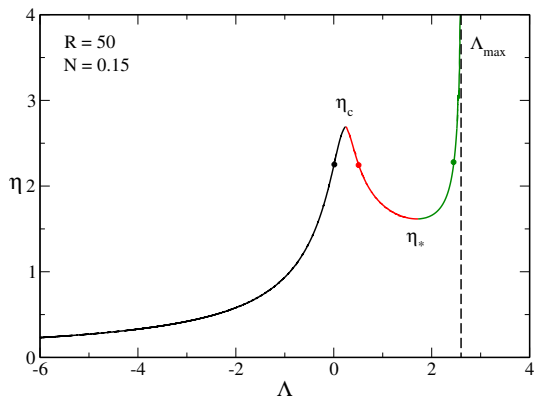


FIG. 64: Caloric curve for $R = 50$ and $N = 0.15$. By varying α in Fig. 62, the first intersections ($\Lambda_1(\alpha), \eta_1(\alpha)$) form the gaseous branch (black), the second intersections ($\Lambda_2(\alpha), \eta_2(\alpha)$) form the core-halo branch (red) and the third intersections ($\Lambda_3(\alpha), \eta_3(\alpha)$) form the condensed branch (green). It turns out that two branches merge at an extremum of temperature: η_c corresponds to the merging of the first and second intersections (for $\alpha = \alpha_M$) and η_* corresponds to the merging of the second and third intersections (for $\alpha = \alpha_m$).

resented in color in Fig. 64. In the present example, they correspond to the gaseous, core-halo and condensed phases respectively. We have observed (but not proven mathematically) that when $\alpha > \alpha_*$, the merging of two intersections between the curves $\{N_\alpha(\Phi_0)\}$ and the line level N , occurring at some $\alpha_e(N, R)$, corresponds to the merging of two branches in the caloric curve $\eta(\Lambda)$ occurring at an extremum of temperature η_e .⁵⁰ We have also observed (but not proven mathematically) that when $\alpha < \alpha_*$, the merging of two intersections between the curves $\{N_\alpha(\Phi_0)\}$ and the line level N , occurring at some $\alpha'_e(N, R)$, corresponds to the merging of two branches in the caloric curve $\eta(\Lambda)$ occurring at an extremum of energy Λ_e .⁵¹ In the present example, we have $\alpha > \alpha_*$. As

⁵⁰ By using this result, it is easy to obtain the curves $\eta_c(N)$, $\eta_*(N)$ and $\eta'_c(N)$ in the canonical phase diagram of Fig. 23, since they correspond to $\alpha > \alpha_*$ (see below). Indeed, each extremum of $N_\alpha(\Phi)$ determines an extremum inverse temperature $\eta_c(N)$ for the corresponding value of $N = N(\alpha)$. Thus, by considering the first three extrema (when they exist) and running α from α_* to $+\infty$, we get the full curves $\eta_c(N)$, $\eta_*(N)$ and $\eta'_c(N)$. Unfortunately, it is not possible to use a similar method to obtain the curves $\Lambda_c(N)$, $\Lambda_*(N)$, $\Lambda'_c(N)$ and $\Lambda''_c(N)$ in the microcanonical phase diagram of Fig. 37. They have to be obtained “by hand” directly from the caloric curves.

⁵¹ By using this result, it is easy to obtain the curve $\Lambda_{\min}(N)$ in the microcanonical phase diagram of Fig. 25, since it corresponds to $\alpha < \alpha_*$ (see below). Indeed, each extremum of $N_\alpha(\Phi)$ determines an extremum energy $\Lambda_e(N)$ for the corresponding value of $N = N(\alpha)$. Thus, by considering the first extremum and running α from $-\infty$ to α_* , we get the full curve $\Lambda_{\min}(N)$. Unfortunately, it is not possible to use a similar method to obtain the curve $\eta_{\min}(N)$ in the canonical phase diagram of Fig. 23. It has to be

a result the merging of the first and second intersections in Fig. 62, occurring at some α_M , corresponds to the temperature minimum η_c in the caloric curve of Fig. 64. Similarly, the merging of the second and third intersections in Fig. 62, occurring at some α_m , corresponds to the temperature maximum η_* in the caloric curve of Fig. 64.

We now generalize this procedure to different values of N and R . The main difference between the case of classical particles studied in [7] and the case of fermions studied in the present paper is the following. When quantum mechanics is taken into account, we find that for $\alpha \rightarrow +\infty$ the $\{N_\alpha(\Phi_0)\}$ curves tend towards an invariant curve corresponding to the OV-curve $N_{OV}(\Phi_0)$ [6]. Close to this curve, i.e. for α large and N small, the $\{N_\alpha(\Phi_0)\}$ curves can have a complex behavior with several oscillations responsible for the phase transitions studied in this paper. The nature of these oscillations, and consequently the nature of phase transitions, depends on the particle number N and on the radius of the system R . We consider below the cases treated in the main text.

1. $R = 50$

In this subsection, we consider a system of size $R = 50$ and make the link between the topological properties of the curves $\{N_\alpha(\Phi_0)\}$ and the caloric curves analysed in Sec. V.

We first consider the case $\alpha < 0$ (see Fig. 65). For $\alpha \rightarrow -\infty$, we find that $\mathcal{N}(\alpha) \rightarrow 0$ and $\Psi(\alpha) \rightarrow +\infty$. This corresponds to the ultrarelativistic regime. As α increases, $\mathcal{N}(\alpha)$ increases and $\Psi(\alpha)$ decreases: the peak of the curve $N_\alpha(\Phi_0)$ grows and moves towards the left. At $\alpha = \alpha_* = -2.75$, $\mathcal{N}(\alpha)$ reaches its maximum value $N_{\max} = 8.821$. For larger values of α , $\mathcal{N}(\alpha)$ and $\Psi(\alpha)$ both decrease: the peak of the curve $N_\alpha(\Phi_0)$ decays and moves towards the left. For $\alpha \rightarrow 0^-$, $\mathcal{N}(\alpha) \rightarrow N_0 = 8.408$ and $\Psi(\alpha) \rightarrow -1$: the peak of the curve $N_\alpha(\Phi_0)$ is squeezed near $\Phi_0 = -1$.⁵²

We now consider the case $\alpha > 0$ (see Fig. 66). For $\alpha > 0$, we find that $\mathcal{N}(\alpha)$ decreases and $\Psi(\alpha)$ increases: the peak of the curve $N_\alpha(\Phi_0)$ decays and moves towards the right. For $\alpha \rightarrow +\infty$, the curve $N_\alpha(\Phi_0)$ tends towards the OV-curve $N_{OV}(\Phi_0)$: $\mathcal{N}(\alpha)$ tends towards $N_{OV} = 0.39853$ and $\Psi(\alpha)$ tends towards 0.695.

The curves $\{N_\alpha(\Phi_0)\}$ with $\alpha < \alpha_*$ (i.e. the ones that go up as α increases) are associated with the hot spiral (radiation) studied in [7]. The hot spiral corresponds to the ultrarelativistic limit valid for high values of the energy and of the temperature. This spiral is present for

obtained “by hand” directly from the caloric curves.

⁵² Apart from this mathematical property, $\alpha = 0$ does not play a particular role in the problem. If we had plotted N as a function of $b_0 = 1/T_0$ instead of Φ_0 [see Eq. (4)] the specificity of the value $\alpha = 0$ would not have arisen.

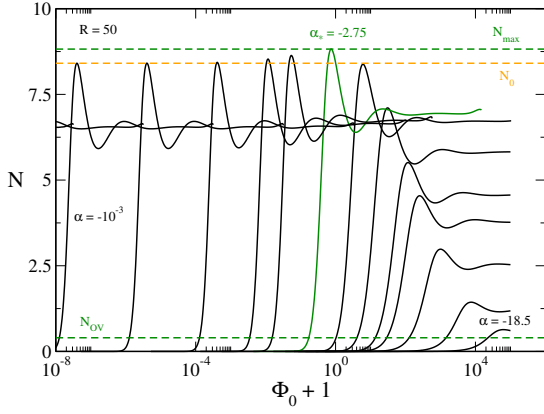


FIG. 65: Evolution of the curve $N_\alpha(\Phi_0)$ for different values of $\alpha < 0$ for $R = 50$ (for illustration the curves go from $\alpha = -18.5$ to $\alpha = -10^{-3}$). We have indicated different characteristics values of N : $N_0 = 8.408$ and $N_{\max} = 8.821$.

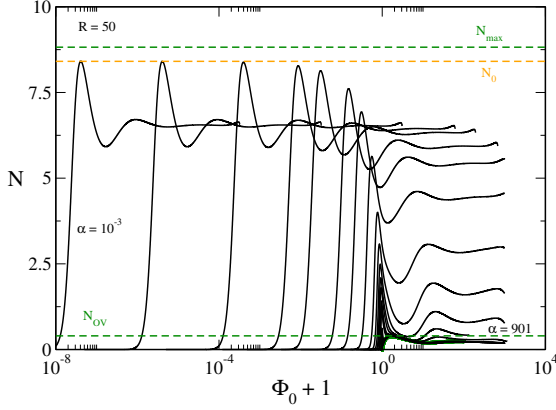


FIG. 66: Evolution of the curve $N_\alpha(\Phi_0)$ for different values of $\alpha > 0$ for $R = 50$ (for illustration the curves go from $\alpha = 10^{-3}$ to $\alpha = 901$). The OV curve has been plotted in green. We have indicated different characteristics values of N : $N_{OV} = 0.39853$, $N_0 = 8.408$ and $N_{\max} = 8.821$.

any value of N , except for N close to N_{\max} where the caloric curve presents a different behavior described in Sec. VI of [7] and in Sec. IX B of the present paper.

The curves $\{N_\alpha(\Phi_0)\}$ with $\alpha > \alpha_*$ (i.e. the ones that go down as α increases) are associated with the part of the caloric curve corresponding to mid and low values of the energy and of the temperature. Figure 67 is a zoom of Fig. 66 close to the OV curve, i.e. for small values of N . This is the region of interest where canonical phase transitions appear (they are related to the appearance of turning points of temperature). We have indicated on this figure the different characteristic values of N that have been identified in Sec. V. They can be related to the topological properties of the curves $\{N_\alpha(\Phi_0)\}$ as follows:

(i) $N_{OV} = 0.39853$ and $N_1 = 0.18131$ are intrinsic properties of the OV curve $N_{OV}(\Phi_0)$. They correspond

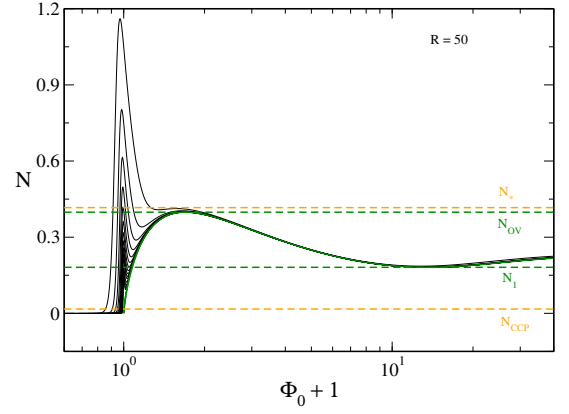


FIG. 67: Some curves $N_\alpha(\Phi_0)$ for $R = 50$ together with different characteristics values of N : $N_{CCP} = 0.01697$, $N_1 = 0.18131$, $N_{OV} = 0.39853$, and $N_* = 0.41637$.

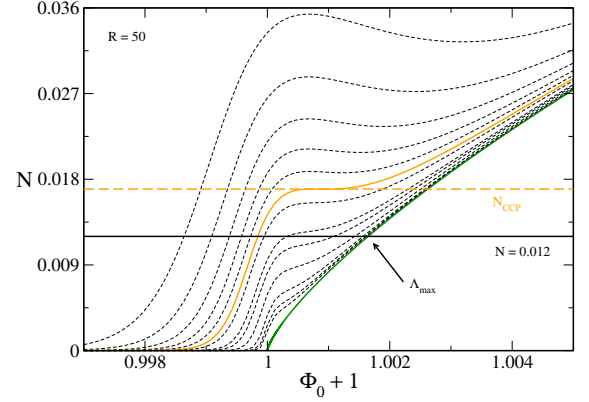


FIG. 68: Illustration of the intersections in the case $N < N_{CCP} = 0.01697$ (specifically $R = 50$ and $N = 0.012$).

to its first maximum and to its first minimum.

(ii) $N_{CCP} = 0.01697$ and $N_* = 0.41637$ can be related to the first and second inflexion points of the curves $\{N_\alpha(\Phi_0)\}$ (see Figs. 68 and 71). Indeed, we have seen that an extremum of temperature in the caloric curve corresponds to a merging of two intersections in the $N = \{N_\alpha(\Phi_0)\}$ plots. As a result, the canonical phase transitions appear (at $N = N_{CCP}$) and disappear (at $N = N_*$) when the curve $\{N_\alpha(\Phi_0)\}$ presents an inflexion point. This is how we can precisely determine N_{CCP} and N_* .

Let us now describe in more detail the different intersections as a function of N .

For $N < N_{CCP}$ (see Fig. 68), we have just one intersection between the line level N and the curves $\{N_\alpha(\Phi_0)\}$. This explains why the caloric curve of Fig. 4 is monotonic. We note that the intersection between the line level N and the OV-curve ($\alpha \rightarrow +\infty$) corresponds to the ground state $T = 0$ (i.e. $\eta \rightarrow +\infty$). This leads to the vertical asymptote at $\Lambda = \Lambda_{\max}$ in the caloric curve of

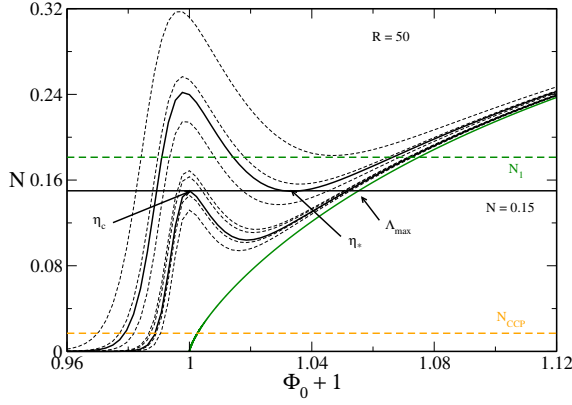


FIG. 69: Illustration of the intersections in the case $N_{CCP} = 0.01697 < N < N_1 = 0.18131$ (specifically $R = 50$ and $N = 0.15$).

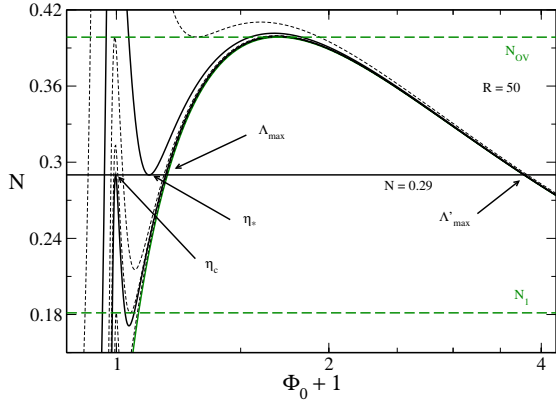


FIG. 70: Illustration of the intersections in the case $N_1 = 0.18131 < N < N_{OV} = 0.39853$ (specifically $R = 50$ and $N = 0.29$).

Fig. 4. We note that, for $N < N_{CCP}$, $\Phi_0 \ll 1$ showing that we are in the Newtonian limit.

For $N_{CCP} < N < N_1$ (see Fig. 69), we are above the first inflexion point so we can have up to three intersections between the line level N and the curves $\{N_\alpha(\Phi_0)\}$. This determines three branches in the caloric curve of Fig. 5. This is why it has an N -shape. The first and second intersections merge at $\alpha = \alpha_M$. Correspondingly, the first and second branches in the caloric curve merge at η_c , the first turning point of temperature. The second and third intersections merge at $\alpha = \alpha_m$. Correspondingly, the second and third branches in the caloric curve merge at η_s , the second turning point of temperature.

For $N_1 < N < N_{OV}$ (see Fig. 70), the novelty is that there is a second intersection between the line level N and the OV-curve $N_{OV}(\Phi_0)$. This corresponds to an unstable equilibrium state at $T = 0$ (i.e. $\eta \rightarrow +\infty$). This gives rise to the second vertical asymptote at $\Lambda = \Lambda'_{max}$ in the caloric curve of Fig. 7. There are also secondary

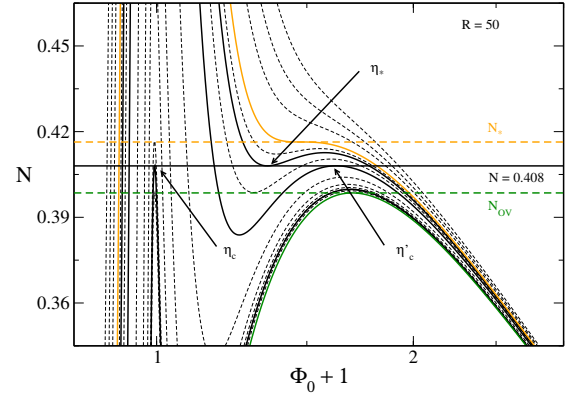


FIG. 71: Illustration of the intersections in the case $N_{OV} = 0.39853 < N < N_* = 0.41637$ (specifically $R = 50$ and $N = 0.408$).

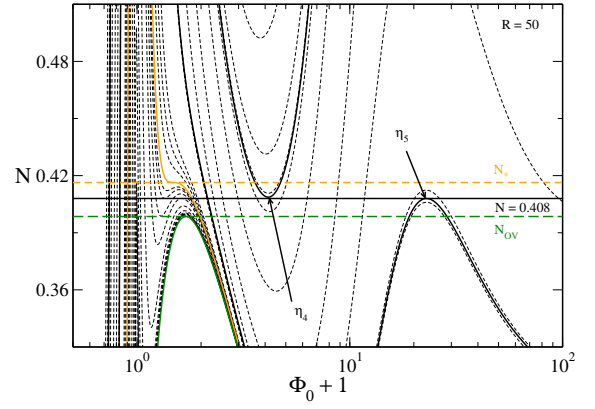


FIG. 72: Illustration of the intersections in the case $N_{OV} = 0.39853 < N < N_* = 0.41637$ (specifically $R = 50$ and $N = 0.408$).

intersections leading to the unstable spiral of Fig. 7 as discussed in the next paragraph.

For $N_{OV} < N < N_*$ (see Figs. 71 and 72) we can have up to four fundamental intersections between the line level N and the curves $\{N_\alpha(\Phi_0)\}$. This gives rise to four fundamental branches in the caloric curve of Fig. 16. The first and second intersections merge at $\alpha = \alpha_M$. Correspondingly, the first and second branches in the caloric curve merge at η_c , the first turning point of temperature. The second and third intersections merge at $\alpha = \alpha_m$. Correspondingly, the second and third branches in the caloric curve merge at η_s , the second turning point of temperature. The third and fourth intersections merge at $\alpha = \alpha'_M$. Correspondingly, the third and fourth branches in the caloric curve merge at η'_c , the third turning point of temperature. Furthermore, there are additional intersections giving rise to the spiral (that will become the cold spiral for larger values of N) in the caloric curve of Fig. 16. These intersections are less relevant since they correspond to unstable states. Note that there is

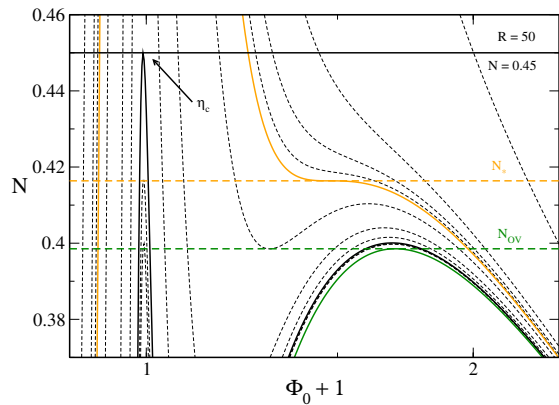


FIG. 73: Illustration of the intersections in the case $N > N_* = 0.41637$ (specifically $R = 50$ and $N = 0.45$).

no intersection with the OV curve so there is no vertical asymptote corresponding to $\eta \rightarrow +\infty$. Finally, we note that $\Phi_0 \sim 1$ showing that we are in the relativistic regime.

For $N > N_*$ (see Fig. 73), we are above the second inflexion point so we can have at most two fundamental intersections between the line level N and the curves $\{N_\alpha(\Phi_0)\}$. This determines two fundamental branches in the caloric curve of Fig. 20. The first and second intersections merge at $\alpha = \alpha_M$. Correspondingly, the first and second branches in the caloric curve merge η_c , the first turning point of temperature. There are also secondary intersections giving rise to the spiral (made of unstable equilibrium states) as described in the previous paragraph.

For larger values of N the discussion is similar to the one given in [7].

2. $R = 600$

We now consider a system of size $R = 600$ corresponding to the case analysed in Sec. VI. The novelty with respect to the previous situation is that microcanonical phase transitions can appear (they are related to the appearance of turning points of energy).

Some curves $N_\alpha(\Phi_0)$ are plotted in Fig. 74 for different values of α . We have indicated on this figure the different characteristic values of N that have been identified in Sec. VI. As we have seen in the previous section $N_{\max} = 106.057$, $N_{OV} = 0.39853$, $N_1 = 0.18131$, $N_{CCP} = 9.719 \times 10^{-6}$ and $N_* = 0.418$ can be related to the topological properties of the curves $\{N_\alpha(\Phi_0)\}$. Unfortunately, $N_{MCP} = 0.00965$ and $N'_* = 1.5$ cannot be determined from a simple graphical construction because there does not seem to be a simple manner to relate a turning point of energy in the caloric curve $\eta(\Lambda)$ to the topological properties of the curves $\{N_\alpha(\Phi_0)\}$. Therefore, in Sec. VI, we had to determine N_{MCP} and N'_* “by

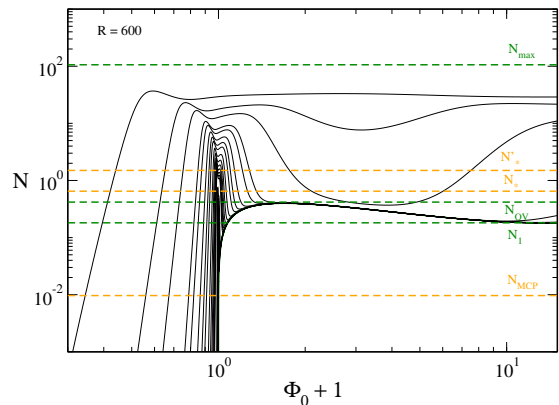


FIG. 74: Some curves $N_\alpha(\Phi_0)$ for $R = 600$ together with different characteristics values of N : $N_{CCP} = 9.719 \times 10^{-6}$, $N_{MCP} = 0.00965$, $N_1 = 0.18131$, $N_{OV} = 0.39853$, $N_* = 0.418$, $N'_* = 1.5$ and $N_{\max} = 106.057$.

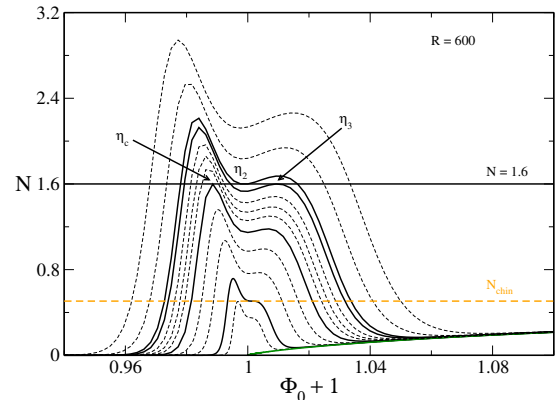


FIG. 75: Illustration of the intersections in the case $N > N_{\text{chin}} = 0.5062$ (specifically $R = 600$ and $N = 1.6$).

hand” directly from the study of the caloric curves as a function of N .

Apart from the occurrence of microcanonical phase transitions, there is another novelty with respect to the previous situation ($R = 50$). A new inflexion point appears at $N_{\text{chin}} = 0.5062$ (see Fig. 75). For $N < N_{\text{chin}}$ we have two fundamental intersections in the $N = \{N_\alpha(\Phi_0)\}$ plot leading to two branches of solutions in the caloric curve $\eta(\Lambda)$ that merge at the temperature minimum η_c (see Fig. 27).⁵³ For $N > N_{\text{chin}}$ we have four fundamental intersections in the $N = \{N_\alpha(\Phi_0)\}$ plot leading to four branches of solutions that merge at the temperature minimum η_c , at the temperature maximum η_2 and at the temperature minimum η_3 respectively (see Fig. 76). In that case, the dinosaur has a “chin”. This is essentially

⁵³ In this paragraph, we do not consider the temperature maximum η_* that is far away from the dinosaur’s head.

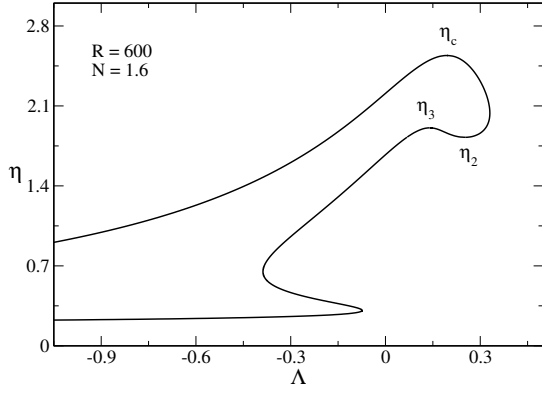


FIG. 76: Caloric curve for $N > N_{\text{chin}} = 0.5062$ (specifically $R = 600$ and $N = 1.6$).

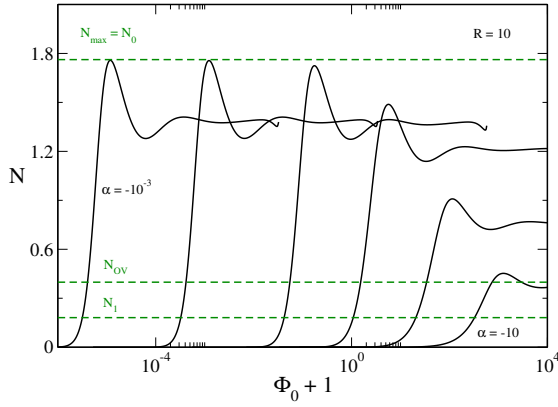


FIG. 77: Evolution of the curve $N_\alpha(\Phi_0)$ for different values of $\alpha < 0$ for $R = 10$ (for illustration the curves go from $\alpha = -10$ to $\alpha = -10^{-3}$).

a curiosity since the solutions in this part of the caloric curve are unstable.

3. $R = 10$

We consider a system of size $R = 10$ corresponding to the case analyzed in Sec. VIII. Some curves $N_\alpha(\Phi_0)$ are plotted in Figs. 77 and 78 for $\alpha < 0$ and $\alpha > 0$ respectively. The difference with the case $R = 50$ studied in Appendix C1 is that there is no canonical phase transition. This is manifested by the absence of inflexion points in the family of curves $\{N_\alpha(\Phi_0)\}$. We also note that, for $R = 10$, N_{max} is very close to N_0 .⁵⁴ However, this is essentially a mathematical curiosity without physical consequences.

⁵⁴ They become equal when $\alpha_* = 0$ corresponding to $R = R_t = 12.255$ (see Fig. 63).

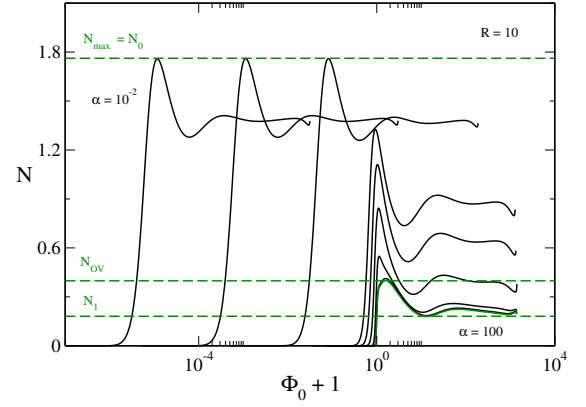


FIG. 78: Evolution of the curve $N_\alpha(\Phi_0)$ for different values of $\alpha > 0$ for $R = 10$ (for illustration the curves go from $\alpha = 10^{-2}$ to $\alpha = 100$).

Let us describe the different intersections as a function of N . As already mentioned, the intersections with the curves $\alpha < \alpha_* \simeq 0$ (see Fig. 77) give rise to the hot spiral. This case has already been studied in [7]. Therefore, we consider below the intersections with the curves $\alpha > \alpha_* \simeq 0$ (see Fig. 78).

For $N < N_1$, we have just one intersection between the line level N and the curves $\{N_\alpha(\Phi_0)\}$. Therefore, the caloric curve is monotonic and is similar to Fig. 4. The intersection between the line level N and the OV-curve corresponds to the ground state $T = 0$ (i.e. $\eta \rightarrow +\infty$). This leads to the vertical asymptote at $\Lambda = \Lambda_{\text{max}}$ in the caloric curve.

For $N_1 < N < N_{\text{OV}}$, there is a second intersection between the line level N and the OV-curve $N_{\text{OV}}(\Phi_0)$. This corresponds to an unstable equilibrium state at $T = 0$ (i.e. $\eta \rightarrow +\infty$). This gives rise to the second vertical asymptote at $\Lambda = \Lambda'_{\text{max}}$ in the caloric curve of Fig. 39. There are also secondary intersections leading to the cold spiral that is apparent on Fig. 39.

For $N > N_{\text{OV}}$, there are two fundamental intersections between the line level N and the curves $\{N_\alpha(\Phi_0)\}$. This gives rise to two fundamental branches in the caloric curve of Fig. 40. The first and second intersections merge at $\alpha = \alpha_M$. Correspondingly, the first and second branches in the caloric curve merge at η_c , the first turning point of temperature. Furthermore, there are additional intersections giving rise to the cold spiral in the caloric curve of Fig. 40. These intersections are less relevant since they correspond to unstable states. Note that there is no intersection with the OV curve so there is no vertical asymptote corresponding to $\eta \rightarrow +\infty$.

For larger values of N the discussion is similar to the one given in [7].

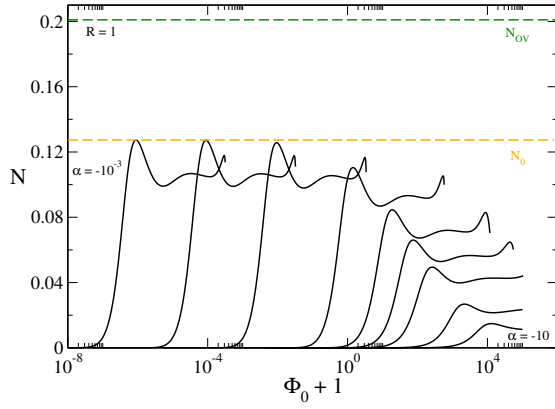


FIG. 79: Evolution of the curve $N_\alpha(\Phi_0)$ for different values of $\alpha < 0$ for $R = 1$ (for illustration the curves go from $\alpha = -10$ to $\alpha = -10^{-3}$).

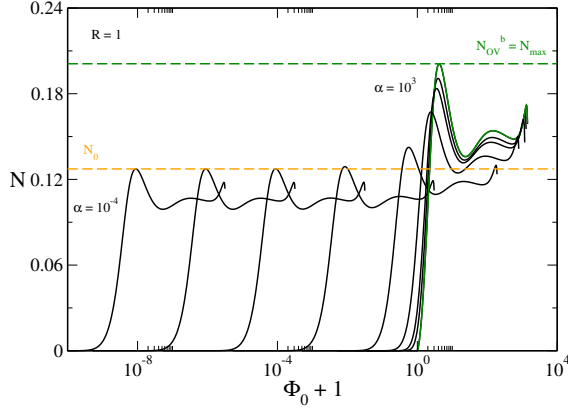


FIG. 80: Evolution of the curve $N_\alpha(\Phi_0)$ for different values of $\alpha > 0$ for $R = 1$ (for illustration the curves go from $\alpha = 10^{-4}$ to $\alpha = 10^3$).

4. $R = 1$

We consider a system of size $R = 1$ corresponding to the case analyzed in Sec. IX. Some curves $N_\alpha(\Phi_0)$ are plotted in Figs. 79 and 80 for $\alpha < 0$ and $\alpha > 0$ respectively.⁵⁵ The difference with the previous case is that now $N_{OV}(\Phi_0)$ is very close to $N_{\max}(\Phi_0)$. This is because $\alpha_* \gg 1$ (see Fig. 63). Therefore N_{OV}^b is very close to N_{\max} and N_1^b is very close to N'_S .

Let us describe the different intersections as a function of N (note that most of the curves correspond to $\alpha < \alpha_*$).

For $N < N'_S \simeq N_1^b$ (see Fig. 81), we have one inter-

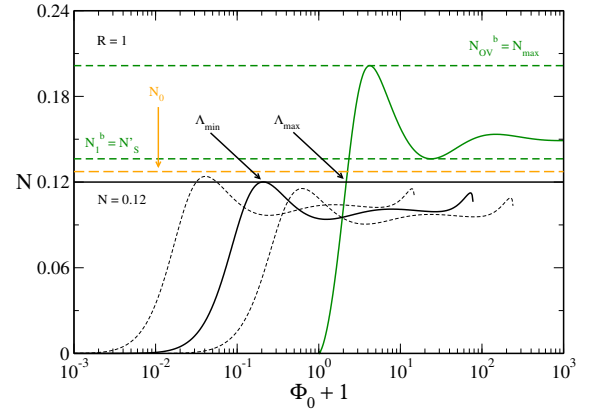


FIG. 81: Illustration of the intersections in the case $N < N'_S \simeq N_1^b$ (specifically $R = 1$ and $N = 0.12$).

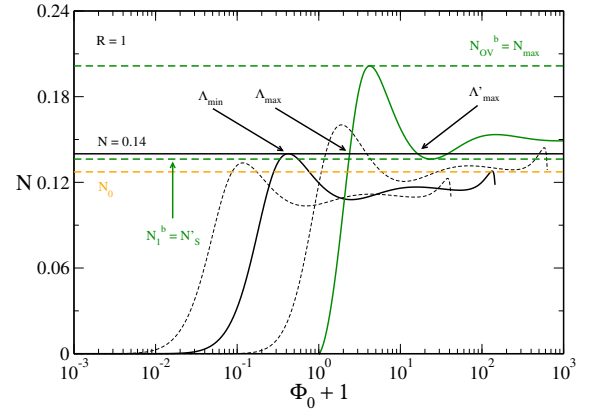


FIG. 82: Illustration of the intersections in the case $N'_S \simeq N_1^b < N < N_{\max} \simeq N_{OV}^b$ (specifically $R = 1$ and $N = 0.14$).

section between the line level N and the OV-curve which corresponds to the ground state $T = 0$ (i.e. $\eta \rightarrow +\infty$). This leads to the vertical asymptote at $\Lambda = \Lambda_{\max}$ in the caloric curve of Fig. 43. In addition, we can have up to an infinity of intersections with the curves $N_\alpha(\Phi_0)$ leading to the hot spiral displayed in the caloric curve of Fig. 43.

For $N'_S \simeq N_1^b < N < N_{\max} \simeq N_{OV}^b$ (see Fig. 82), we have two fundamental intersections between the line level N and the OV-curve (corresponding to $\alpha \rightarrow +\infty$) leading to the asymptotes $\eta = +\infty$ at Λ_{\max} (stable ground state) and Λ'_{\max} (unstable ground state) in the caloric curve of Fig. 44. For smaller values of α , the two fundamental intersections between the line level N and the curves $\{N_\alpha(\Phi_0)\}$ lead to two fundamental branches in the caloric curve of Fig. 44. These intersections merge at $\alpha = \alpha_n$. Since $\alpha_n < \alpha_*$, this is associated with a turning point of energy at Λ_{\min} in the caloric curve of Fig. 44. There may also be a third intersection with the OV-curve and secondary intersections with the curves $\{N_\alpha(\Phi_0)\}$ forming a third branch exhibiting an asymp-

⁵⁵ Since $R = 1 < R_t = 12.255$, implying $\alpha_* > 0$, we note that $N_{\max}(\Phi_0)$ is reached after $N_0(\Phi_0)$ (see Figs. 79 and 80) while it was reached before $N_0(\Phi_0)$ in the case $R = 50$ (see Figs. 65 and 66).

tote at Λ''_{\max} and a spiral. However, these solutions are not represented on the caloric curve because they are associated with unstable states of high order.

Appendix D: Condition to be degenerate

In the nonrelativistic limit, the system is degenerate when the thermal pressure $P = \rho k_B T/m$ is small as compared to the quantum pressure $P = (1/5)(3/4\pi g)^{2/3} h^2 \rho^{5/3}/m^{8/3}$ arising from the Pauli exclusion principle. This condition can be written as

$$k_B T \ll \frac{1}{5} \left(\frac{3}{4\pi g} \right)^{2/3} \frac{h^2}{m^{5/3}} \rho^{2/3} \quad (\text{D1})$$

which is the nonrelativistic Sommerfeld criterion (the right hand side of Eq. (D1) is of the order of the Fermi temperature T_F). To get an estimate of the importance of degeneracy, we replace the density ρ by the average density $\bar{\rho} = 3M/4\pi R^3$. In this manner, we obtain the condition

$$\eta \gg 0.917 \mu^{2/3}. \quad (\text{D2})$$

As stated above this condition is only valid in an average sense. A system which does not satisfy this condition in average may still have a degenerate core and a nondegenerate halo as in Appendix E 2.

In the ultrarelativistic limit, the system is degenerate when the thermal pressure $P = \rho k_B T/m$ is small as compared to the quantum pressure $P = (1/4)(3/4\pi g)^{1/3} h c \rho^{4/3}/m^{4/3}$ arising from the Pauli exclusion principle. This can be written as

$$k_B T \ll \frac{1}{4} \left(\frac{3}{4\pi g} \right)^{1/3} \frac{h c}{m^{1/3}} \rho^{1/3} \quad (\text{D3})$$

which is the ultrarelativistic Sommerfeld criterion. Proceeding as above, we obtain the condition

$$\eta \gg 1.10 \left(\frac{M}{M_{\text{OV}}} \right)^{2/3}, \quad (\text{D4})$$

where M_{OV} is the OV critical mass given by Eq. (B1).

Appendix E: Thermodynamics of nonrelativistic self-gravitating systems

In this Appendix, we recall and complete important results concerning the thermodynamics of nonrelativistic self-gravitating systems (classical particles and fermions) that are needed in our analysis. We refer to Appendix F for useful formulae that are used throughout this Appendix.

1. Classical particles

We first consider a self-gravitating system of nonrelativistic classical particles confined within a spherical box of radius R . We show below that there is no statistical equilibrium state in a strict sense but that long-lived metastable states can exist under certain conditions.

a. Canonical ensemble

In the canonical ensemble, one can make the free energy $F = E - TS$ diverge towards $-\infty$ at fixed mass M in the most efficient manner by approaching all the particles at the same point (see Appendix B of [68]). Indeed, let us consider a homogeneous sphere of radius a containing all the particles. When $a \rightarrow 0$ the potential energy $W = -3GM^2/(5a)$ diverges to $-\infty$. The entropy $S \sim 3Nk_B \ln a$ diverges to $-\infty$ but it is subdominant. As a result, the free energy $F = E - TS \sim W \sim -3GM^2/(5a)$ diverges to $-\infty$. Therefore, there is no global minimum of free energy. In a sense, the most probable structure in the canonical ensemble is a Dirac peak containing all the mass.

On the other hand, there exist metastable gaseous states with a temperature $T > T_c = 0.397GMm/(k_B R)$ [3, 57]. They have a density contrast $\mathcal{R} < 32.1$ [3, 57] and they are very long-lived [4]. When $T < T_c$, or when $T > T_c$ and $\mathcal{R} > 32.1$, there are no metastable states anymore and the system collapses (isothermal collapse) [57]. According to the previous thermodynamical argument, it is expected to form a Dirac peak containing all the mass. By solving the Smoluchowski-Poisson equations describing the canonical evolution of self-gravitating Brownian particles [60, 68] it is found that the Dirac peak is formed in the postcollapse regime of the dynamics.

b. Microcanonical ensemble

In the microcanonical ensemble, one can make the entropy S diverge towards $+\infty$ at fixed mass M and energy E by forming a core-halo structure and letting the size of the core go to zero (see Appendix A of [68]). Indeed, let us consider a homogeneous core made of N_C particles in a sphere of radius R_C . Its potential energy $W_C = -3GM_C^2/(5R_C)$ tends to $-\infty$ when $R_C \rightarrow 0$. In order to conserve the total energy, the kinetic energy of the halo $K_h = (3/2)N_h k_B T$ must tend to $+\infty$ like $K_h \sim -W_C$ meaning that its temperature $T \sim 2GM_C^2/(5R_C N_h k_B)$ tends to $+\infty$. As a result, the entropy of the system behaves as $S \sim -(3/2)k_B(N_h - N_C) \ln R_C$ and tends to $+\infty$ when $R_C \rightarrow 0$. Therefore, there is no global maximum of entropy at fixed energy. We note that the divergence of the entropy is the most efficient when the core contains a few particles ($N_C \ll N_h$). Actually, we only need to approach 2 particles to each other and make a tight binary. Its potential energy $-Gm^2/a$ diverges towards

$-\infty$. The released energy serves to heat the halo made of the $N - 2$ other particles. This produces the most efficient divergence of entropy (note that the divergence of entropy is weak — logarithmic). In a sense, the most probable structure in the microcanonical ensemble is a tight binary surrounded by a hot halo. This can be seen as a Dirac peak of zero mass but infinite potential energy + a hot halo.

On the other hand, there exist metastable gaseous states with an energy $E > E_c = -0.335GM^2/R$ [3]. They have a density contrast $\mathcal{R} < 709$ [2, 3] and they are very long-lived [4]. When $E < E_c$, or when $E > E_c$ and $\mathcal{R} > 709$, there are no metastable states anymore and the system collapses (gravothermal catastrophe) [3]. It is expected to form a binary surrounded by a hot halo. Dynamical models describing the collisional evolution of globular clusters (fluid equations, orbit-averaged Fokker-Planck equation...) show that the binary is formed in the postcollapse regime of the dynamics [55, 58, 59]. The energy released by the binary can stop the collapse and induce a re-expansion of the halo. Then, in principle, a series of gravothermal oscillations should follow [69, 70].

2. Fermions

We now consider a self-gravitating system of nonrelativistic fermions confined within a spherical box of radius R . In that case, there exists a statistical equilibrium state at any energy E and temperature T [5]. We consider a situation where we are close to the classical limit ($\mu \rightarrow +\infty$ or $\hbar \rightarrow 0$). When $T > T_c$ and $E > E_c$ there exist metastable gaseous states that are not affected by quantum mechanics (see Appendix E 1). When $T < T_c$ and $E < E_c$ there are no metastable states anymore. The system collapses and becomes very dense until quantum mechanics (Pauli's exclusion principle) comes into play. Generically, the system forms a core-halo structure with a completely degenerate fermionic core of mass M_C and radius R_C surrounded by an (almost classical) isothermal halo of mass $M_h = M - M_C$ and radius R . We can obtain the value of M_C from a simple analytical model developed in [41]. We summarize this model below by using dimensional variables in order to understand more easily the physical mechanisms at play.

We model the core as a completely degenerate fermion ball. Its mass-radius relation is

$$M_C R_C^3 = \chi \frac{\hbar^6}{g^2 m^8 G^3}. \quad (\text{E1})$$

Its energy (kinetic + potential) is

$$E_C = -\frac{3}{7\chi^{1/3}} \frac{G^2 M_C^{7/3} g^{2/3} m^{8/3}}{\hbar^2}. \quad (\text{E2})$$

Its entropy is zero: $S_C = 0$.

We model the halo by a classical gas at temperature T with a uniform density.⁵⁶ Its kinetic energy is

$$K_h = \frac{3}{2} N_h k_B T. \quad (\text{E3})$$

Its potential (gravitational) energy, taking into account the presence of the core, is

$$W_h = -\frac{3GM_C M_h}{2R} - \frac{3GM_h^2}{5R}. \quad (\text{E4})$$

Its entropy is

$$S_h = -N_h k_B \ln \left(\frac{M_h}{V} \right) + \frac{3}{2} N_h k_B \ln \left(\frac{2\pi k_B T}{m} \right) + \frac{5}{2} N_h k_B + N_h k_B \ln \eta_0. \quad (\text{E5})$$

In the foregoing expressions, we have assumed $R_C \ll R$ which can be checked a posteriori.

The total mass of the system is $M = M_C + M_h$, its total energy is $E = E_C + K_h + W_h$, its total entropy is $S = S_h$ and its total free energy is $F = E - TS$. The mass M_C of the core is obtained by maximizing the entropy at fixed mass and energy in the microcanonical ensemble or by minimizing the free energy at fixed mass in the canonical ensemble. The extremization problem gives in both ensembles [41]:

$$\begin{aligned} & -\frac{G^2 M_C^{4/3} g^{2/3} m^{8/3}}{\chi^{1/3} \hbar^2} - \frac{3G(M - 2M_C)}{2R} \\ & + \frac{6G(M - M_C)}{5R} - \frac{k_B T}{m} \ln \left(\frac{M - M_C}{V} \right) \\ & + \frac{3}{2} \frac{k_B T}{m} \ln \left(\frac{2\pi k_B T}{m} \right) + \frac{k_B T}{m} \ln \eta_0 = 0. \end{aligned} \quad (\text{E6})$$

This equation may have several solutions that have been analyzed in detail in [41]. Below, we restrict ourselves to the stable condensed state.

a. Canonical ensemble

In the canonical ensemble, when $\hbar \rightarrow 0$, we expect that the core contains a large mass $M_C/M \sim 1$ (see Appendix E 1 a). Guided by this ansatz, which can be checked a posteriori, one can see from Eq. (E6) that the core mass is given by

$$1 - \frac{M_C}{M} \sim \frac{\eta_0 V}{M} \left(\frac{2\pi k_B T}{m} \right)^{3/2} e^{\frac{3GM_C}{2Rk_B T}} e^{-\frac{G^2 M^{4/3} g^{2/3} m^{11/3}}{\chi^{1/3} \hbar^2 k_B T}}. \quad (\text{E7})$$

⁵⁶ We will see that its temperature is very large in the situations considered. This justifies the uniform density approximation.

When $h \rightarrow 0$, the core mass tends towards M exponentially rapidly. Therefore the core contains almost all the mass: $M_C \sim M$. Its radius is given by

$$R_C = \chi^{1/3} \frac{h^2}{g^{2/3} m^{8/3} G M^{1/3}}. \quad (\text{E8})$$

When $h \rightarrow 0$, it tends to zero as h^2 . The energy of the core is

$$E_C = -\frac{3}{7\chi^{1/3}} \frac{G^2 M^{7/3} g^{2/3} m^{8/3}}{h^2}. \quad (\text{E9})$$

When $h \rightarrow 0$, it tends to $-\infty$ as $-h^{-2}$. The free energy, which is dominated by the energy of the core, $F \sim E_C$, behaves in a similar manner. In the classical limit $h \rightarrow 0$, we recover the Dirac peak containing all the mass. This structure leads to the divergence of the free energy in agreement with the arguments of Appendix E 1 a. We note that these results are independent of the presence, or not, of the box.

In terms of dimensionless variables [41], the preceding results can be written as

$$1 - \alpha_C \sim \frac{\sqrt{\pi}}{6} \mu \frac{e^{3\eta/2}}{\eta^{3/2}} e^{-\lambda\eta\mu^{2/3}}, \quad (\text{E10})$$

$$\frac{R_C}{R} \sim \frac{1}{\lambda\mu^{2/3}}, \quad (\text{E11})$$

$$\Lambda_C \sim \Lambda_{\max} = \frac{3}{7} \lambda\mu^{2/3}, \quad (\text{E12})$$

where $\alpha_C = M_C/M$. We note that letting $h \rightarrow 0$ (classical limit) in the dimensional equations is equivalent to letting $\mu \rightarrow +\infty$ in the dimensionless equations.

Remark: Using the results of Ref. [41], the maximum temperature of the condensed phase, and the corresponding core mass, are given by

$$\eta_* \sim \frac{2 \ln \mu}{\lambda\mu^{2/3}}, \quad 1 - \alpha_* \sim \frac{3}{8 \ln \mu}. \quad (\text{E13})$$

Coming back to dimensional variables, we get⁵⁷

$$k_B T_* \sim \frac{1}{6\chi^{1/3}} \frac{g^{2/3} G^2 M^{4/3} m^{11/3}}{h^2 (-\ln h)}. \quad (\text{E14})$$

On the other hand, the temperature of transition, and the corresponding core mass, are given by

$$\eta_t \sim \frac{14 \ln \mu}{3\lambda\mu^{2/3}}, \quad 1 - \alpha_t \sim \frac{\sqrt{\pi}}{6} \left(\frac{3\lambda}{14} \right)^{3/2} \frac{1}{\mu^{8/3} (\ln \mu)^{3/2}}. \quad (\text{E15})$$

Coming back to dimensional variables, we get

$$k_B T_t \sim \frac{1}{14\chi^{1/3}} \frac{g^{2/3} G^2 M^{4/3} m^{11/3}}{h^2 (-\ln h)}. \quad (\text{E16})$$

⁵⁷ Here and in the following, we give the logarithmic correction in the dominant approximation. Furthermore, $-\ln h$ should be understood as $(1/3) \ln \mu$ where $\mu = (gm^4/h^3)\sqrt{512\pi^4 G^3 M R^3}$ is dimensionless.

b. Microcanonical ensemble

In the microcanonical ensemble, we expect that the core contains a small mass $M_C/M \ll 1$ (see Appendix E 1 b). Guided by this ansatz, which can be checked a posteriori, one can see from Eq. (E6) that the core mass is given by

$$\frac{M_C}{M} \sim \frac{7}{12(-\ln h)}. \quad (\text{E17})$$

When $h \rightarrow 0$, the core mass tends towards 0 extremely slowly (logarithmically). Therefore, the core contains a fraction of the total mass and this fraction goes to zero as $(-\ln h)^{-1}$ when $h \rightarrow 0$. The radius of the core is given by

$$R_C \sim \left(\frac{12}{7} \right)^{1/3} \chi^{1/3} \frac{h^2 (-\ln h)^{1/3}}{g^{2/3} m^{8/3} G M^{1/3}}. \quad (\text{E18})$$

When $h \rightarrow 0$, it tends to zero as $h^2 (-\ln h)^{1/3}$. The energy of the core is

$$E_C \sim -\frac{3}{7\chi^{1/3}} \left(\frac{7}{12} \right)^{7/3} \frac{G^2 M^{7/3} g^{2/3} m^{8/3}}{h^2 (-\ln h)^2}. \quad (\text{E19})$$

When $h \rightarrow 0$, it tends to $-\infty$ as $-h^{-2} (-\ln h)^{-2}$. Since the energy of the core is very negative the kinetic energy of the halo must be very positive in order to conserve the total energy. It must behave as $K_h \sim -E_C$. Therefore, the temperature of the halo must be very large:

$$k_B T_{\text{cond}} \sim \frac{2}{7\chi^{1/3}} \left(\frac{7}{12} \right)^{7/3} \frac{G^2 M^{4/3} g^{2/3} m^{11/3}}{h^2 (-\ln h)^2}. \quad (\text{E20})$$

When $h \rightarrow 0$, it diverges to $+\infty$ as $h^{-2} (-\ln h)^{-2}$. The entropy behaves as $S \sim -6Nk_B \ln h$. Subtracting the term $-3Nk_B \ln h$ that we get even in the absence of gravity (see Appendix F), we obtain

$$\Delta S \sim -3Nk_B \ln h. \quad (\text{E21})$$

When $h \rightarrow 0$, the entropy diverges to $+\infty$ as $-\ln h$. In the classical limit $h \rightarrow 0$, we recover the core-halo structure made of a core having a small mass, a small radius and a huge potential energy (Dirac peak of zero mass) surrounded by a very hot halo.⁵⁸ This core-halo structure leads to the (logarithmic) divergence of the entropy

⁵⁸ We note that the collapse at *low* energies in the microcanonical ensemble (gravothermal catastrophe) produces *hot* systems ($T \rightarrow +\infty$) with a core-halo structure. Actually, although the temperature is uniform throughout the system, the halo is hot while the core is cold. Indeed, the halo is nondegenerate (Boltzmannian) because $T \gg T_F$, where T_F is the Fermi temperature (see Appendix D), while the core is completely degenerate because $T \ll T_F$. Fundamentally, this core-halo structure is the consequence of the negative specific heat of self-gravitating systems as explained in Ref. [3].

in agreement with the results of Appendix E 1 b. We note that these results are independent of the presence, or not, of the box. They are also independent of the value of the energy E provided that it is not too extreme.

In terms of dimensionless variables [41], the preceding results can be rewritten as

$$\alpha_C \sim \frac{7}{4 \ln \mu}, \quad (\text{E22})$$

$$\frac{R_C}{R} \sim \frac{1}{\lambda} \left(\frac{4}{7}\right)^{1/3} \frac{(\ln \mu)^{1/3}}{\mu^{2/3}}, \quad (\text{E23})$$

$$\Lambda_C \sim \frac{3}{7} \lambda \left(\frac{7}{4}\right)^{7/3} \frac{\mu^{2/3}}{(\ln \mu)^{7/3}}, \quad (\text{E24})$$

$$\eta_{\text{cond}} \sim \frac{7}{2\lambda} \left(\frac{4}{7}\right)^{7/3} \frac{(\ln \mu)^{7/3}}{\mu^{2/3}}, \quad (\text{E25})$$

where $\alpha_C = M_C/M$. More generally (without specifying the value of the core mass α_C), in the case where the energy of the core tends to $-\infty$ and the energy of the halo tends to $+\infty$ we have the relation

$$\eta_{\text{cond}} \sim \frac{1 - \alpha_C}{\alpha_C^{7/3}} \frac{7}{2\lambda \mu^{2/3}}. \quad (\text{E26})$$

When α_C is given by Eq. (E22) obtained from Eq. (E6), we recover Eq. (E23). Finally, we note that letting $h \rightarrow 0$ (classical limit) in the dimensional equations is equivalent to letting $\mu \rightarrow +\infty$ in the dimensionless equations.

Remark: Using the results of Ref. [41], the maximum energy of the condensed phase, and the corresponding core mass, are given by

$$\Lambda_* \sim -\frac{9\lambda}{28} \frac{\mu^{2/3}}{(\ln \mu)^{7/3}}, \quad \alpha_* \sim \frac{1}{\ln \mu}. \quad (\text{E27})$$

Coming back to dimensional variables, we get

$$E_* \sim \frac{1}{28(3\chi)^{1/3}} \frac{g^{2/3} G^2 M^{7/3} m^{8/3}}{h^2 (-\ln h)^{7/3}}. \quad (\text{E28})$$

The energy of transition Λ_t , and the corresponding core mass α_t , have the same scalings.

Appendix F: Useful formulae

In this Appendix, we regroup basic formulae that are useful in our study.

1. Energy and entropy

The energy of a nonrelativistic self-gravitating system can be written as

$$E = \int f \frac{v^2}{2} d\mathbf{r} d\mathbf{v} + \frac{1}{2} \int \rho \Phi d\mathbf{r} = K + W, \quad (\text{F1})$$

where K is the kinetic energy and W the potential (gravitational) energy [71].

The Fermi-Dirac entropy functional is given by

$$S = -k_B \frac{\eta_0}{m} \int \left\{ \frac{f}{\eta_0} \ln \frac{f}{\eta_0} + \left(1 - \frac{f}{\eta_0}\right) \ln \left(1 - \frac{f}{\eta_0}\right) \right\} d\mathbf{r} d\mathbf{v}, \quad (\text{F2})$$

where $\eta_0 = gm^4/h^3$ is the maximum allowed value of the distribution function $f(\mathbf{r}, \mathbf{v})$ fixed by Pauli's exclusion principle [45]. In the classical (nondegenerate) limit $f \ll \eta_0$, it reduces to the Boltzmann entropy functional

$$S = -k_B \int \left(\frac{f}{m} \ln \frac{f}{\eta_0} - \frac{f}{m} \right) d\mathbf{r} d\mathbf{v}. \quad (\text{F3})$$

The distribution function that maximizes the Boltzmann entropy at fixed density ρ and energy E is the Boltzmann distribution

$$f(\mathbf{r}, \mathbf{v}) = \left(\frac{m}{2\pi k_B T} \right)^{3/2} \rho(\mathbf{r}) e^{-\frac{mv^2}{2k_B T}}, \quad (\text{F4})$$

where T is the temperature [1, 57]. Using Eq. (F4), the kinetic energy and the entropy of a nonrelativistic classical isothermal self-gravitating system are

$$K = \frac{3}{2} N k_B T \quad (\text{F5})$$

and

$$S = -k_B \int \frac{\rho}{m} \ln \rho d\mathbf{r} + \frac{3}{2} N k_B \ln \left(\frac{2\pi k_B T}{m} \right) + \frac{5}{2} N k_B + N k_B \ln \eta_0. \quad (\text{F6})$$

Remark: We note that the Boltzmann entropy defined by Eq. (F3) diverges like $S \sim N k_B \ln \eta_0 \sim -3N k_B \ln h \rightarrow +\infty$ when $h \rightarrow 0$. This divergence is present in the famous Sackur-Tetrode formula for the entropy of a perfect gas (without self-gravity). In order to see the absence of statistical equilibrium states for classical self-gravitating systems, marked by the divergence of the entropy when $h \rightarrow 0$, we first have to subtract the term $-3N k_B \ln h$ from the total entropy (see Appendix E 2 b).

2. Homogeneous sphere

The potential (gravitational) energy of a spatially homogeneous sphere of mass M and radius R is [71]:

$$W = -\frac{3GM^2}{5R}. \quad (\text{F7})$$

Using Eqs. (F1), (F5) and (F7), the total energy of a nonrelativistic classical isothermal self-gravitating system with a uniform density is

$$E = \frac{3}{2} N k_B T - \frac{3GM^2}{5R}. \quad (\text{F8})$$

Using Eq. (F6) its entropy is

$$S_B = -Nk_B \ln \left(\frac{M}{V} \right) + \frac{3}{2} Nk_B \ln \left(\frac{2\pi k_B T}{m} \right) + \frac{5}{2} Nk_B + Nk_B \ln \eta_0, \quad (\text{F9})$$

where $V = (4/3)\pi R^3$ is the volume of the system.

3. Completely degenerate nonrelativistic self-gravitating Fermi gas

The mass-radius relation of a completely degenerate fermion star ($T = 0$) in the nonrelativistic limit is

$$M_C R_C^3 = \chi \frac{h^6}{g^2 m^8 G^3}, \quad R_C = \chi^{1/3} \frac{h^2}{g^{2/3} m^{8/3} G M_C^{1/3}} \quad (\text{F10})$$

with

$$\chi = \frac{1}{8} \left(\frac{3}{4\pi} \right)^2 \frac{\omega_{3/2}}{16\pi^2} = 5.97241 \times 10^{-3}, \quad (\text{F11})$$

where $\omega_{3/2} = 132.3843$ [8].

Its energy (kinetic + potential) is [8]:

$$E_C = -\frac{3GM_C^2}{7R_C}. \quad (\text{F12})$$

Combined with the mass-radius relation (F10), we get

$$E_C = -\frac{3}{7\chi^{1/3}} \frac{G^2 M_C^{7/3} g^{2/3} m^{8/3}}{h^2}. \quad (\text{F13})$$

This is the energy of the ground state.

Remark: In terms of dimensionless variables [41], the mass-radius relation can be written as

$$\frac{R_C}{R} = \frac{1}{\lambda \alpha_C^{1/3} \mu^{2/3}}, \quad (\text{F14})$$

where $\alpha_C = M_C/M$ and

$$\lambda = \frac{1}{(512\pi^4 \chi)^{1/3}} = 0.149736... \quad (\text{F15})$$

Similarly, the energy-mass relation can be written as

$$\Lambda_C = \frac{3}{7} \lambda \alpha_C^{7/3} \mu^{2/3}. \quad (\text{F16})$$

In writing these expressions, we have implicitly assumed that the fermion star of mass M_C and radius R_C constitutes the core of a larger system of mass M and radius R as in Appendix E.

4. Ground state of a self-gravitating Fermi gas in a box

In terms of dimensionless variables [41], the minimum energy (ground state) of a nonrelativistic self-gravitating Fermi gas enclosed within a box is given by (see Eq. (F16) with $\alpha_C = 1$):

$$\Lambda_{\max} = \frac{3}{7} \lambda \mu^{2/3}. \quad (\text{F17})$$

This expression is valid for a self-confined fermion star such that $R_C < R$ (i.e., the density of the fermion star vanishes before reaching the box). Using Eq. (F14) with $\alpha_C = 1$, we find that Eq. (F17) is valid for $\mu > \lambda^{-3/2} = 17.26$. When $\mu < 17.26$, the fermion star at $T = 0$ (ground state) is box-confined ($R_C > R$) and its energy $\Lambda_{\max}^b(\mu)$ is represented in Fig. 2 of [45].

Introducing the normalized variables of Appendix B and using Eq. (20), we find from Eq. (F17) that the minimum energy of a nonrelativistic self-gravitating Fermi gas is given by

$$\frac{\Lambda_{\max}}{R} = \frac{3}{7} \lambda \left(\frac{4\sqrt{2}}{\pi} \right)^{2/3} N^{1/3} = 0.0950 N^{1/3}. \quad (\text{F18})$$

This expression is valid for $N > 91.9/R^3$ so that the fermion star is self-confined ($R_C < R$). This equation can be used to locate the vertical asymptote Λ_{\max} in the caloric curves of this paper. However, it is only valid in the nonrelativistic regime $N \ll N_{\text{OV}}$. In the relativistic regime, the minimum energy Λ_{\max} of the self-gravitating Fermi gas, as well as the energy Λ'_{\max} of the unstable fermion star at $T = 0$, are represented in Fig. 14 of [6]. At the point $N = N_1$ where the second asymptote (corresponding to the unstable fermion star at $T = 0$) appears, we find that

$$\frac{\Lambda'_{\max}}{R} = -0.53617, \quad \frac{\Lambda_{\max}}{R} = 0.0570. \quad (\text{F19})$$

At the point $N = N_{\text{OV}}$ where the two asymptotes meet each other, we find that

$$\frac{\Lambda'_{\max}}{R} = \frac{\Lambda_{\max}}{R} = 0.08985. \quad (\text{F20})$$

Appendix G: Temperature-dependent OV maximum particle number

For $R = 50$ and $N \rightarrow N_{\text{OV}}^+$, we find from Fig. 24 that

$$\eta'_c(N) \sim 0.104 (N - N_{\text{OV}})^{-1/2}. \quad (\text{G1})$$

For a given normalized temperature $\eta > \eta_c \simeq 2.52$, the system collapses towards a black hole when $\eta'_c(N) < \eta$, i.e., when $N \geq N_{\text{OV}}(\eta)$ with

$$N_{\text{OV}}(\eta) = N_{\text{OV}} + 0.0108/\eta^2. \quad (\text{G2})$$

This can be seen as a temperature-dependent OV maximum particle number. We note that $N_{\text{OV}}(\eta)$ is very close to N_{OV} since $N_{\text{OV}}(\eta_c) = N_c^{\text{CE}} = 1.00427 N_{\text{OV}}$ (see Sec. XIII C). The relation (G1) remains valid, with a different prefactor, for other values of $R > R_{\text{CCP}}$. On the other hand, for $R_{\text{OV}} < R < R_{\text{CCP}}$, we have a similar relation for $\eta_c(N)$ close to N_{OV} (see Fig. 41 for $R = 10$):

$$\eta_c(N) \sim 0.516 (N - N_{\text{OV}})^{-1/2}. \quad (\text{G3})$$

Using the same argument as before, this yields

$$N_{\text{OV}}(\eta) = N_{\text{OV}} + 0.266/\eta^2. \quad (\text{G4})$$

More generally, writing Eqs. (G1) and (G3) under the form

$$\eta_c^{(\prime)}(N) \sim a(R) (N - N_{\text{OV}})^{-1/2}, \quad (\text{G5})$$

we get

$$N_{\text{OV}}(\eta) = N_{\text{OV}} + a(R)^2/\eta^2. \quad (\text{G6})$$

If we substitute $\eta = \beta GNm^2/R$ into Eq. (G6) and replace N by N_{OV} at leading order, we obtain

$$N_{\text{OV}}(T_\infty) = N_{\text{OV}} + a(R)^2 \frac{R^2 (k_B T_\infty)^2}{G^2 N_{\text{OV}}^2 m^4}. \quad (\text{G7})$$

We make the guess that the product $a(R)R$ in Eq. (G7) is independent of R . This can be checked on the two values that we have computed since the products $0.104 \times 50 = 5.2$ and $0.516 \times 10 = 5.16$ are almost the same. As a result, we guess that $a(R)(R/R_{\text{OV}}) \simeq 5.2/3.3569 \simeq 1.5$, i.e., $a(R) \simeq 1.5(R_{\text{OV}}/R)$. Substituting this relation into Eq. (G7), we finally obtain (using the results of Appendix B):

$$N_{\text{OV}}(T_\infty) \simeq N_{\text{OV}} + 160 \left(\frac{k_B T_\infty}{mc^2} \right)^2. \quad (\text{G8})$$

This relation is expected to be valid for $k_B T_\infty \ll mc^2$. It gives the first order correction to the OV maximum number due to thermal effects.

-
- [1] T. Padmanabhan, Phys. Rep. **188**, 285 (1990)
- [2] V.A. Antonov, Vest. Leningr. Gos. Univ. **7**, 135 (1962)
- [3] D. Lynden-Bell, R. Wood, Mon. Not. R. Astron. Soc. **138**, 495 (1968)
- [4] P.H. Chavanis, Astron. Astrophys. **432**, 117 (2005)
- [5] P.H. Chavanis, Int. J. Mod. Phys. B **20**, 3113 (2006)
- [6] G. Alberti, P.H. Chavanis, in preparation
- [7] G. Alberti, P.H. Chavanis, in preparation
- [8] S. Chandrasekhar, *An Introduction to the Theory of Stellar Structure* (Dover, 1942)
- [9] S.L. Shapiro, S.A. Teukolsky *Black Holes, White Dwarfs, and Neutron Stars* (Wiley Interscience, 1983)
- [10] N. Bilić, G.B. Tupper, R.D. Viollier, Lect. Notes Phys. **616**, 24 (2003)
- [11] H.J. de Vega, P. Salucci, N.G. Sanchez, Mon. Not. R. Astron. Soc. **442**, 2717 (2014)
- [12] R. Ruffini, C.R. Argüelles, J.A. Rueda, Mon. Not. R. Astron. Soc. **451**, 622 (2015)
- [13] P.H. Chavanis, M. Lemou, F. Méhats, Phys. Rev. D **91**, 063531 (2015)
- [14] P.H. Chavanis, M. Lemou, F. Méhats, Phys. Rev. D **92**, 123527 (2015)
- [15] V. Domcke, A. Urbano, JCAP **01**, 002 (2015)
- [16] L. Randall, J. Scholtz, J. Unwin, Mon. Not. R. Astron. Soc. **467**, 1515 (2017)
- [17] P.H. Chavanis, Eur. Phys. J. B **87**, 9 (2014)
- [18] *Dynamics and thermodynamics of systems with long range interactions*, edited by T. Dauxois, S. Ruffo, E. Arimondo, M. Wilkens, Lecture Notes in Physics **602**, (Springer, 2002)
- [19] J. Katz, Found. Phys. **33**, 223 (2003)
- [20] A. Campa, T. Dauxois, S. Ruffo, Physics Reports **480**, 57 (2009)
- [21] A. Campa, T. Dauxois, D. Fanelli, S. Ruffo, *Physics of long-range interacting systems* (Oxford University Press, 2014)
- [22] P. Hertel and W. Thirring, Commun. Math. Phys. **24**, 22 (1971)
- [23] J.M. Lévy-Leblond, J. Math. Phys. **10**, 806 (1969)
- [24] P. Hertel, H. Narnhofer and W. Thirring, Commun. Math. Phys. **28**, 159 (1972)
- [25] J. Messer, Z. Physik **33**, 313 (1979)
- [26] B. Baumgartner, Commun. Math. Phys. **48**, 207 (1976)
- [27] P. Hertel, Acta Phys. Austr. Suppl. **17**, 209 (1977)
- [28] H. Narnhofer and G.L. Sewell, Commun. Math. Phys. **71**, 1 (1980)
- [29] H. Narnhofer and G.L. Sewell, Commun. Math. Phys. **79**, 9 (1981)
- [30] W. Braun and K. Hepp, Commun. Math. Phys. **56**, 101 (1977)
- [31] P. Hertel and W. Thirring, Thermodynamic Instability of a System of Gravitating Fermions. In: H.P. Dürr (Ed.): *Quanten und Felder* (Braunschweig: Vieweg 1971)
- [32] J. Messer, J. Math. Phys. **22**, 2910 (1981)
- [33] J. Messer, Phys. Lett. **83A**, 304 (1981)
- [34] W. Thirring, Z. Physik **235**, 339 (1970)
- [35] E.B. Aronson, C.J. Hansen, Astrophys. J. **177**, 145 (1972)
- [36] R.D. Carlitz, Phys. Rev. D **5**, 3231 (1972)
- [37] S.W. Hawking, Phys. Rev. D **13**, 191 (1976)
- [38] P.H. Chavanis, B. Denet, M. Le Berre and Y. Pomeau, preprint
- [39] N. Bilić and R.D. Viollier, Phys. Lett. B **408**, 75 (1997)
- [40] P.H. Chavanis, J. Sommeria, Mon. Not. R. Astron. Soc. **296**, 569 (1998)
- [41] P.H. Chavanis, Phys. Rev. E **65**, 056123 (2002)
- [42] P.H. Chavanis, The self-gravitating Fermi gas, in *Dark Matter in Astro- and Particle Physics*, edited by H.V. Klapdor-Kleingrothaus and R.D. Viollier (Springer, 2002)
- [43] P.H. Chavanis, I. Ispolatov, Phys. Rev. E **66**, 036109 (2002)

- [44] P.H. Chavanis, M. Rieutord, *Astron. Astrophys.* **412**, 1 (2003)
- [45] P.H. Chavanis, *Phys. Rev. E* **69**, 066126 (2004)
- [46] D. Lynden-Bell, *Mon. Not. R. Astron. Soc.* **136**, 101 (1967)
- [47] N. Bilić and R.D. Viollier, *Eur. Phys. J. C* **11**, 173 (1999)
- [48] P.H. Chavanis, G. Alberti, in preparation
- [49] J.R. Oppenheimer, G.M. Volkoff, *Phys. Rev.* **55**, 374 (1939)
- [50] R. Genzel, F. Eisenhauer, S. Gillessen, *Rev. Mod. Phys.* **82**, 3121 (2010)
- [51] N. Bilić and R.D. Viollier, *Gen. Rel. Grav.* **31**, 1105 (1999)
- [52] H. Poincaré, *Acta Math.* **7**, 259 (1885)
- [53] J. Katz, *Mon. Not. R. Astron. Soc.* **183**, 765 (1978)
- [54] J. Katz, *Mon. Not. R. Astron. Soc.* **189**, 817 (1979)
- [55] H. Cohn, *Astrophys. J.* **242**, 765 (1980)
- [56] T. Padmanabhan, *Astrophys. J. Supp.* **71**, 651 (1989)
- [57] P.H. Chavanis, *Astron. Astrophys.* **381**, 340 (2002)
- [58] D. Lynden-Bell, P.P. Eggleton, *Mon. Not. R. Astron. Soc.* **191**, 483 (1980)
- [59] S. Inagaki, D. Lynden-Bell, *Mon. Not. R. Astron. Soc.* **205**, 913 (1983)
- [60] C. Sire, P.H. Chavanis, *Phys. Rev. E* **69**, 066109 (2004)
- [61] Z. Roupas, *Class. Quantum Grav.* **32**, 135023 (2015)
- [62] R.D. Sorkin, R.M. Wald, Z.Z. Jiu, *Gen. Relativ. Gravit.* **13**, 1127 (1981)
- [63] P.H. Chavanis, *Astron. Astrophys.* **381**, 709 (2002)
- [64] P.H. Chavanis, *Astron. Astrophys.* **483**, 673 (2008)
- [65] Ya. B. Zel'dovich, *Soviet Physics JETP* **15**, 446 (1962)
- [66] Z. Roupas, P.H. Chavanis, in preparation
- [67] P.H. Chavanis, *Astron. Astrophys.* **556**, A93 (2013)
- [68] C. Sire, P.H. Chavanis, *Phys. Rev. E* **66**, 046133 (2002)
- [69] D. Sugimoto, E. Bettwieser, *Mon. Not. R. Astron. Soc.* **204**, 19 (1983)
- [70] D. Heggie, N. Ramamani, *Mon. Not. R. Astron. Soc.* **237**, 757 (1989)
- [71] J. Binney, S. Tremaine, *Galactic Dynamics* (Princeton Series in Astrophysics, 1987)